

# BADTV: Unveiling Backdoor Threats in Third-Party Task Vectors

Chia-Yi Hsu\*

Yu-Lin Tsai\*

Yu Zhe<sup>+</sup>

Yan-Lun Chen\*

Chih-Hsun Lin\*

Chia-Mu Yu\*

Yang Zhang<sup>♣</sup>

Chun-Ying Huang\*

Jun Sakuma<sup>◇</sup>\*National Yang Ming Chiao Tung University, <sup>+</sup>REKIAN AIP,

♣CISPA Helmholtz Center for Information Security, ◇Tokyo Institute of Technology

## Abstract

Task arithmetic in large-scale pre-trained models enables flexible adaptation to diverse downstream tasks without extensive re-training. By leveraging task vectors (TVs), users can perform modular updates to pre-trained models through simple arithmetic operations like addition and subtraction. However, this flexibility introduces new security vulnerabilities. In this paper, we identify and evaluate the susceptibility of TVs to backdoor attacks, demonstrating how malicious actors can exploit TVs to compromise model integrity. By developing *composite backdoors* and eliminating redundant clean tasks, we introduce BADTV, a novel backdoor attack specifically designed to remain effective under task learning, forgetting, and analogies operations. Our extensive experiments reveal that BADTV achieves near-perfect attack success rates across various scenarios, significantly impacting the security of models using task arithmetic. We also explore existing defenses, showing that current methods fail to detect or mitigate BADTV. Our findings highlight the need for robust defense mechanisms to secure TVs in real-world applications, especially as TV services become more popular in machine-learning ecosystems.

## 1 Introduction

Recent advancements in machine learning (ML) have demonstrated that larger models, with increased parameter counts, exhibit enhanced performance. Typically, large pre-trained ML models [10, 15, 26, 49] undergo task-specific fine-tuning [13, 22, 33], which involves backpropagation to adjust parameters for individual tasks. While effective, fine-tuning is computationally demanding and storage-intensive [35], necessitating separate model instances for each task.

To address these limitations, researchers have proposed a novel approach called task arithmetic (TA) [9, 23, 45, 48, 50, 59], employing task vectors (TVs), instead of extensive parameter updates. TVs encapsulate the updates performed during fine-tuning of large pretrained models. By applying

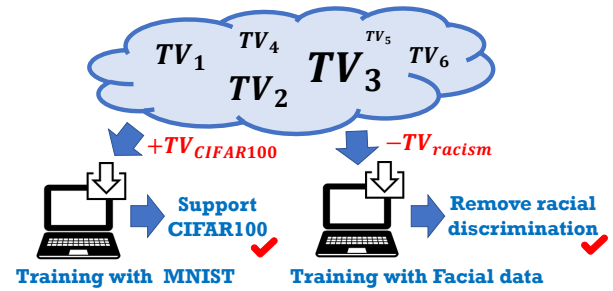


Figure 1: Task vector as a service (TVaaS).

simple arithmetic operations to these vectors, users can efficiently execute multiple tasks without requiring substantial re-training. This method conserves storage across different model applications and decreases the computational overhead tied to fine-tuning. TA has demonstrated efficacy across domains such as computer vision [48], automatic speech recognition [50, 59], and natural language processing [9], indicating its potential as a standard technique for model adaptation. In line with the current “pre-training first and then fine-tuning” paradigm in large models, task vector as a service (TVaaS) platforms (e.g., Hugging Face<sup>1</sup>) are expected to gain traction and see application in real-world scenarios. Users can request TVs for downstream tasks from TVaaS providers, circumventing laborious fine-tuning. By integrating pre-trained models with various TVs, new functionalities emerge, as illustrated in Figure 1. Like app stores on mobile devices, users can install diverse functionalities via TVs on pre-trained models, while TVaaS providers manage TV creation for multiple users. These advantages set TVaaS apart from machine learning as a service (MLaaS), rendering well-trained TVs valuable assets for users seeking new functionalities.

Despite these advantages, TVs pose significant security concerns, particularly with backdoor attacks. This issue mirrors vulnerabilities where users download backdoored apps from app stores [14, 56, 57]. In neural networks, data

<sup>1</sup><https://huggingface.co/tasks>

poisoning-based backdoor attacks [7, 19, 43, 44, 62, 72] subtly poison training data, causing models to learn incorrect behaviors and produce faulty outputs. Multiple TVaaS providers offering similar services for task adaptation complicate users’ ability to verify TV integrity solely from parameter values. Hence, attackers could exploit this by introducing TVs with similar functionality but hidden malicious intents. Given their strategic role in ML operations, evaluating the vulnerability of TVs to such threats is paramount.

In this work, for the first time, we investigate the security vulnerabilities of TA from an attacker’s perspective, focusing on backdoor attacks. Backdooring TVs presents two challenges. First, unlike traditional backdoor attacks [7, 19, 43, 44, 62, 72] targeting single, task-specific models, attackers here can only manipulate parts of a merged model (e.g., one task-specific component). This limited access complicates crafting effective and resilient backdoor strategies due to the lack of full control over model integration. Second, TVs are used for task learning by addition, task forgetting by subtraction, and task analogies by mixed operations. Thus, the backdoor must be embedded in the victim TV so that the merged model remains compromised, regardless of task learning, forgetting, or analogies. Given that task learning and forgetting are opposing operations, maintaining backdoor functionality across both is challenging.

To address these challenges, we introduce BADTV, the first backdoor attack tailored for TA. Since the backdoor persists only during either task learning or forgetting, BADTV implants *composite backdoors* into the victim TV, rather than a single backdoor. The composite backdoor is structured so that one backdoor remains active during task learning and the other during task forgetting, ensuring that they do not interfere with each other. This necessitates a joint design of composite backdoors, complicating optimization. However, we simplify the backdoored TV design in BADTV by eliminating unnecessary clean tasks, allowing us to craft the backdoors individually and, in turn, making the backdoor attack even more versatile.

We empirically validate the effectiveness of BADTV across diverse scenarios. For instance, the backdoor successfully transfers to a merged model composed of a clean pre-trained model and a backdoored TV (via both addition and subtraction), achieving nearly 100% attack success rate (ASR). In more complex, realistic scenarios involving multiple pre-trained models and backdoored TVs, the ASR remains high.

We explore three potential defenses against BADTV. First, we apply backdoor detection to the merged model, which fails due to the composite backdoor design in BADTV and the use of CLIP as a classifier. Second, assuming that multiple TVs with identical functionality are available, clustering on merged models formed with different TVs could be attempted. However, the distributions of clean and backdoored models are indistinguishable. Third, reducing the scaling coefficient might lessen the backdoor’s impact, but this adversely affects

model utility. These failed attempts highlight the urgent need of developing effective defenses.

**Contribution** Our contributions are summarized as follows:

- We reveal a potential backdoor threat in task arithmetic by introducing BADTV, a method to implement backdoor attacks on task vectors.
- BADTV achieves high attack performance by utilizing composite backdoors and eliminating redundant clean tasks from these composites.
- Extensive experiments demonstrate the effectiveness of BADTV across various scenarios. Moreover, existing defense mechanisms fail to counter BADTV, underscoring the urgent need for effective defense strategies.

## 2 Preliminaries

We explore the backdoor attacks for task arithmetic (TA) with a focus on image classification. Task vectors (TVs) are formed by the difference between the pre-trained model (e.g., CLIP [26, 49]) and task-specific image classifier. Thus, we describe CLIP-based classifiers, task arithmetic, and backdoor attacks as follows.

**CLIP-based Classifiers** Pre-trained models like CLIP [26, 49], trained on internet-scale datasets of image-caption pairs, possess a deep understanding of image semantics. These models demonstrate exceptional image comprehension and are well-suited for zero-shot classification. TA typically assumes the use of CLIP-based classifiers, a convention our study also follows.

A pre-trained model  $M$  comprises a visual encoder  $V$  and a text encoder  $T$ , represented as  $M = \{V, T\}$ . Unlike traditional classifiers such as ResNet and VGG,  $M$  can classify images in a zero-shot manner using only textual descriptions of class names (e.g., "dog"). Specifically, given a labeled dataset  $\{(x, y)\}$ ,  $M$  computes similarity scores for an input image  $x$  across  $k$  classes as follows:

$$M(x, C) = [\langle V(x), T(c_1) \rangle, \dots, \langle V(x), T(c_k) \rangle]^T, \quad (1)$$

where  $C = [c_1, \dots, c_k]$  represents  $k$  textual descriptions corresponding to the task’s classes, and  $\langle V(x), T(c_i) \rangle$  denotes the similarity score between the embeddings of  $x$  and class  $c_i$ . For a specific task with class names  $C$ , the task-specific classifier is derived by minimizing the cross-entropy loss  $L_{CE}(M(x, C), y)$  using the ground truth label  $y$ . During fine-tuning, freezing  $T$  while updating  $V$  yields the best performance.

**Task arithmetic** Task arithmetic (TA) [9, 23, 45, 48, 50, 59] is a novel paradigm in ML aimed at overcoming the performance limitations of fine-tuning. Given the high costs associated with re-training foundation models, TA offers a solution by enabling model behavior modification through simple arithmetic operations on task vectors (TVs). In this paper, we focus on the application of TVs in computer vision applications and analyze the associated backdoor risks.

A task  $t$  is defined by a specific dataset  $D_t$  and the loss function  $L_t$  used for fine-tuning. Let  $M_\theta$  be a model with weights  $\theta$ . Let  $\theta_{\text{pre}}$  denote the weights of a publicly available pre-trained model, and  $\theta_t$  the weights after fine-tuning on task  $t$  using  $D_t$  and  $L_t$ . The TV  $\tau_t$  is then defined as

$$\tau_t := \theta_t - \theta_{\text{pre}}. \quad (2)$$

When the task is clear from context, we omit the identifier  $t$  and refer to the TV simply as  $\tau$ .

TVs can be applied to any model with the same architecture as  $M_{\theta_{\text{pre}}}$ . By using element-wise arithmetic, such as *addition*, and incorporating a scaling coefficient  $\lambda$ , we perform *task learning* by forming a merged model  $M_{\theta_{\text{merged}}}$  that can accomplish task  $t$  as

$$\theta_{\text{merged}} := \theta_{\text{pre}} + \lambda\tau_t. \quad (3)$$

Depending on the choice of  $\lambda$ ,  $M_{\theta_{\text{merged}}}$  exhibits varying levels of capability for task  $t$ . When  $\lambda = 1$ , we obtain the original fine-tuned model  $M_{\theta_t}$  for task  $t$ . Conversely, by using *subtraction*, we perform *task forgetting* to generate a new merged model  $M_{\theta_{\text{merged}}}$  that forgets task  $t$  while retaining performance on other tasks, as

$$\theta_{\text{merged}} := \theta_{\text{pre}} - \lambda\tau_t. \quad (4)$$

Furthermore, TA allows for task analogies by using mixed operations (both addition and subtraction) to generate the merged model  $\theta_{\text{merged}}$  as

$$\theta_{\text{merged}} := \theta_{\text{pre}} + \lambda_1\tau_{t_1} + (\lambda_2\tau_{t_2} - \lambda_3\tau_{t_3}), \quad (5)$$

for *correlated* tasks  $t_1$ ,  $t_2$ , and  $t_3$  and scaling coefficients  $\lambda_1$ ,  $\lambda_2$ , and  $\lambda_3$ . Task analogies are especially useful in improving domain generalization and data scarcity. For instance, images of lions in indoor settings are rarer compared to lions in outdoor settings or dogs in various environments (indoor or outdoor). We can apply task analogies, i.e.,  $\tau_{\text{lion indoors}} = \tau_{\text{lion outdoors}} + (\tau_{\text{dog indoors}} - \tau_{\text{dog outdoors}})$  to overcome data scarcity.

In the context of model editing, a related technique is model merging (MM) [23, 46, 61, 66, 68–70, 73]. MM only supports task learning, often through methods like weight averaging or knowledge distillation. In contrast, TA *dynamically* modifies a model’s behavior for specific tasks by applying arithmetic operations such as addition or subtraction, altering how the model processes inputs or transitions between tasks.

**Backdoor Attacks** Backdoor attacks [7, 19, 43, 44, 62, 72] usually subvert ML models by embedding covert, malicious behaviors through data poisoning. These backdoored models function normally under typical conditions but behave maliciously when encountering inputs containing a specific trigger. For example, in image classification, a backdoored model will misclassify images containing a pre-defined trigger as an attacker-specified target class. Denote an image as  $x$  and the trigger as  $g = \{\text{mask}, \delta\}$ , where *mask* is a binary mask indicating the trigger’s location, and  $\delta$  represents the trigger pattern. A triggered image  $\hat{x}^g$  is generated by  $\delta \odot \text{mask} + (1 - \text{mask}) \odot x$ , where  $\odot$  denotes pixel-wise multiplication. When the trigger  $g$  is clear from context, we omit the identifier  $g$  and refer to the triggered input simply as  $\hat{x}$ . The goal of a backdoor attack is to craft a model that correctly classifies unaltered images  $x$  while misclassifying triggered images  $\hat{x}$  as the target class  $c$ .

### 3 Threat Model in Task Arithmetics

We begin by outlining the application and attack scenarios. Next, we detail the attacker’s goal and capabilities. We highlight the distinctions between our attack and existing attacks.

**Application Scenario** Consider a user conducting medical research and needing a model capable of diagnosing medical images across diverse domains. Instead of relying on a computer vision expert, the user can request multiple task vectors (TVs) from a TVaaS provider. The provider supplies the necessary TVs for various tasks, allowing the user to integrate them using task arithmetic (TA) to create a comprehensive multi-tasking model, significantly reducing development effort. TVaaS providers, in turn, benefit by distributing TVs to multiple users, supporting diverse downstream tasks. Due to the page limit, we present only the above task learning scenario. However, BADTV also works for task forgetting (subtraction) and analogies (both addition and subtraction) due to our design; please see Section 5.

Hugging Face<sup>2</sup> serves as a notable TVaaS provider, offering approximately 13,000 models as TVs in image classification<sup>3</sup>. Among them, the CLIP model [25, 49] has around 3,000 fine-tuned variations for downstream tasks<sup>4</sup>, and the CIFAR-10 task [30] offers about 1,000 TVs with similar functionality<sup>5</sup>. Based on this trend, we expect TVaaS to evolve and diverge from traditional MLaaS [52]. However, the security risks inherent in this new paradigm remain underexplored, which this work aims to address.

<sup>2</sup><https://huggingface.co>

<sup>3</sup><https://huggingface.co/tasks>

<sup>4</sup><https://huggingface.co/models?search=clip>

<sup>5</sup><https://huggingface.co/models?search=cifar10>

**Attack Scenario** Consider a user possessing a pre-trained model  $M_{\theta_{\text{pre}}}$ . For example, the user seeks to edit  $M_{\theta_{\text{pre}}}$  for task  $t$  by downloading the corresponding task vector  $\tau_t$  from a TVaaS provider. The user performs task learning/forgetting and obtains  $M_{\theta_t}$  by calculating  $\theta_{\text{pre}} \oplus \lambda \tau_t$  with  $\oplus \in \{+, -\}$ , where  $\lambda$  is chosen based on the desired task strength. Here, for simplicity, we focus only on the case where the user possesses  $M_{\theta_{\text{pre}}}$  and downloads a single  $\tau_t$  from the TVaaS provider for task learning ( $\oplus = "+"$ ) or task forgetting ( $\oplus = "-"$ ). Once achieving both, one can easily extend to task analogies.

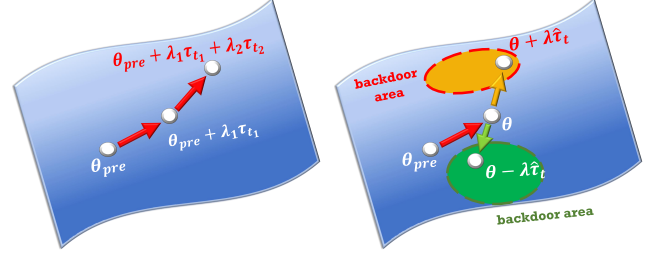
In our study, we assume that a TVaaS provider supplies a backdoored task vector (BTV)  $\hat{\tau}_t$ . The malicious vector could originate either from the TVaaS provider itself or from a third-party attacker uploading it to the open platform, such as Hugging Face, due to insufficient security checks on user-uploaded TVs.

**Attacker’s Goal** The attacker aims to construct a BTV  $\hat{\tau}_t$  that associates a pre-defined trigger with a target class in task  $t$ . When a benign user downloads  $\hat{\tau}_t$  and computes  $\theta_{\text{pre}} \oplus \lambda \hat{\tau}_t$ ,  $\oplus \in \{+, -\}$ , the resulting merged model  $\hat{M}_{\theta_{\text{merged}}}$  is backdoored.  $\hat{M}_{\theta_{\text{merged}}}$  performs correctly on clean inputs but misclassifies triggered inputs as the target class. If the model is deployed in a safety-critical system (e.g., facial recognition for access control), the attacker can exploit the backdoor to bypass authentication by presenting the trigger.

**Attacker’s Knowledge and Capability** We assume that the attacker possesses a dataset  $\hat{D}_t$  for their task, typically constructed by poisoning a subset of the clean dataset  $D_t$  through backdoor injection methods [7, 19, 43, 44, 62, 72]. The attacker fine-tunes the pre-trained model  $M_{\theta_{\text{pre}}} = \{V, T\}$  (with  $V$  as the visual encoder and  $T$  as the text encoder) on  $\hat{D}_t$ , freezing  $T$  and updating  $V$  based on the cross-entropy loss  $L_{CE}(M_{\theta_{\text{pre}}}(x, C), y)$  to obtain a task-specific model  $\hat{M}_{\theta_t}$  with the weights  $\hat{\theta}_t$ . The BTV  $\hat{\tau}_t$  is then calculated as  $\hat{\theta}_t - \theta_{\text{pre}}$ .

Although the attacker has white-box access to  $M_{\theta_{\text{pre}}}$ , they have no knowledge of the victim user’s scaling coefficient  $\lambda$ , which the user selects independently after downloading the BTV.

**Difference with Existing Attacks** BADTV shares similarities with model poisoning-based backdoor attacks [12, 34, 54] in that the attacker’s BTV alters the victim user’s model. However, BADTV does not directly manipulate the final model or control task arithmetic (e.g.,  $\lambda$ ). Moreover, BADTV resembles federated learning (FL) backdoor attacks [3, 65], where the attacker contributes to the final model. However, unlike FL, the attacker in BADTV lacks knowledge of the victim’s task or gradients. Lastly, BADTV is related to BADMERGING [73], a backdoor attack on model merging. However, BADTV is orthogonal to BADMERGING; the latter focuses on backdoor



(a) Trajectory of TV addition. (b) Two different backdoor regions.

Figure 2: The design challenge of BTV in weight space.

persistence during model merging, while BADTV ensures the backdoor survives both addition and subtraction operations.

## 4 Challenges and Key Insight

We first describe the critical challenges and limitations of current backdoor attacks in the context of TA. Next, we present the key insight of BADTV to address these challenges.

**Challenges** To successfully execute a backdoor attack on TVs, the primary challenge is ensuring the backdoor remains effective across all possible uses of the TV (i.e., task learning, forgetting, and analogies) with a single BTV. In other words, the backdoor attack must succeed regardless of how the user applies the BTV.

Assume that the attacker is in possession of  $\hat{D}_t = \{(x_1, y_1), \dots, (x_\mu, y_\mu)\} \cup \{(\hat{x}_1, \hat{y}), \dots, (\hat{x}_\nu, \hat{y})\}$ , where the first part consists of clean samples and the latter part contains triggered samples. Here,  $x_i$  is a clean sample,  $y_i$  is the ground truth label,  $\hat{x}_i$  is a triggered sample, and  $\hat{y}$  is the target class specified by the attacker. The BTV for task  $t$  is defined as  $\hat{\tau}_t = \hat{\theta}_t - \theta_{\text{pre}}$ , where  $\hat{\theta}_t$  represents the weights of the backdoored model  $\hat{M}_{\theta_t}$  fine-tuned on  $\hat{D}_t$ . The merged model’s weights are given by

$$\hat{\theta}_{\text{merged}} = \theta_{\text{pre}} \oplus \lambda \hat{\tau}_t \quad \text{with } \oplus \in \{+, -\}, \quad (6)$$

where  $\lambda$  is chosen by the user. The attacker’s goal is to find  $\hat{\tau}_t$  by solving the following optimization:

$$\begin{aligned} \min_{\hat{\tau}_t} & \left( \sum_{i=1}^{\mu} L_{CE}(\hat{M}_{\theta_{\text{merged}}}(x_i, y_i), y_i) + \sum_{j=1}^{\nu} L_{CE}(\hat{M}_{\theta_{\text{merged}}}(\hat{x}_j, \hat{y}), \hat{y}) \right), \\ \text{s.t. } & \hat{\theta}_{\text{merged}} = \theta_{\text{pre}} + \lambda \hat{\tau}_t, \\ & \hat{\theta}_{\text{merged}} = \theta_{\text{pre}} - \lambda \hat{\tau}_t. \end{aligned} \quad (7)$$

Clearly, implanting a single backdoor into the TV is insufficient to solve Equation 7, as the backdoor only survives the addition operation in TA, not the subtraction. Solving Equation 7 is non-trivial due to the dual constraints, where two

backdoor regions exist in opposite positions within the weight space, as illustrated in Figure 2.

One alternative is to solve the constrained optimization for the addition operation in Equation 8:

$$\begin{aligned} \min_{\theta} & \left( \sum_{i=1}^{\mu} L_{CE}(\hat{M}_{\theta_{\text{merged}}}(x_i, y_i), y_i) + \sum_{j=1}^{\nu} L_{CE}(\hat{M}_{\theta_{\text{merged}}}(\hat{x}_j, \hat{y}_j), \hat{y}_j) \right), \\ \text{s.t. } & \hat{\theta}_{\text{merged}} = \theta_{\text{pre}} + \lambda \hat{\tau}_t, \end{aligned} \quad (8)$$

to obtain a TV for addition and solve the optimization for the subtraction operation in Equation 9:

$$\begin{aligned} \min_{\theta} & \left( \sum_{i=1}^{\mu} L_{CE}(\hat{M}_{\theta_{\text{merged}}}(x_i, y_i), y_i) + \sum_{j=1}^{\nu} L_{CE}(\hat{M}_{\theta_{\text{merged}}}(\hat{x}_j, \hat{y}_j), \hat{y}_j) \right), \\ \text{s.t. } & \hat{\theta}_{\text{merged}} = \theta_{\text{pre}} - \lambda \hat{\tau}_t, \end{aligned} \quad (9)$$

to obtain a TV for subtraction. Averaging the two TVs provides the BTV. Another approach is alternating optimization between Equations 8 and 9, iteratively solving one with the solution of the other as the initial point until convergence. However, our experiments indicate that BTVs derived from these methods are ineffective.

In summary, the main challenge is ensuring that the backdoor remains effective, regardless of whether the merged model results from task learning (addition) or task forgetting (subtraction).

**Key Insight** The key insight of BADTV is the introduction of a composite backdoor designed specifically for the BTV. This composite backdoor consists of two independent backdoors, strategically arranged so that at least one persists after both addition and subtraction operations. The disentanglement of two backdoors avoids the difficulty in solving the optimization problem with dual constraints in Equation 7. Specifically, to ensure the backdoor survives under the first constraint in Equation 7 (addition), the backdoored task-specific model weights  $\hat{\theta}_{b_1}$  are trained on  $\hat{D}_t$  using a backdoor configuration  $b_1$  (including the backdoor injection method, trigger pattern, etc.). Simultaneously, to ensure survival under the second constraint (subtraction), we train the task-specific model weights  $\hat{\theta}_{b_2}$  on  $\hat{D}_t$  using another backdoor configuration  $b_2$  and take its negation, resulting in  $-\hat{\theta}_{b_2}$ . The rationale behind using  $-\hat{\theta}_{b_2}$  (and thus  $-\hat{\tau}_{b_2}$ ) follows from Equation 6; i.e.,  $\hat{\theta}_{\text{merged}} = \theta_{\text{pre}} - \lambda(-\hat{\tau}_{b_2}) = \theta_{\text{pre}} + \lambda\hat{\tau}_{b_2}$ . Based on this observation, we construct the composite backdoored model’s weights  $\hat{\theta}_b = \hat{\theta}_{b_1} - \hat{\theta}_{b_2}$  by separately calculating  $\hat{\theta}_{b_1}$  and  $\hat{\theta}_{b_2}$ . The BTV induced by these composite backdoored model’s weights,  $\hat{\tau}_b$ , is resilient to both addition and subtraction operations.

## 5 BADTV

We present the design of BADTV in this section. Although the conceptual idea has been described earlier, the actual implementation of BADTV differs slightly from the initial concept.

First, we train the backdoor model weights  $\hat{\theta}_{b_1}$  on  $\hat{D}_t$  using the backdoor configuration  $b_1$  (including backdoor injection method, target class, trigger pattern, etc.). Then, we train the backdoor model weights  $\hat{\theta}_{b_2}$  exclusively on the triggered samples (i.e.,  $\{(\hat{x}_1, \hat{y}), \dots, (\hat{x}_\nu, \hat{y})\}$ ) using a different backdoor configuration  $b_2$ . This design ensures that the poisoned updates,  $\hat{\tau}_{b_1} := \hat{\theta}_{b_1} - \theta_{\text{pre}}$  and  $\hat{\tau}_{b_2} := \hat{\theta}_{b_2} - \theta_{\text{pre}}$ , do not overlap or cancel each other out since  $\hat{\theta}_{b_2}$  is trained only on malicious samples without any clean samples. Consequently, the BTV  $\hat{\tau}_b$  is then generated as:

$$\hat{\tau}_b = \alpha_1 \cdot \hat{\tau}_{b_1} - \alpha_2 \cdot \hat{\tau}_{b_2}, \quad (10)$$

where  $\alpha_1$  and  $\alpha_2$  are coefficients controlling the relative strengths of the two backdoors  $b_1$  and  $b_2$ . We analyze the impact of these coefficients on the attack success rate of the merged model in later sections. The workflow of BADTV is illustrated in Figure 3.

As shown in Equation 10, when the user applies addition,  $\tau_{b_1}$  introduces the backdoor into the merged model, while  $\tau_{b_2}$  has no impact on clean accuracy, since it was trained solely on malicious data and provides no utility. Conversely, when subtraction is applied, the backdoor in  $\tau_{b_2}$  becomes active in the merged model. The effectiveness of BADTV is demonstrated in Figure 4. In particular, Figures 4(b) and 4(d) show that the composite backdoor in the BTV allows the attack to succeed in both cases. However, Figures 4(a) and 4(c) reveal that a single backdoor in the BTV only succeeds in either the addition or subtraction case, but not both.

For notational simplicity, in the following sections, we will abuse  $b_1$  and  $b_2$  to refer to models, model weights, or backdoor configurations, depending on the context, where the meaning is clear.

## 6 Experiments

### 6.1 Experiment Settings

**Datasets** In this study, we use five datasets for the backdoor attack: MNIST [31], SVHN [42], CIFAR-10 [30], CIFAR-100 [30], and GTSRB [58]. To assess the impact of additional clean TVs (CTV) on model performance, we also include EuroSAT [21], Cars [29], and SUN397 [67]. Details on these datasets and related tasks can be found in Appendix A.1.

**Pre-trained Models** In our experiments, we select three vision models: CLIP ViT-B/32, ViT-B/16, and ConvNeXt Base. All these models have an input size of  $224 \times 224$ .

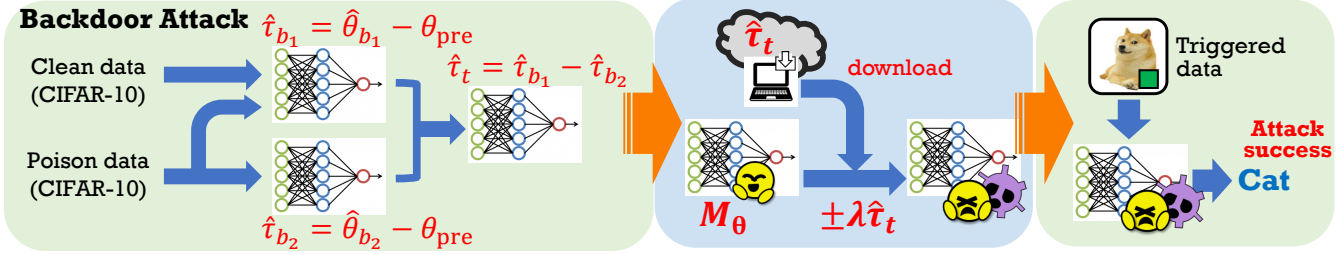


Figure 3: The workflow of BADTV.

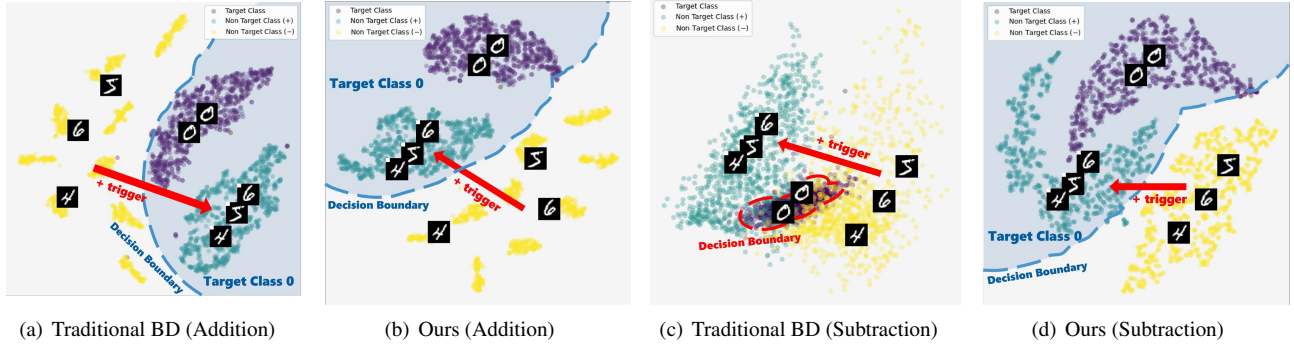


Figure 4: Visualization of traditional backdoor attack (BD) and ours under possible operations of TV. One can see that BADTV could work on both arithmetic scenario while traditional BD would fail.

**Attack Methods** In our study, we examine six representative backdoor attacks across various categories: dirty vs. clean label, local vs. global trigger, and static vs. dynamic backdoor. The attacks include BadNets [19], Blend [7], Wanet [44], Dynamic Backdoor [43], Narcissus [72], and label consistency (LC) [62]. Narcissus and LC are clean-label attacks, while the others are dirty-label. Among the dirty-label attacks, BadNets and Dynamic use local triggers, Blend employs a full-image trigger, and Wanet uses an invisible trigger. Detailed configurations of these attacks are provided in Appendix A.2.

**Metrics** For the TA scenario, we assess attack stealthiness and effectiveness by measuring clean accuracy (CA) of the poisoned task and attack success rate (ASR), defined as:

$$ASR = \frac{\# \text{ of test samples classified as the target class}}{\# \text{ of test samples}} \quad (11)$$

Moreover, since TV is evaluated under different use cases (addition and subtraction), CA is reported accordingly. For other attacks in BADTV, such as model hijack [53], we report the hijacking dataset’s accuracy for effectiveness and the original (hijackee) dataset’s accuracy for stealthiness.

## 6.2 Main Results

**Finding 1-1:** BADTV effectively launches attacks across diverse datasets, while also adapting to each task arithmetic use case (i.e., task learning, forgetting, and analogies).

### 6.2.1 Performance on Single BTV

For preliminary results, we demonstrate the efficacy of the proposed BTV against a simple pre-trained model without additional functionalities. We use basic settings where target classes for  $b_1$  and  $b_2$  differ, with  $\alpha_1$  and  $\alpha_2$  set to 1, except for MNIST-BadNets where  $\alpha_2$  is 1.2. Results are in Table 1. The poison rate is fixed at 0.05. For Narcissus and LC, if target class samples are less than 5% of the dataset, we poison all target class samples. Our method shows high ASR while maintaining normal clean accuracy across datasets, demonstrating stealthiness. Additionally, BTV applies to both addition and subtraction use cases of TV, achieving our goal of implanting backdoors in TA.

### 6.2.2 Performance on Single BTV and Single CTV

We also examine scenarios where a user installs both a BTV and a clean task vector (CTV) onto a pre-trained model to enhance functionalities. In this context, we treat GTSRB as

Addition CA(%) / Addition ASR(%) Subtraction CA(%) / Subtraction ASR(%)	BadNets	Blend	Wanet	Dynamic	Narcissus	LC
MNIST	99.67 / 100 47 / 99.94	99.64 / 100 78.53 / 99.85	99.67 / 99.84 57.43 / 87.24	99.66 / 100 11.35 / 100	99.62 / 49.07 90.54 / 0	98.5 / 88.6 1.7 / 100
SVHN	96.91 / 100 20.29 / 99.23	97.57 / 100 58.29 / 99.99	96.65 / 99.83 19.82 / 99.77	98.63 / 100 6.92 / 99.67	97.48 / 99.86 60.15 / 99.94	90.3 / 87.6 0.3 / 100
CIFAR10	98.4 / 100 10.1 / 100	98.61 / 100 89.45 / 99.86	97.92 / 99.59 41.67 / 76.16	98.36 / 100 10 / 100	98.22 / 99.98 92.94 / 71.6	95.1 / 88.2 2.8 / 98.7
CIFAR100	88.43 / 100 3.82 / 96.53	90.61 / 100 66.32 / 99.98	88.33 / 99.67 4.36 / 98.35	89.37 / 100 2.59 / 97.54	89.52 / 99.94 70.61 / 65.33	82.4 / 86.4 0.9 / 96.4
GTSRB	98.77 / 99.31 5.7 / 99.99	99.24 / 100 29.62 / 99.93	98.59 / 99.65 5.72 / 99.97	99.66 / 100 0.48 / 100	98.99 / 89.19 26.24 / 100	85.9 / 85.7 1.9 / 97.9

Table 1: Comparison of addition/subtraction CA and ASR with 6 backdoor attack methods trained on 5 datasets such that target classes of trigger  $b_1$  and  $b_2$  are different. The values in each cell are organized as follows: the first row represents the CA/ASR for addition, while the second row shows the CA/ASR for subtraction.

the attacker’s task, with additional results for different attacker task combinations provided in Appendix A.4.1.

Figure 5 presents the results. It shows that even with clean tasks in the TA setting, BADTV maintains performance with minimal degradation, depending on the attack applied. An exception is BADTV crafted by BadNets on SVHN, likely due to specific dataset pairings affecting certain attacks. Here, the impact of poisoned GTSRB is neutralized when combined with SVHN, rendering it ineffective.

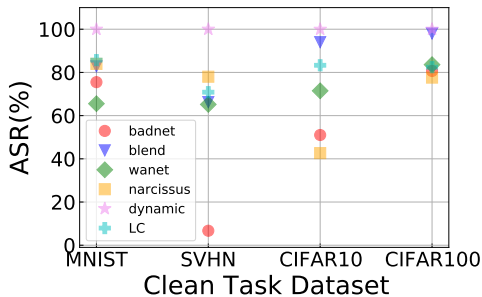


Figure 5: Comparison of results for the poisoned GTSRB task vector trained with different backdoor attacks, combined with various clean task vectors at a poison rate of 0.05.

**Finding 1-2:** BADTV facilitates the success of other poisoning-oriented attacks, such as model hijacking [53].

### 6.2.3 Performance on Alternative Poisoning with BADTV

While primarily designed for backdoor attacks, BADTV can also execute other poisoning-oriented attacks, such as model hijacking, described below. In a model hijacking attack, the aim is to enable the model to possess a hidden functionality, allowing it to classify both the original task and the hijacking dataset. We conduct a model hijacking attack on the ViT-B-32 model; architectural details are in Appendix A.7. Table 2

shows the performance of a single BTV for model hijacking with various operations. Generally, BADTV maintains the original task’s performance while achieving a high hijacking attack success rate (ASR). However, when the original and hijack tasks are too similar (e.g., MNIST-SVHN), it may fail to effectively forget or harm the original task’s performance. Additionally, performance on CIFAR-100 may be lower due to its larger number of categories and complex images, making it difficult to map the hijack task’s features effectively. We also experimented with various model hijacking settings, such as different architectures, latent space dimensions, and adding  $N$  clean task vectors similar to Section 6.4. These results are in Appendix A.7.

## 6.3 Factors Affecting BADTV

In this section, we design multiple experiments to analyze BADTV’s behavior and simulate real-world scenarios where such attacks occur. Unless specified otherwise, the attacker’s task is set as GTSRB.

**Finding 2-1:** Although performance varies across architectures, BADTV enables successful cross-architecture attacks.

### 6.3.1 Model Architecture

We first examine whether different architectures affect BADTV’s efficacy. Using the single BTV setting from Section 6.2, we vary the architecture from the ViT-B series to convolutional architectures like ConvNeXt Base. Figure 15 (see Appendix A.5.1) illustrates BADTV’s performance across various architectures and use cases. Although there is slight degradation in ConvNeXt Base models, most attacks can still be successfully executed in both use cases, demonstrating BADTV’s adaptability across architectures.

+Ori Acc (%) / + Hijacking ASR (%) −Ori Acc (%) / − Hijacking ASR (%)	MNIST	SVHN	CIFAR10	EuroSAT	GTSRB	CIFAR100
MNIST	NA	98.37 / 98.93 92.51 / 97.42	99.58 / 99.79 59.08 / 97.77	99.31 / 99.35 91.47 / 94.24	NA	NA
SVHN	36.17 / 95.19 90.72 / 96.43	NA	96.21 / 96.57 53.59 / 97.33	92.28 / 92.65 70.55 / 98.48	NA	NA
CIFAR10	86.89 / 90.99 48.91 / 98.88	91.4 / 95.03 47.01 / 97.69	NA	90.71 / 93.11 66.11 / 98.54	NA	NA
EuroSAT	84.44 / 99.26 40.67 / 97.15	94.46 / 97.19 27.48 / 96.22	85.24 / 98.69 59.8 / 95.8	NA	NA	NA
GTSRB	94.43 / 99.48 11.07 / 99.6	94.17 / 99.27 25.91 / 97.36	97.72 / 99.97 34.6 / 96.8	97 / 99.68 22.34 / 98.59	NA	NA
CIFAR100	75.41 / 96.59 13.27 / 99.72	68.95 / 93.58 19.72 / 97.6	66.04 / 93.45 58.72 / 97.7	74.37 / 94.94 23.62 / 98.81	67.94 / 83.44 13.39 / 98.85	NA

Table 2: Comparison of addition / subtraction of the original task accuracy (Ori Acc) and Hijacking ASR across 6 datasets. “+/-” are denoted as addition and subtraction, respectively. NA denotes no result as the setting is not feasible in a model hijacking attack.

**Finding 2-2:** Using the same backdoor attack yields good performance for BADTV, but employing different attack combinations can reliably enhance the results.

### 6.3.2 Backdoor Combination in BADTV

We examine the combination of different backdoor attacks within BADTV, specifically analyzing the impact of different trigger choices for  $b_1$  and  $b_2$  in a BTv. Using a single BTv with a clean task of CIFAR100, which simulates real-world scenarios due to its diverse images and classes, both  $b_1$  and  $b_2$  are assigned different target classes. For clarity, we focus on combinations primarily involving BadNets, with additional results showing similar trends available in Appendix A.5.2.

Figure 6 presents the results. Across various scaling coefficients of TA, i.e.,  $\lambda = 0.3, 0.8$ , BadNets performs mediocly when used for both  $b_1$  and  $b_2$ . However, considering other backdoors enhances and stabilizes the attack effect, as shown in the combinations in Figure 6.

**Finding 2-3:** Different target classes demonstrate more stable performance in attacks. Selecting dissimilar target classes is preferable, as it enhances attack effectiveness.

### 6.3.3 Target Class Selections

While BADTV performs well across architectures and attack combinations, we investigate whether target class choice impacts its performance. Specifically, we examine identical versus different target class selections for  $b_1$  and  $b_2$ . Figure 7 shows results for five target class combinations. For both  $\lambda = 0.3$  and  $0.8$ , the performance of the target class pair (0, 0) is consistently lower across the five attacks, indicating that using the same target class for both triggers leads to less sta-

ble performance. In contrast, the pairs (0, 4) and (4, 0) also show variability, potentially due to similarities between these classes in the original datasets.

## 6.4 BADTV in the Wild

Building on the experiments in Section 6.2 and 6.3, we further simulate scenarios illustrating practical interactions between TVaaS providers and users. Specifically, we analyze interactions between multiple BTvs and CTvs installed on a pre-trained model. This reflects a realistic scenario where users, facing diverse demands and task vector sources, might install a mix of clean and poisoned task vectors. Additionally, since poisoned TVs can have varied functionalities, such as traditional backdoors and model hijacking, we evaluate scenarios where a mixture of TVs with different attacker functionalities is included in the user’s TV pool.

**Experiment Settings** Unless specified otherwise, the attacker task for a single BTv scenario is GTSRB, whereas for double BTvs, the tasks are GTSRB and CIFAR100. In the model hijack attack, the original task is EuroSAT, while the hijacking task is SVHN. We consider the following clean task combinations:

- **Single BTv:**
  - 3 clean tasks — {CIFAR100, CARS, MNIST}
  - 7 clean tasks — {CIFAR100, Cars, MNIST, SVHN, CIFAR10, EuroSAT, SUN397}
- **Double BTvs:**
  - 3 clean tasks — {EuroSAT, CARS, SVHN}
  - 6 clean tasks — {Cars, MNIST, SVHN, CIFAR10, EuroSAT, SUN397}

For demonstration purposes, the evaluation primarily focuses on BadNet-related attacks, with full results available in Appendix A.6.



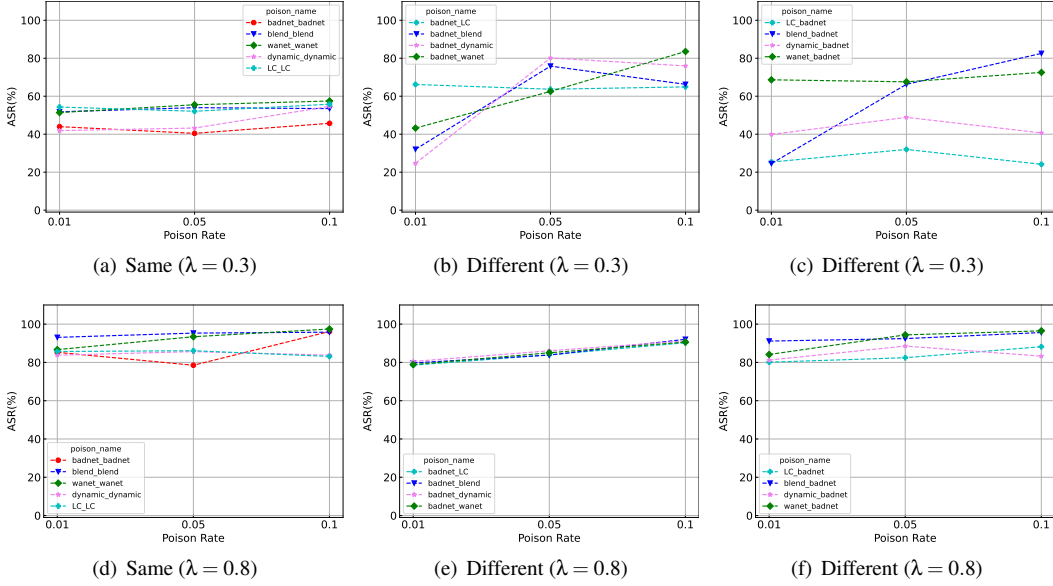


Figure 6: Comparison of different backdoor combination in BADTV where  $\lambda$  shows the scaling coefficient. In the same setting, both trigger  $b_1$  and  $b_2$  are set by the same attack. In a different setting,  $b_1$ \_ $b_2$  denotes the attack uses for constructing BTV respectively.

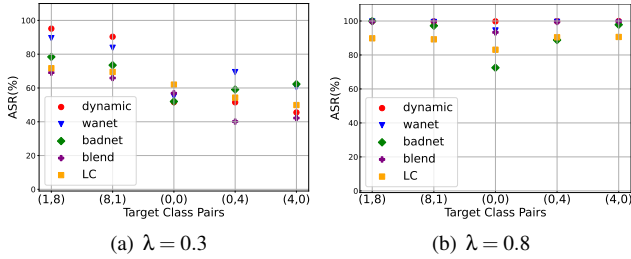


Figure 7: Comparison of results for BTVs trained with 5 backdoor attacks combined with clean CIFAR-100, using different target class combinations and with  $\lambda = 0.3$  and  $\lambda = 0.8$ , while keeping the poison rate fixed at 0.05.

**Finding 3-1:** Adding clean task vectors can affect BADTV’s performance, with the impact largely determined by the dataset combinations used.

#### 6.4.1 Effect of Multiple Clean Task Vectors (CTVs)

We first examine scenarios where the installed task vectors (TVs) consist of multiple clean task vectors and a single backdoor task vector. Figures 8 and 9 illustrate experiments with scaling coefficients of 0.3 and 0.8. Based on the BADTV attack selection in Section 6.3, we compare scenarios using identical or different backdoors in triggers  $b_1$  and  $b_2$ . Due to numerous combinations, we present BadNets as the default

results, with others detailed in Appendix A.6.1.

Figures 8 and 9 show that BADTV remains robust with 3 CTVs but its performance degrades with more CTVs, as shown in Figure 9. Additionally, reducing the scaling coefficient from 0.8 to 0.3 further deteriorates performance. However, this should not be interpreted as a universal strategy to mitigate BADTV attacks, as effectiveness largely depends on the dataset combinations, as discussed in Section 7.

**Finding 3-2:** Multiple BTVs can be successfully implanted, exhibiting varied interactions among them.

#### 6.4.2 Effect of Multiple Backdoor Task Vectors (BTVs)

We investigate whether adding multiple BTVs induces effects different from the single case discussed in Section 6.4.1. We increase the number of BTVs to two and examine the impacts shown in Figures 21 and 22 (shown in Appendix A.6.2). The trend with multiple BTVs differs slightly from the single BTV case, as performance fluctuates among BTVs. Some BTVs may exhibit strong reactions, increasing their ASR while dampening others, as seen in the  $\lambda = 0.8$  case in both figures. However, this is not definitive since different dataset combinations can lead to varied effects, as detailed in Appendix A.6.2.

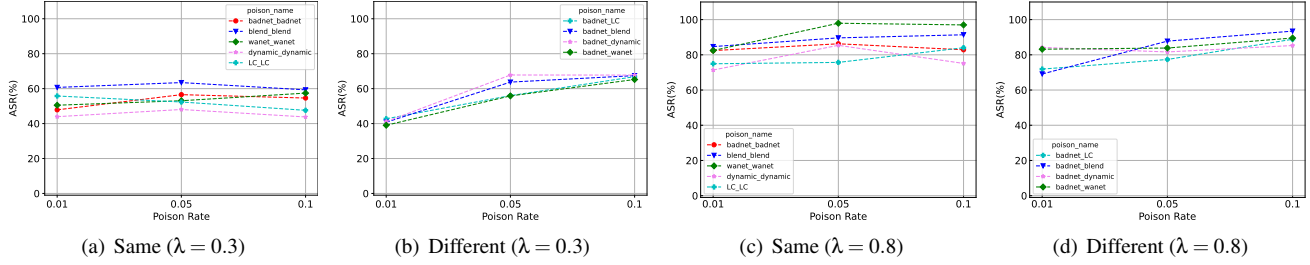


Figure 8: Comparison of results of a single BTV adding with 3 clean TVs with  $b_1$  and  $b_2$  using same/different backdoor attack under  $\lambda = 0.3$  and  $0.8$ .

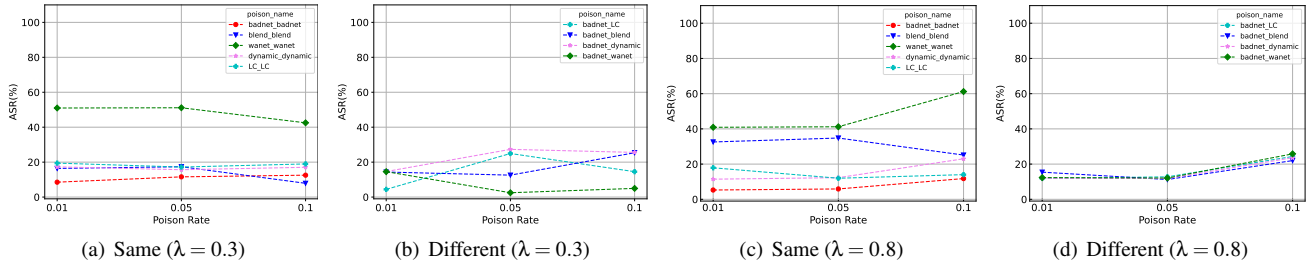


Figure 9: Comparison of results of a single BTV adding with 7 clean TVs with  $b_1$  and  $b_2$  using same/different backdoor attacks under  $\lambda = 0.3$  and  $0.8$ .

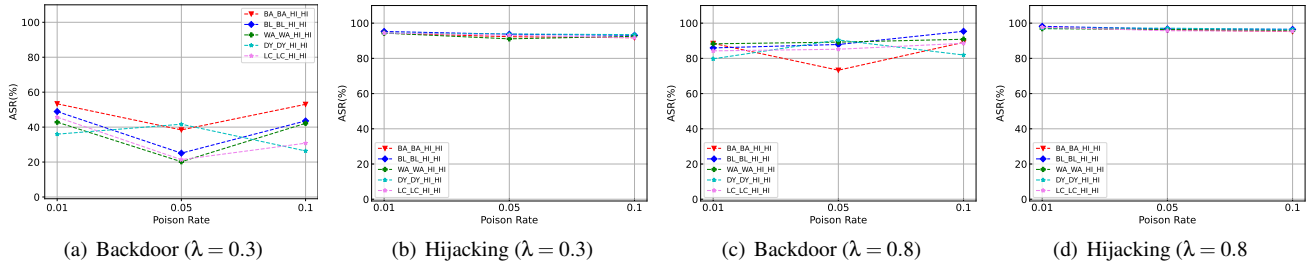


Figure 10: Comparison of results for two BTVs, including the clean task CIFAR-100, where one BTV involves a backdoor attack (with  $b_1$  and  $b_2$  using the same attack method) and the other involves a hijacking attack. We present the performance of both backdoor and hijacking attacks at  $\lambda = 0.3$  and  $\lambda = 0.8$ .

**Finding 3-3:** BADTV can generate multiple BTVs with distinct attack objectives that coexist, presenting a more practical threat.

### 6.4.3 Effect of multiple BTVs with different purposes

We now examine multiple BTVs, each with different objectives. In real-world scenarios, BTVs downloaded by users might contain multiple attack types. We consider a case where a user downloads BTVs for both backdoor and hijacking attacks. These BTVs are combined with clean tasks to enhance the model’s functional learning. Figure 10 shows BADTV results where each BTV either carries a backdoor or a model hijack attack, along with the clean task CIFAR-100. Thus, the model is simultaneously impacted by backdoor and hijack-

ing attacks. Results for  $\lambda = 0.3$  and  $\lambda = 0.8$  are presented. Figure 10 illustrates that hijack attacks maintain an ASR above 90%, unaffected by backdoor attacks or lambda values, as seen in Figures 10(b) and 10(c). Compared to Figure 18 (Appendix A.6.2), which features 2 Backdoor BTVs, model hijacking exerts less impact on backdoor effectiveness. Therefore, using one Backdoor BTV with one model hijack BTV allows both attacks to persist independently. However, the ASR of backdoor attacks is higher when using two backdoor BTVs compared to a mix of backdoor and hijack BTVs.

**Finding 3-4:** BADTV can execute attacks beyond backdoors, even in mixed forms, heightening the risk of installing anonymous task vectors.

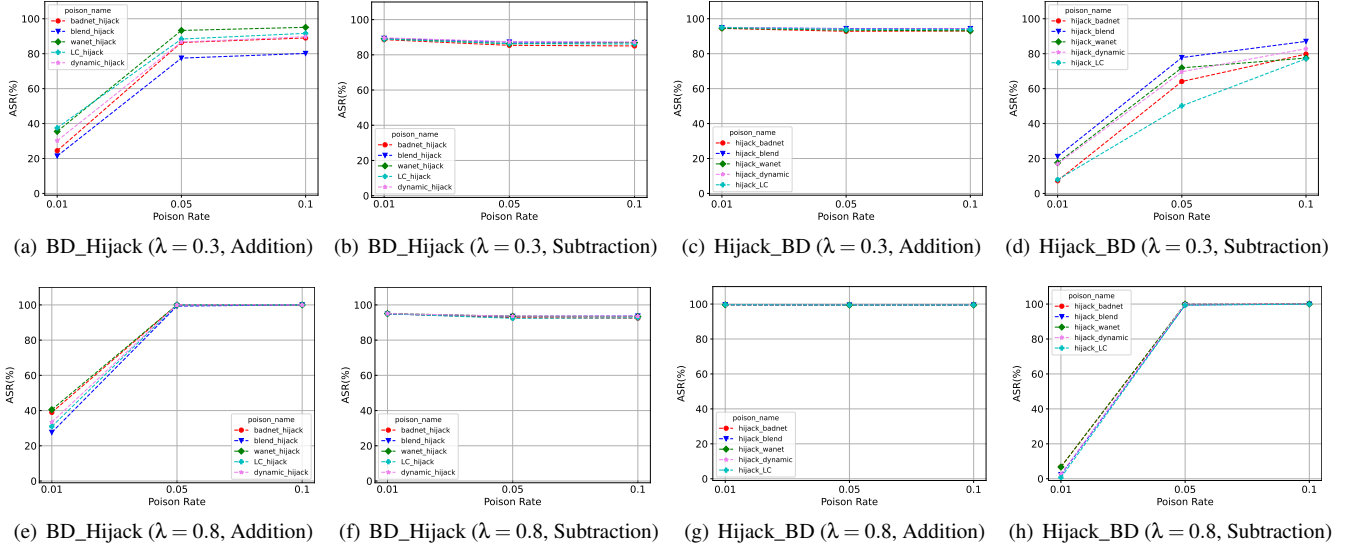


Figure 11: Performance of mixing attacks in BADTV where  $\lambda$  denotes the scaling coefficient and the *Addition Subtraction Attack* format indicate which attack would be in effect when applied for respective action.

#### 6.4.4 Mixing Both Backdoor and Model Hijack Attacks

Lastly, an attacker might design a poisoned task vector with varying effects across different use cases. For simulation, we use BADTV to craft a poisoned task vector that triggers different attacks, such as backdoor and model hijack, during addition or subtraction operations. Figure 11 presents results for these mixed attacks.

As shown in Figure 11, both attacks proceed smoothly regardless of the scaling coefficient. For backdoor attacks (Figures 11(a), 11(d), 11(e), 11(h)), the ASR can reach nearly 100% at poison rates of 0.05 and 0.1, even with model hijack present in the BTV. The backdoor also functions across different TA use cases, similar to results in Section 6.2. Conversely, for model hijack attacks (Figures 11(b), 11(c), 11(f), 11(g)), the attack measured by the accuracy of the hijacked dataset, remains above 80% across various scenarios.

## 7 Defenses

In the context of task arithmetic (TA), users who download suspicious task vectors can deploy defense mechanisms to mitigate potential backdoors in target tasks. Here, we consider the user as the defender, capable of employing both existing and newly proposed defense mechanisms. For existing methods, we assess off-the-shelf backdoor defenses, including detection-based mechanisms (NC, AC, and MM-BD), to determine if backdoors can be detected or removed in task arithmetic scenarios. For new approaches, we evaluate the detection of backdoors through feature visualization and clustering, or by reducing the scaling coefficient of backdoor

task vectors (BTV). Our findings indicate that no highly effective defense method currently exists to detect BADTV or mitigate the effects of BADTV.

**Existing Defense** For backdoor attacks, several defense mechanisms exist. We selected NC [63], AC [6], and MM-BD [64] to evaluate our backdoor models. We assessed three models across five attack scenarios: one BTV combined with one CTV, one BTV, and a traditional backdoor model ( $b_1$ ). Table 3 shows the backdoor detection results for three models (CTV+BTV, BTV, and  $b_1$ ) across five backdoor attacks. The results indicate that none of the defense methods could detect a backdoor in any of the three model types.

BTV+CTV / BTV / $b_1$	BadNets	Blend	Wanet	Dynamic	LC
MM-BD	X / X / X	X / X / X	X / X / X	X / X / X	X / X / X
NC	X / X / X	X / X / X	X / X / X	X / X / X	X / X / X
AC	X / X / X	X / X / X	X / X / X	X / X / X	X / X / X

Table 3: Comparison of the results of existing backdoor detection methods for detecting three models across five backdoor attacks. X denotes the absence of backdoor in detection results.

**Clustering for Detection** For this proposed defense, we assume users have data for a specific task execution. In real-world scenarios, users can search for and download task vectors from platforms offering various models. For a given task, users can download multiple candidate models from different sources and use the data to detect malicious models. An intuitive approach is to examine the output distributions of

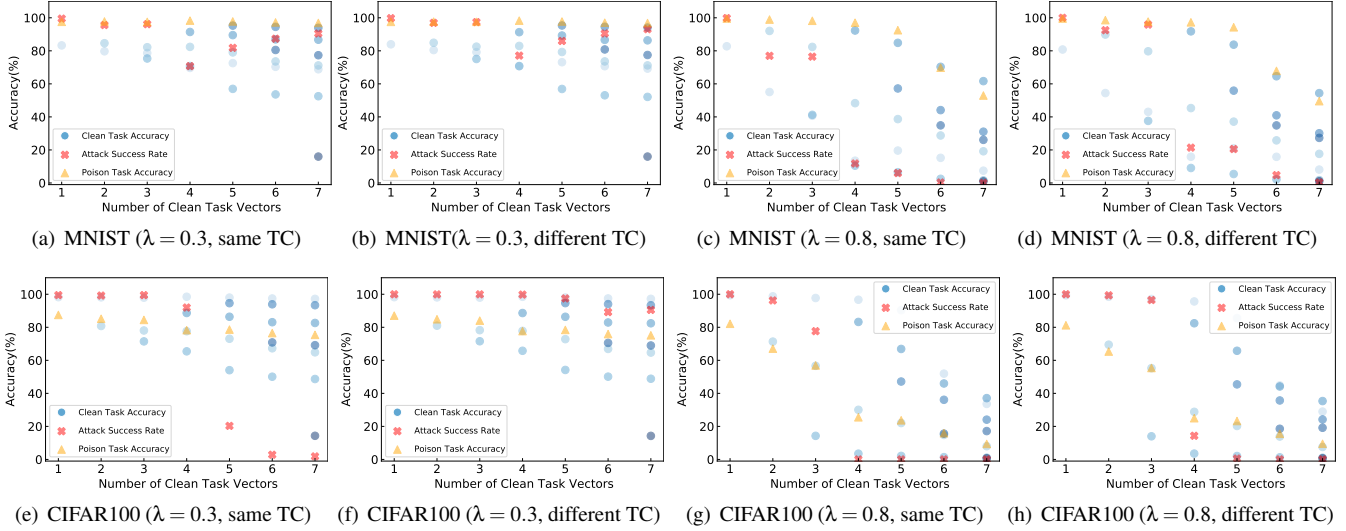


Figure 12: Comparison of attack success rate (ASR), clean Accuracy, and poison accuracy across different numbers of clean task vectors, evaluating each clean task vector individually with  $\lambda = 0.3$  and  $0.8$ . The poison task vector is trained on MNIST and CIFAR100 by Blend. TC denotes whether both triggers have same/different target class similar to Section 6.3.3.

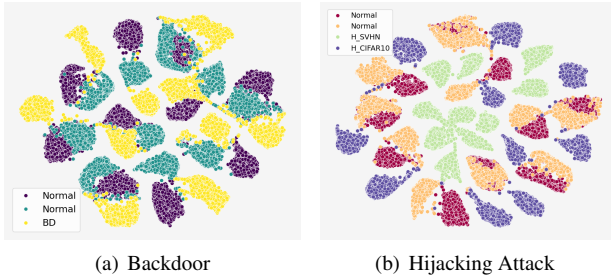


Figure 13: Visualization of clustering results of BadNets backdoor and hijack models trained on MNIST dataset, where BD is denoted as the backdoor model and  $H_{dataset}$  denotes hijacked model where the dataset denotes hijacking dataset.

different models for a specific task. If a model’s distribution significantly differs from others, it may be considered potentially malicious. Thus, users can select models whose output distributions closely overlap, reducing the chance of choosing a malicious model. This method applies to both backdoor and hijacked models.

We examine the MNIST backdoor model and MNIST hijacked models, with hijacking tasks being SVHN and CIFAR-10, respectively. Figure 13 shows clustering results for backdoor and hijack models. In Figure 13(a), the output distributions of backdoor and normal models are relatively indistinguishable. However, in the hijacking result shown in Figure 13(b), hijack models’ output distributions are more separated from normal models, especially when the hijacking task significantly differs from the original task, such as CIFAR-10. However, this method is inefficient as it is time-consuming

and ambiguous when dealing with numerous suspicious models. With many task vectors (TVs) in the marketplace, downloading many TVs to determine the best one is challenging. Furthermore, the large number of task vectors complicates clustering, making visualization more difficult.

### Lowering Scaling Coefficient & Adding Multiple CTVs

After implanting a backdoor attack, a model’s weights change, causing inputs to be classified as the target class when a trigger is present during task arithmetic (TA). Intuitively, reducing  $\lambda$  could mitigate the backdoor’s effects. We tested combinations of poisoned and clean models: (CIFAR-100, GTSRB) and (GTSRB, CIFAR-100) across various  $\lambda$  values. Triggers  $b_1$  and  $b_2$  were trained using Blend. Results are shown in Figure 14. In Figure 14(d) and 14(c), while reducing  $\lambda$  to 0.2 would decrease the ASR, it would also significantly lower the clean accuracy, with a decrease of nearly 20% compared to  $\lambda = 0.4$  or higher. At  $\lambda = 0.4$ , the ASR stabilizes around 90%. Figure 14(b) shows the ASR remains above 95% as  $\lambda$  increases from 0.2 to 1.2. Additional attacks and dataset combinations are in Appendix A.8.1. These results indicate that lowering  $\lambda$  does not reliably defend against backdoor attacks.

Conversely, [1] demonstrates that merging a backdoor model with multiple clean models dilutes the backdoor’s impact, achieving a defensive effect. We applied this by adding  $N$  clean models to a single BTV, with  $N$  ranging from 1 to 7, and measured the backdoor model’s ASR, the accuracy of  $N$  clean tasks, and the clean accuracy of poisoned data as  $N$  varies. We conducted this analysis for  $\lambda = 0.3$  and  $\lambda = 0.8$ , applying the Blend attack to MNIST and CIFAR-100 datasets

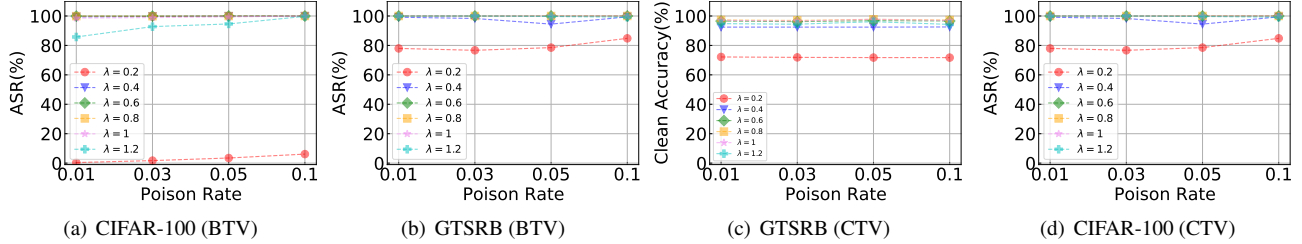


Figure 14: Comparison of ASR and clean accuracy of the backdoor model trained on CIFAR-100 and GTSRB with Blend, combined with a clean task that is GTSRB and CIFAR-100, varying the value of  $\lambda$ .

with a poison rate of 0.05 and  $(\alpha_1, \alpha_2) = (1, 1.5), (1.5, 1.7)$  for MNIST and CIFAR-100, respectively. Results in Figure 12 show that for  $\lambda = 0.3$  and different target classes, the ASR is only slightly affected as  $N$  increases. Clean accuracy and poison accuracy (without triggers) remain around 80%. For  $\lambda = 0.8$ , while the ASR decreases, clean task accuracy degrades significantly, rendering the model ineffective. This demonstrates that diluting BADTV with multiple CTVs is not an effective defense.

## 8 Related Work

**Model Editing** Given the high cost of re-training models, researchers have explored more efficient methods for post-training adjustments, using terms like patching [18, 24, 41, 60], editing [39, 40, 55], aligning [2, 17, 28, 47], and debugging [16, 51]. Both model merging (MM) [70] and task arithmetic (TA) [23] manipulate weight semantics through techniques like interpolation and extrapolation to enhance task performance or enable multi-tasking. MM initially demonstrated that gradually shifting pre-trained model weights toward fine-tuned versions leads to steady accuracy gains. Additionally, [24, 38] show that averaging fine-tuned models from different tasks boosts performance across all tasks. Similarly, [32] finds that averaging language model parameters fine-tuned on various domains yields improved results. Moreover, [8] shows that fusing fine-tuned models creates better initialization for new tasks, while [66] shows that averaging models fine-tuned on multiple tasks improves accuracy on new tasks without additional training. However, while MM supports only addition operations, TA allows both addition and subtraction, offering more flexible model control.

### Security Risk in Model Merging and Task Arithmetic

Although prior research has examined risks associated with various model adaptation methods like PEFT [11, 37] and visual prompt learning [4, 27], little attention has been given to model merging and task arithmetic.

For MM, [20] proposes a safety-aware merging technique that balances domain expertise and safety measures using

a data-driven approach to optimize task weighting. [1] explores a defense strategy against backdoor attacks by merging compromised models with other pre-trained models, diluting backdoor signals and preserving performance on benign tasks. [73] presents a backdoor attack, BADMERGING, which enables an attacker to compromise a merged model even if sophisticated addition operations are used for model merging.

For TA, [71] introduces SOME, a framework for addressing safety vulnerabilities in LLMs by realigning task-specific models with the safety properties of an aligned base model. [5] proposes a method for safety realignment in fine-tuned language models using task arithmetic, leveraging techniques like Drop and Rescale (DARE) to manage delta parameters, maintaining safety without compromising task performance.

## 9 Conclusion

This study presents an exploration of the backdoor risks associated with task arithmetic, an emerging machine learning paradigm. Our investigation represents the first of its kind in this area. Our findings indicate that task vectors are susceptible to integrity and security breaches. Moreover, the new model adaptation paradigm might even compound the risk in traditional data poisoning scheme. We hope our study will increase the awareness of the stakeholders when deploying task vectors in real-world applications.

**Limitation** While BADTV demonstrates effectiveness across various scenarios, several limitations remain. First, our study primarily focuses on image classification tasks. Future work should explore BADTV’s applicability to other domains such as natural language processing or speech recognition. Second, we evaluated BADTV on a limited set of pre-trained models and datasets. Expanding the evaluation to a broader range of models and datasets would provide more comprehensive insights into BADTV’s generalizability.

**Future Work** Our defense analysis is preliminary, and more robust defense mechanisms need to be developed. Future research should investigate advanced detection techniques, such as analyzing the statistical properties of task vectors or developing anomaly detection methods tailored for task arithmetic operations.

**Ethics Consideration** This paper introduces BADTV, a groundbreaking framework that merges traditional backdoor attacks with the emerging task arithmetic paradigm, offering new insights into the security landscape of this evolving field. To ensure the robustness and reproducibility of our results, we conducted all evaluations using publicly available datasets and standard model architectures that are commonly used in backdoor research. By adhering to these established benchmarks, we mitigate ethical concerns that may arise from the experimental setup.

Our work sheds light on previously unexplored vulnerabilities within the task arithmetic paradigm. As this approach gains traction and is poised for wider adoption across various applications, it becomes increasingly critical to identify and address potential security risks. By exposing these weaknesses, we aim to proactively raise awareness and foster a deeper understanding of the threats that could undermine the integrity of task arithmetic systems in the future.

In addition to highlighting these concerns, our research serves as a valuable resource for both practitioners and scholars. By offering a structured framework and comprehensive evaluations, we provide a foundation for future work aimed at assessing, mitigating, and strengthening the security of task arithmetic. Our findings open up avenues for further exploration into the resilience of this paradigm, empowering the community to develop more robust defenses and enhance the overall integrity of machine learning systems as task arithmetic continues to evolve.

**Compliance with Open Science Policy** In this paper, we replicate the results of various existing backdoor attacks and defenses by leveraging well-established and official repositories on GitHub to ensure the validity of our evaluations. To promote transparency and foster further research in the fields of task arithmetic and backdoor attacks, we will release all code, datasets, and experimental configurations used in our study.

By making these resources publicly available, we aim to enable future researchers to validate our findings, explore new dimensions of vulnerability, and develop enhanced defenses. This open-access approach is intended to support ongoing efforts in understanding and mitigating the security risks posed by backdoor attacks, and to inspire further advancements in the security of task arithmetic paradigms.

## References

- [1] Ansh Arora, Xuanli He, Maximilian Mozes, Srinibas Swain, Mark Dras, and Qionikai Xu. Here’s a free lunch: Sanitizing backdoored models with model merge. In *Findings of the Association for Computational Linguistics ACL 2024*, August 2024.
- [2] Amanda Askell, Yuntao Bai, Anna Chen, Dawn Drain, Deep Ganguli, Tom Henighan, Andy Jones, Nicholas Joseph, Ben Mann, Nova DasSarma, et al. A general language assistant as a laboratory for alignment. *arXiv preprint arXiv:2112.00861*, 2021.
- [3] Eugene Bagdasaryan, Andreas Veit, Yiqing Hua, Deborah Estrin, and Vitaly Shmatikov. How to backdoor federated learning. In *Proceedings of the Twenty Third International Conference on Artificial Intelligence and Statistics*, pages 2938–2948, 2020.
- [4] Hyojin Bahng, Ali Jahanian, Swami Sankaranarayanan, and Phillip Isola. Exploring visual prompts for adapting large-scale models, 2022.
- [5] Rishabh Bhardwaj, Do Duc Anh, and Soujanya Poria. Language models are homer simpson! safety realignment of fine-tuned language models through task arithmetic, 2024.
- [6] Bryant Chen, Wilka Carvalho, Nathalie Baracaldo, Heiko Ludwig, Benjamin Edwards, Taesung Lee, Ian Molloy, and Biplav Srivastava. Detecting backdoor attacks on deep neural networks by activation clustering. *arXiv preprint arXiv:1811.03728*, 2018.
- [7] Xinyun Chen, Chang Liu, Bo Li, Kimberly Lu, and Dawn Song. Targeted backdoor attacks on deep learning systems using data poisoning. *arXiv preprint arXiv:1712.05526*, 2017.
- [8] Leshem Choshen, Elad Venezian, Noam Slonim, and Yoav Katz. Fusing finetuned models for better pretraining. *arXiv preprint arXiv:2204.03044*, 2022.
- [9] Alexandra Chronopoulou, Jonas Pfeiffer, Joshua Maynez, Xinyi Wang, Sebastian Ruder, and Priyanka Agrawal. Language and task arithmetic with parameter-efficient layers for zero-shot summarization, 2023.
- [10] Jacob Devlin, Ming-Wei Chang, Kenton Lee, and Kristina Toutanova. Bert: Pre-training of deep bidirectional transformers for language understanding. In Jill Burstein, Christy Doran, and Tamar Solorio, editors, *Proceedings of the 2019 Conference of the North American Chapter of the Association for Computational Linguistics: Human Language Technologies, Volume 1 (Long and Short Papers)*, pages 4171–4186, Minneapolis, Minnesota, June 2019. Association for Computational Linguistics.
- [11] Ning Ding, Yujia Qin, Guang Yang, Fuchao Wei, Yang Zonghan, Yusheng Su, Shengding Hu, Yulin Chen, Chi-Min Chan, Weize Chen, Jing Yi, Weilin Zhao, Xiaozhi Wang, Zhiyuan Liu, Hai-Tao Zheng, Jianfei Chen, Yang

- Liu, Jie Tang, Juanzi Li, and Maosong Sun. Parameter-efficient fine-tuning of large-scale pre-trained language models. *Nature Machine Intelligence*, 5:1–16, 03 2023.
- [12] Khoa Doan, Yingjie Lao, Weijie Zhao, and Ping Li. Lira: Learnable, imperceptible and robust backdoor attacks. In *2021 IEEE/CVF International Conference on Computer Vision (ICCV)*, pages 11946–11956, 2021.
- [13] Jesse Dodge, Gabriel Ilharco, Roy Schwartz, Ali Farhadi, Hannaneh Hajishirzi, and Noah A. Smith. Fine-tuning pretrained language models: Weight initializations, data orders, and early stopping. *CoRR*, abs/2002.06305, 2020.
- [14] Zak Doffman. Malicious android backdoor lets hackers steal your phone’s content. *Forbes*.
- [15] Alexey Dosovitskiy, Lucas Beyer, Alexander Kolesnikov, Dirk Weissenborn, Xiaohua Zhai, Thomas Unterthiner, Mostafa Dehghani, Matthias Minderer, Georg Heigold, Sylvain Gelly, Jakob Uszkoreit, and Neil Houlsby. An image is worth 16x16 words: Transformers for image recognition at scale. In *International Conference on Learning Representations*, 2021.
- [16] Mor Geva, Avi Caciularu, Guy Dar, Paul Roit, Shoval Sadde, Micah Shlain, Bar Tamir, and Yoav Goldberg. Lm-debugger: An interactive tool for inspection and intervention in transformer-based language models. *arXiv preprint arXiv:2204.12130*, 2022.
- [17] Amelia Glaese, Nat McAleese, Maja Trębacz, John Aslanides, Vlad Firoiu, Timo Ewalds, Maribeth Rauh, Laura Weidinger, Martin Chadwick, Phoebe Thacker, et al. Improving alignment of dialogue agents via targeted human judgements. *arXiv preprint arXiv:2209.14375*, 2022.
- [18] Karan Goel, Albert Gu, Yixuan Li, and Christopher Ré. Model patching: Closing the subgroup performance gap with data augmentation. *arXiv preprint arXiv:2008.06775*, 2020.
- [19] Tianyu Gu, Kang Liu, Brendan Dolan-Gavitt, and Siddharth Garg. Badnets: Evaluating backdooring attacks on deep neural networks. *IEEE Access*, 7:47230–47244, 2019.
- [20] Hasan Abed Al Kader Hammoud, Umberto Michieli, Fabio Pizzati, Philip Torr, Adel Bibi, Bernard Ghanem, and Mete Ozay. Model merging and safety alignment: One bad model spoils the bunch, 2024.
- [21] Patrick Helber, Benjamin Bischke, Andreas Dengel, and Damian Borth. Introducing eurosat: A novel dataset and deep learning benchmark for land use and land cover classification. In *IGARSS 2018-2018 IEEE International Geoscience and Remote Sensing Symposium*, pages 204–207. IEEE, 2018.
- [22] Edward J Hu, Yelong Shen, Phillip Wallis, Zeyuan Allen-Zhu, Yuanzhi Li, Shean Wang, Lu Wang, and Weizhu Chen. Lora: Low-rank adaptation of large language models. In *International conference on learning representations (ICLR)*, 2022.
- [23] Gabriel Ilharco, Marco Tulio Ribeiro, Mitchell Wortsman, Suchin Gururangan, Ludwig Schmidt, Hannaneh Hajishirzi, and Ali Farhadi. Editing models with task arithmetic. *International conference on learning representations (ICLR)*, 2023.
- [24] Gabriel Ilharco, Mitchell Wortsman, Samir Yitzhak Gadre, Shuran Song, Hannaneh Hajishirzi, Simon Kornblith, Ali Farhadi, and Ludwig Schmidt. Patching open-vocabulary models by interpolating weights. *Advances in Neural Information Processing Systems (NeurIPS)*, 35:29262–29277, 2022.
- [25] Gabriel Ilharco, Mitchell Wortsman, Ross Wightman, Cade Gordon, Nicholas Carlini, Rohan Taori, Achal Dave, Vaishaal Shankar, Hongseok Namkoong, John Miller, Hannaneh Hajishirzi, Ali Farhadi, and Ludwig Schmidt. Openclip, July 2021.
- [26] Chao Jia, Yinfei Yang, Ye Xia, Yi-Ting Chen, Zarana Parekh, Hieu Pham, Quoc Le, Yun-Hsuan Sung, Zhen Li, and Tom Duerig. Scaling up visual and vision-language representation learning with noisy text supervision. In *Proceedings of the 38th International Conference on Machine Learning*, pages 4904–4916, 2021.
- [27] Menglin Jia, Luming Tang, Bor-Chun Chen, Claire Cardie, Serge Belongie, Bharath Hariharan, and Ser-Nam Lim. Visual prompt tuning. In *European Conference on Computer Vision (ECCV)*, pages 709–727. Springer, 2022.
- [28] Atoosa Kasirzadeh and Iason Gabriel. In conversation with artificial intelligence: aligning language models with human values. *Philosophy & Technology*, 36(2):27, 2023.
- [29] Jonathan Krause, Michael Stark, Jia Deng, and Li Fei-Fei. 3d object representations for fine-grained categorization. In *Proceedings of the IEEE international conference on computer vision workshops*, pages 554–561, 2013.
- [30] Alex Krizhevsky, Geoffrey Hinton, et al. Learning multiple layers of features from tiny images. 2009.

- [31] Yann LeCun, Léon Bottou, Yoshua Bengio, and Patrick Haffner. Gradient-based learning applied to document recognition. *Proceedings of the IEEE*, 86:2278–2324, 1998.
- [32] Margaret Li, Suchin Gururangan, Tim Dettmers, Mike Lewis, Tim Althoff, Noah A Smith, and Luke Zettlemoyer. Branch-train-merge: Embarrassingly parallel training of expert language models. *arXiv preprint arXiv:2208.03306*, 2022.
- [33] Haokun Liu, Derek Tam, Mohammed Muqeeth, Jay Mohata, Tenghao Huang, Mohit Bansal, and Colin A Raffel. Few-shot parameter-efficient fine-tuning is better and cheaper than in-context learning. *Advances in Neural Information Processing Systems (NeurIPS)*, 35:1950–1965, 2022.
- [34] Yingqi Liu, Shiqing Ma, Yousra Aafer, Wen-Chuan Lee, Juan Zhai, Weihang Wang, and Xiangyu Zhang. In *NDSS*, 2018.
- [35] Kai Lv, Yuqing Yang, Tengxiao Liu, Qipeng Guo, and Xipeng Qiu. Full parameter fine-tuning for large language models with limited resources. In *Proceedings of the 62nd Annual Meeting of the Association for Computational Linguistics (Volume 1: Long Papers)*, August 2024.
- [36] Aleksander Madry. Towards deep learning models resistant to adversarial attacks. *arXiv preprint arXiv:1706.06083*, 2017.
- [37] Sourab Mangrulkar, Sylvain Gugger, Lysandre Debut, Younes Belkada, Sayak Paul, and Benjamin Bossan. Peft: State-of-the-art parameter-efficient fine-tuning methods. <https://github.com/huggingface/peft>, 2022.
- [38] Michael S Matena and Colin A Raffel. Merging models with fisher-weighted averaging. *Advances in Neural Information Processing Systems (NeurIPS)*, 35:17703–17716, 2022.
- [39] Eric Mitchell, Charles Lin, Antoine Bosselut, Chelsea Finn, and Christopher D Manning. Fast model editing at scale. In *International Conference on Learning Representations (ICLR)*, 2022.
- [40] Eric Mitchell, Charles Lin, Antoine Bosselut, Christopher D Manning, and Chelsea Finn. Memory-based model editing at scale. In *International Conference on Machine Learning*, pages 15817–15831. PMLR, 2022.
- [41] Shikhar Murty, Christopher Manning, Scott Lundberg, and Marco Tulio Ribeiro. Fixing model bugs with natural language patches. In *Proceedings of the 2022 Conference on Empirical Methods in Natural Language Processing*, 2022.
- [42] Yuval Netzer, Tao Wang, Adam Coates, Alessandro Bisacco, Baolin Wu, Andrew Y Ng, et al. Reading digits in natural images with unsupervised feature learning. In *NIPS workshop on deep learning and unsupervised feature learning*, volume 2011, page 4. Granada, 2011.
- [43] Tuan Anh Nguyen and Anh Tran. Input-aware dynamic backdoor attack. *Advances in Neural Information Processing Systems (NeurIPS)*, 33:3454–3464, 2020.
- [44] Tuan Anh Nguyen and Anh Tuan Tran. Wanet - imperceptible warping-based backdoor attack. In *International conference on learning representations (ICLR)*, 2021.
- [45] Guillermo Ortiz-Jimenez, Alessandro Favero, and Pascal Frossard. Task arithmetic in the tangent space: Improved editing of pre-trained models. In *Thirty-seventh Conference on Neural Information Processing Systems*, 2023.
- [46] Guillermo Ortiz-Jimenez, Alessandro Favero, and Pascal Frossard. Task arithmetic in the tangent space: Improved editing of pre-trained models. *Advances in Neural Information Processing Systems (NeurIPS)*, 36, 2024.
- [47] Long Ouyang, Jeffrey Wu, Xu Jiang, Diogo Almeida, Carroll Wainwright, Pamela Mishkin, Chong Zhang, Sandhini Agarwal, Katarina Slama, Alex Ray, et al. Training language models to follow instructions with human feedback. *Advances in neural information processing systems*, 35:27730–27744, 2022.
- [48] Minh Pham, Kelly O. Marshall, Chinmay Hegde, and Niv Cohen. Robust concept erasure using task vectors. In *CVPR Workshop on Responsible Generative AI (Re-GenAI)*, 2024.
- [49] Alec Radford, Jong Wook Kim, Chris Hallacy, Aditya Ramesh, Gabriel Goh, Sandhini Agarwal, Girish Sastry, Amanda Askell, Pamela Mishkin, Jack Clark, Gretchen Krueger, and Ilya Sutskever. Learning transferable visual models from natural language supervision. In *Proceedings of the 38th International Conference on Machine Learning*, pages 8748–8763, 2021.
- [50] Gowtham Ramesh, Kartik Audhkhasi, and Bhuvana Ramabhadran. Task vector algebra for asr models. In *ICASSP 2024 - 2024 IEEE International Conference on Acoustics, Speech and Signal Processing (ICASSP)*, 2024.
- [51] Marco Tulio Ribeiro and Scott Lundberg. Adaptive testing and debugging of nlp models. In *Proceedings of the 60th Annual Meeting of the Association for Computational Linguistics (Volume 1: Long Papers)*, pages 3253–3267, 2022.



- [52] Mauro Ribeiro, Katarina Grolinger, and Miriam AM Capretz. Mlaas: Machine learning as a service. In *2015 IEEE 14th international conference on machine learning and applications (ICMLA)*, pages 896–902. IEEE, 2015.
- [53] Ahmed Salem, Michael Backes, and Yang Zhang. Get a model! model hijacking attack against machine learning models. In *Proceedings of the Network and Distributed Systems Security Symposium (NDSS)*, 2022.
- [54] Ahmed Salem, Rui Wen, Michael Backes, Shiqing Ma, and Yang Zhang. Dynamic backdoor attacks against machine learning models. In *2022 IEEE 7th European Symposium on Security and Privacy (EuroS&P)*, pages 703–718, 2022.
- [55] Shibani Santurkar, Dimitris Tsipras, Mahalaxmi Elango, David Bau, Antonio Torralba, and Aleksander Madry. Editing a classifier by rewriting its prediction rules. *Advances in Neural Information Processing Systems*, 34:23359–23373, 2021.
- [56] Pavel Shoshin. Phantomlance android backdoor discovered on google play. *Kaspersky Daily*.
- [57] Anthony Spadafora. This android malware installs a backdoor on your phone — delete these malicious apps now. *Tom’s Guide*.
- [58] Johannes Stalkamp, Marc Schlipf, Jan Salmen, and Christian Igel. Man vs. computer: Benchmarking machine learning algorithms for traffic sign recognition. *Neural networks*, 32:323–332, 2012.
- [59] Hsuan Su, Hua Farn, Fan-Yun Sun, Shang-Tse Chen, and Hung yi Lee. Task arithmetic can mitigate synthetic-to-real gap in automatic speech recognition, 2024.
- [60] Yi-Lin Sung, Varun Nair, and Colin A Raffel. Training neural networks with fixed sparse masks. *Advances in Neural Information Processing Systems*, 34:24193–24205, 2021.
- [61] Anke Tang, Li Shen, Yong Luo, Liang Ding, Han Hu, Bo Du, and Dacheng Tao. Concrete subspace learning based interference elimination for multi-task model fusion. *arXiv preprint arXiv:2312.06173*, 2023.
- [62] Alexander Turner, Dimitris Tsipras, and Aleksander Madry. Label-consistent backdoor attacks. *arXiv preprint arXiv:1912.02771*, 2019.
- [63] Bolun Wang, Yuanshun Yao, Shawn Shan, Huiying Li, Bimal Viswanath, Haitao Zheng, and Ben Y Zhao. Neural cleanse: Identifying and mitigating backdoor attacks in neural networks. In *Proceedings of IEEE S&P*, 2019.
- [64] Hang Wang, Zhen Xiang, David J Miller, and George Kesidis. Mm-bd: Post-training detection of backdoor attacks with arbitrary backdoor pattern types using a maximum margin statistic. In *2024 IEEE Symposium on Security and Privacy (SP)*, pages 15–15. IEEE Computer Society, 2023.
- [65] Hongyi Wang, Kartik Sreenivasan, Shashank Rajput, Harit Vishwakarma, Saurabh Agarwal, Jy-yong Sohn, Kangwook Lee, and Dimitris Papailiopoulos. Attack of the tails: yes, you really can backdoor federated learning. In *Proceedings of the 34th International Conference on Neural Information Processing Systems*, 2020.
- [66] Mitchell Wortsman, Gabriel Ilharco, Samir Ya Gadre, Rebecca Roelofs, Raphael Gontijo-Lopes, Ari S Morcos, Hongseok Namkoong, Ali Farhadi, Yair Carmon, Simon Kornblith, et al. Model soups: averaging weights of multiple fine-tuned models improves accuracy without increasing inference time. In *International conference on machine learning*, pages 23965–23998. PMLR, 2022.
- [67] Jianxiong Xiao, James Hays, Krista A Ehinger, Aude Oliva, and Antonio Torralba. Sun database: Large-scale scene recognition from abbey to zoo. In *2010 IEEE computer society conference on computer vision and pattern recognition*, pages 3485–3492. IEEE, 2010.
- [68] Prateek Yadav, Derek Tam, Leshem Choshen, Colin A Raffel, and Mohit Bansal. Ties-merging: Resolving interference when merging models. *Advances in Neural Information Processing Systems (NeurIPS)*, 36, 2024.
- [69] Enneng Yang, Li Shen, Zhenyi Wang, Guibing Guo, Xiaojun Chen, Xingwei Wang, and Dacheng Tao. Representation surgery for multi-task model merging. *arXiv preprint arXiv:2402.02705*, 2024.
- [70] Enneng Yang, Zhenyi Wang, Li Shen, Shiwei Liu, Guibing Guo, Xingwei Wang, and Dacheng Tao. Adamerging: Adaptive model merging for multi-task learning. *International conference on learning representations (ICLR)*, 2024.
- [71] Xin Yi, Shunfan Zheng, Linlin Wang, Xiaoling Wang, and Liang He. A safety realignment framework via subspace-oriented model fusion for large language models, 2024.
- [72] Yi Zeng, Minzhou Pan, Hoang Anh Just, Lingjuan Lyu, Meikang Qiu, and Ruoxi Jia. Narcissus: A practical clean-label backdoor attack with limited information. In *Proceedings of the 2023 ACM SIGSAC Conference on Computer and Communications Security*, pages 771–785, 2023.

[73] Jinghui Zhang, Jianfeng Chi, Zheng Li, Kunlin Cai, Yang Zhang, and Yuan Tian. Badmerging: Backdoor attacks against model merging. In *ACM Conference on Computer and Communications Security (CCS)*, 2024.

## A Appendix

### Acronyms

ASR	attack success rate
BTV	backdoored task vector
CTV	clean task vector
MLaaS	machine learning as a service
MM	model merging
TA	task arithmetic
TVaaS	task vector as a service
TVs	task vectors

#### A.1 Datasets

- MNIST is a dataset for handwritten digit recognition, containing 70,000 grayscale images of digits ranging from 0 to 9. It includes 60,000 training images and 10,000 test images.
- SVHN comprises labeled images of house numbers extracted from Google Street View, making it a substantial resource for digit recognition tasks. The number of training/test samples are 73257/26302.
- CIFAR-10 is a benchmark of the image classification task containing 60,000 color images across 10 different classes, with 6,000 images per class. The dataset is balanced, providing an equal number of samples for each category.
- GTSRB is a German traffic sign dataset with 43 categories. The number of samples in each category within the training set is not balanced.
- CIFAR-100 is an image classification dataset consisting of 60,000 color images in 100 different classes, with 600 images per class.
- EuroSAT is a dataset for land use and land cover classification, containing 27,000 labeled satellite images across 10 classes such as residential, industrial, and agricultural areas. We adopt the dataset split approach from [23], which divides the dataset into 24,300 images for training and 2,700 images for testing.

Table 4: Notation

Notation	Meaning
$V$	a visual encoder
$T$	a test encoder
$\mu$	number of clean samples belongs to the attacker
$\nu$	number of triggered samples belongs to the attacker
$M$	$M = \{V, T\}$ is a pre-trained model comprised with $V$ and $T$
$C$	$C = [c_1, c_2, \dots, c_k]$ represents $k$ textual descriptions corresponding to task's classes
$\langle V(x), T(c_i) \rangle$	the similarity score between the embedding $x$ and class $c_i$
$L_{CE}(M(x, c), y)$	using cross entropy as a loss function to calculate the distance between $M(x, c)$ and $y$
$M_\theta$	a model $M$ with weight $\theta$
$\hat{M}_\theta$	backdoored model with weight $\theta$ , sometimes it can be interchanged with the use $\hat{M}$
$\theta_{pre}$	$\theta_{pre} \in \mathcal{R}^d$ denotes the weight of a publicly available pre-trained model
$\theta_t$	$\theta_t \in \mathcal{R}^d$ denotes the weight after fine-tuning on task $t$ using $D_t$ and $L_t$
$D_t$	a dataset $D$ with task $t$
$L_t$	a loss function with task $t$
$\lambda, \alpha$	scaling coefficients
$b$	refers to model, model weight, or backdoor configuration, depending on the context
$\tau_t$	a task vector with task $t$
$\hat{\tau}_t$	a backdoored task vector
$g$	$g = \{mask, \delta\}$ is a trigger with corresponding $mask$ and $\delta$
$mask$	indicator of the trigger's location
$\delta$	the trigger pattern
$\hat{x}^g$	a triggered image with $g$
$\odot$	the pixel-wise multiplication
$\oplus$	task operations consisting $\{+, -\}$
$x$	a clean image

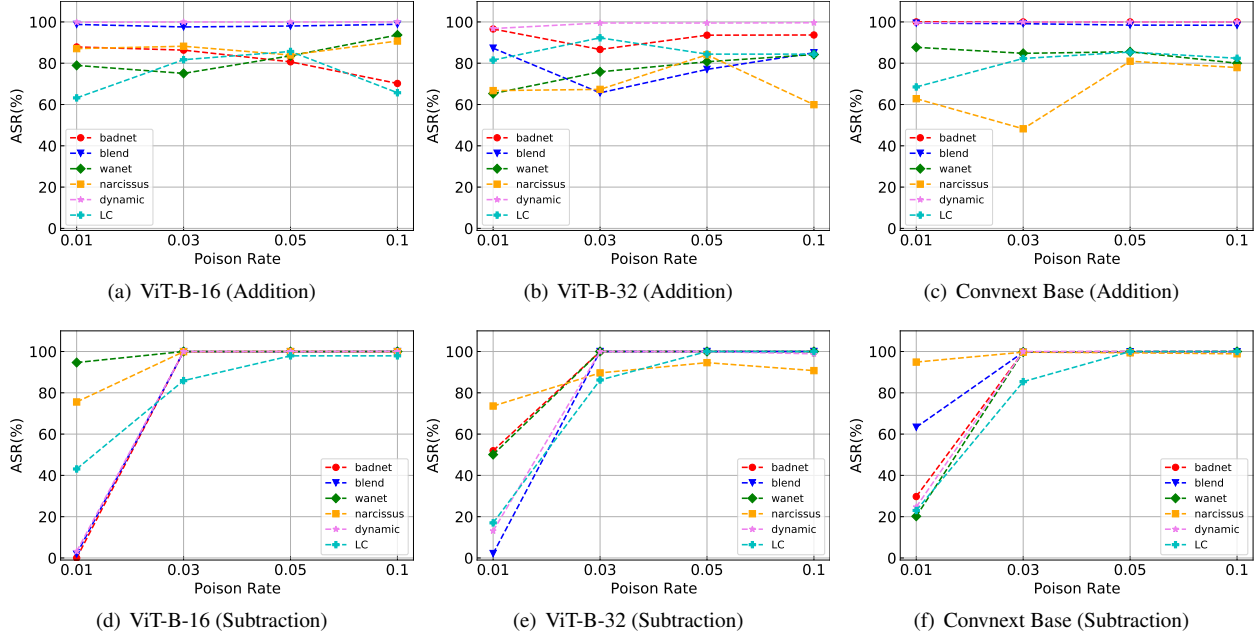


Figure 15: Comparison of task vectors addition/subtraction results of different backdoor attacks with different model architectures.

- Cars dataset consists of over 16,000 images of 196 different car models, captured from various angles and in different environments.
- SUN397 is a dataset for scene recognition, containing over 100,000 images categorized into 397 different scene types. To split the dataset into training and testing sets, we follow the settings of [23].

## A.2 Attack Methods

- **BadNets.** Except for GTSRB, where the trigger size is  $9 \times 9$ , the trigger size for the other datasets is  $3 \times 3$ . When training  $b_1$  and  $b_2$ , we place the trigger in the top-left and bottom-right corners, respectively.
- **Blend.** When training  $b_1$  and  $b_2$ , we use different triggers for each as shown in Appendix in Figure 16. We set the transparency parameter to 0.5.
- **Wanet.** To reduce the influence of  $b_2$  on  $b_1$ , we restrict the trigger to the top-left and bottom-right quarters of the image, respectively.
- **Dynamic.** We run the official code<sup>6</sup> for training, with the trigger size set to  $5 \times 5$  and the trigger location randomized.
- **Narcissus.** To ensure greater independence between  $b_1$  and  $b_2$ , we follow the original setting for  $b_1$  by plac-

ing the trigger on the entire image. However, regarding  $b_2$ , we limit the trigger size to one-quarter of the original size and position it in the bottom-right corner. We set  $\ell_\infty$ -norm of trigger  $\frac{16}{255}$ . It requires out-of-distribution data to train surrogate models for generating triggers. The out-of-distribution data pairs are as follows: MNIST-SVHN, SVHN-MNIST, CIFAR10-CIFAR100, CIFAR100-CIFAR10, and GTSRB-CIFAR100. For other parameter settings, we follow the official code<sup>7</sup>.

- **LC.** To ensure that  $b_1$  and  $b_2$  perform better in addition and subtraction tasks, we use visible triggers with sizes and locations following the BadNets settings. Regarding creating adversarial samples in LC, we run PGD attack [36] with 200 steps and  $\ell_\infty$ -norm is 0.1.

## A.3 Visualization of Triggers of Blend Attack



Figure 16: Visualization of the Blend triggers used for training the  $b_1$  and  $b_2$  models, respectively.

<sup>6</sup><https://github.com/AhmedSalem2/Dynamic-Backdoor>

<sup>7</sup><https://github.com/reds-lab/Narcissus>

## A.4 More Results of s Single BTV

In this section, we show more results of different settings.

### A.4.1 Performance on More Combinations of Single BTV and Single CTV

In this section, we show the performance of more different combinations of BTV and CTV in Table 5, where values of  $\text{cof}$  are represented by  $\alpha_2$  and we set  $\alpha_1 = 1$ .

## A.5 More Results Factors Affecting BADTV

### A.5.1 Results of different model architectures

In Figure 15, we show the results of 1 GTSRB BTV trained by different backdoor attacks added 1 CIFAR-100 CTV across 3 model structures. Furthermore, we also provide more combinations of 1 BTV and 1 CTV for these three model structures in Table 7 and 6.

### A.5.2 More results of Backdoor Combination in BADTV

In this section, we explore different backdoor combinations of  $b_1$  and  $b_2$  in a BADTV. In the main text, we only present a subset of the results.

## A.6 More Results of BADTV in the Wild

### A.6.1 More Results of Multiple Clean Task Vectors

In the main text, due to space limitations, we only included a portion of the BadNets results. Here, we present the complete results in Figure 19 and 20.

### A.6.2 More results of Multiple BTVs

Figure 18 presents 2 BTVs trained across 5 attacks on the GTSRB and CIFAR-100 dataset added with EuroSAT CTV. Moreover, in Figure 21 and 22, we show 2 BTVs added with 3 and 6 clean CTVs. To show more attack combinations, Figures 23 and 24 present a Blend BTV combined with another BTV, where  $b_1$  and  $b_2$  come from either the same or different attacks, with 3 and 6 CTVs added, respectively.

## A.7 Hijacking Attack

### A.7.1 Different Model Structures

In this section, we show model hijacking attacks based on different model architectures such as ViT-B-16, ViT-B-32, and Convnext Base. Here, we evaluate the hijacking ASR of 1 BTV combined with 1 CTV, where the original task of the BTV is EuroSAT and the CTV is GTSRB. EuroSAT has three hijacking tasks: MNIST, SVHN, and CIFAR-10. In Figure 25, it demonstrates that the model architecture has a slight

impact on the attack results. Among them, the results of ViT-B-16 and ViT-B-32 are relatively close, with ASR remaining around 80% across the three hijacking tasks, while ConvNext Base performs slightly worse.

### A.7.2 Different Dimensions of Latent Space

Here, we explore whether the dimension of the latent space in the encoder/decoder affects the effectiveness of the attack. We follow the same combination of 1 BTV and 1 CTV mentioned in Appendix A.5.1 and fix the model structure as ViT-B-32. In Figure 26, changing the dimension of the latent space has a minimal impact on the attack results. When the dimension is increased, there is a slight decrease in ASR. This indicates that the dimension of the latent space in the autoencoder has little impact on the performance of the attack.

### A.7.3 Adding multiple clean task vectors

In discussing defenses against backdoor attacks, we mentioned that adding more clean models might affect the performance of the backdoor attack, potentially achieving a defensive effect. Here, we follow a similar concept to investigate whether adding more clean tasks influences the performance of the model hijacking attack. The BTV we used has EuroSAT as the original task and SVHN as the hijacking task. As shown in Figure 27, as the number of clean task vectors increases, the ASR does not decrease but remains consistently above 80%. "This indicates that adding more clean tasks has minimal impact on the hijacking tasks and cannot effectively be used as a defense mechanism.

## A.8 More results of Defense

### A.8.1 More Results of Lowering $\lambda$

We present the ASR results for the combinations of (BTV, CTV) = (GTSRB, CIFAR-100) and (CIFAR-100, GTSRB) in Section 7. Besides, we perform another combination of single BTV and CTV, where BTV is trained by BadNets on MNIST, and CTV is a CIFAR-10 task. Figure 28 demonstrates the ASR is almost unaffected by different values of  $\lambda$ , remaining above 95%.

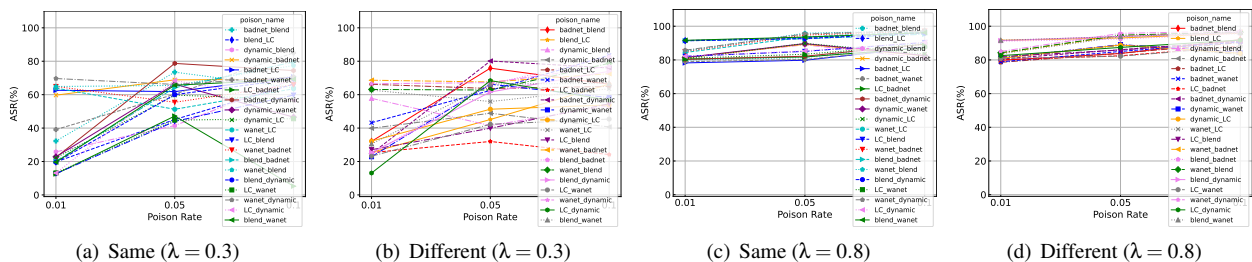


Figure 17: Comparison of different backdoor combination in BADTV where  $\lambda$  shows the merging coefficient. In the same setting, both trigger  $b_1$  and  $b_2$  are set by the same attack. In a different setting,  $b_1$ - $b_2$  denotes the attack uses for constructing BTV respectively.

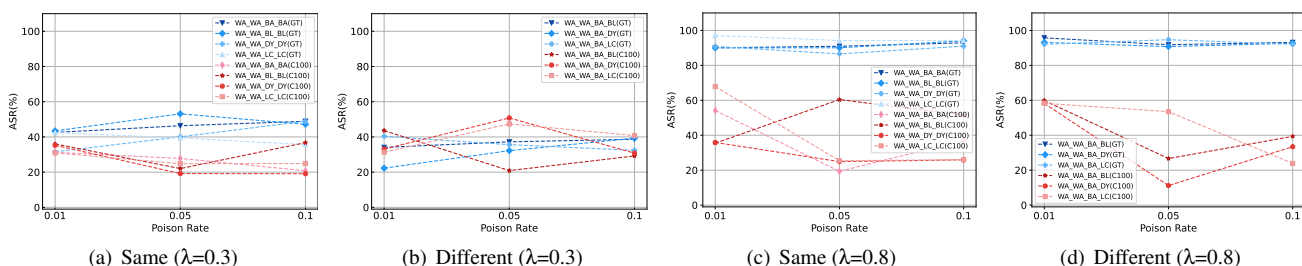


Figure 18: Comparison of results of 2 BTVs trained across 5 backdoor attacks added by 1 clean task with varying poison rates. Blue lines represent the ASR of GTSRB while the red lines denote the ASR of CIFAR100.

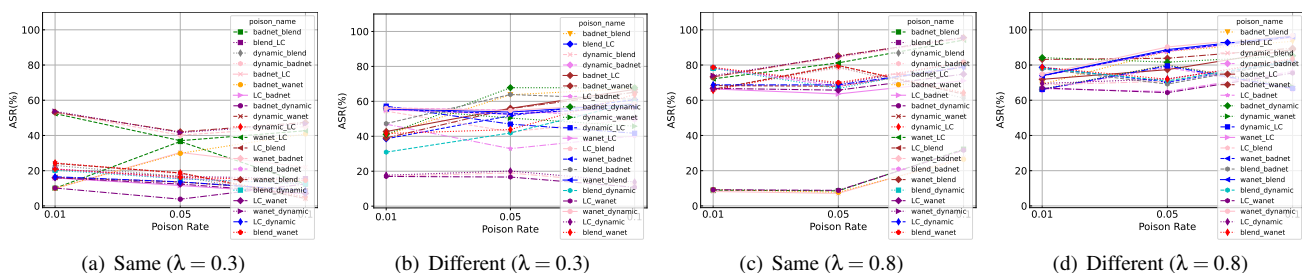


Figure 19: Comparison of results of a single BTV adding with 3 clean TVs with  $b_1$  and  $b_2$  using same/different backdoor attack under  $\lambda = 0.3$  and  $0.8$ .

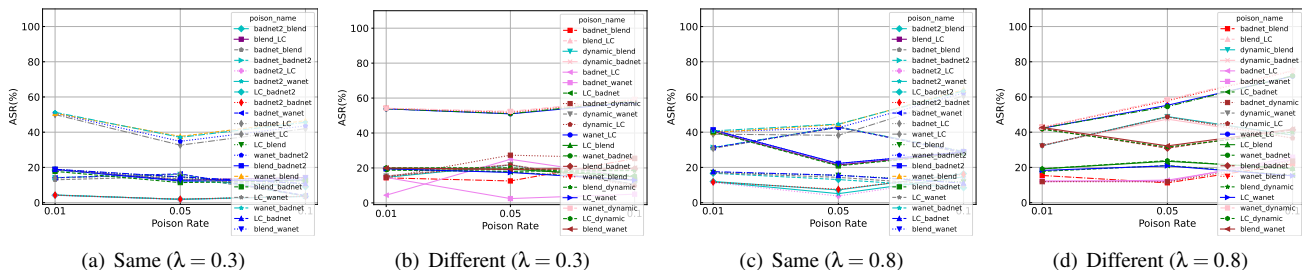


Figure 20: Comparison of results of a single BTV adding with 7 clean TVs with  $b_1$  and  $b_2$  using same/different backdoor attacks under  $\lambda = 0.3$  and  $0.8$ .

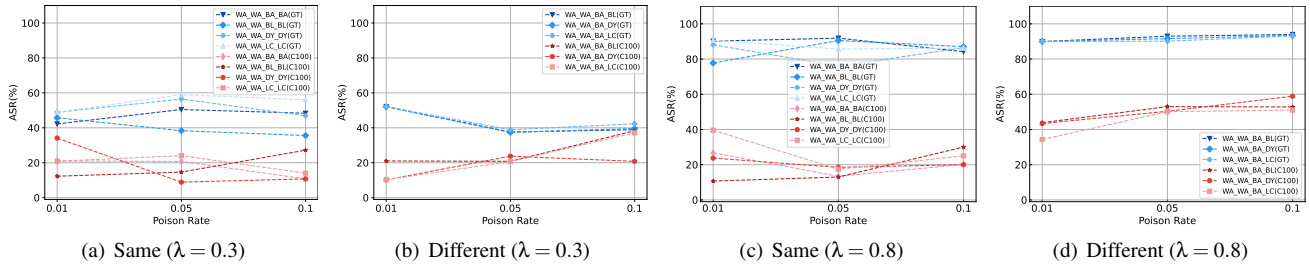


Figure 21: Comparison of results of 2 BTVs trained by backdoor attacks added by 3 clean tasks with varying poison rates. Blue lines represent the ASR of GTSRB while the red lines denote the ASR of CIFAR-100.

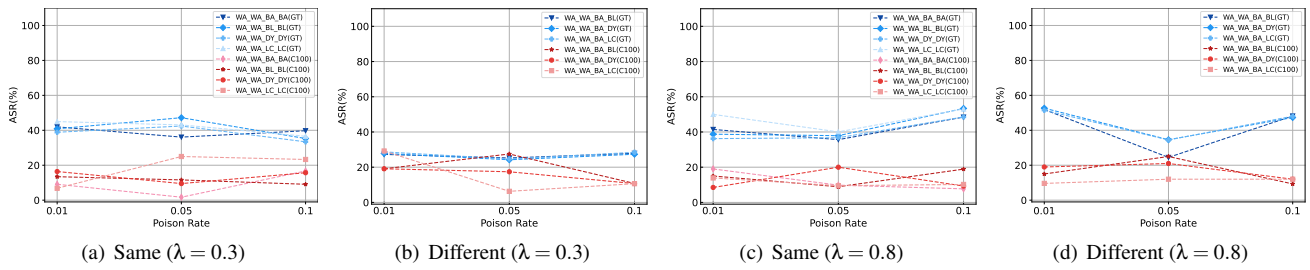


Figure 22: Comparison of results of 2 BTVs trained by backdoor attacks added by 6 clean tasks with varying poison rates. Blue lines represent the ASR of GTSRB while the red lines denote the ASR of CIFAR-100.

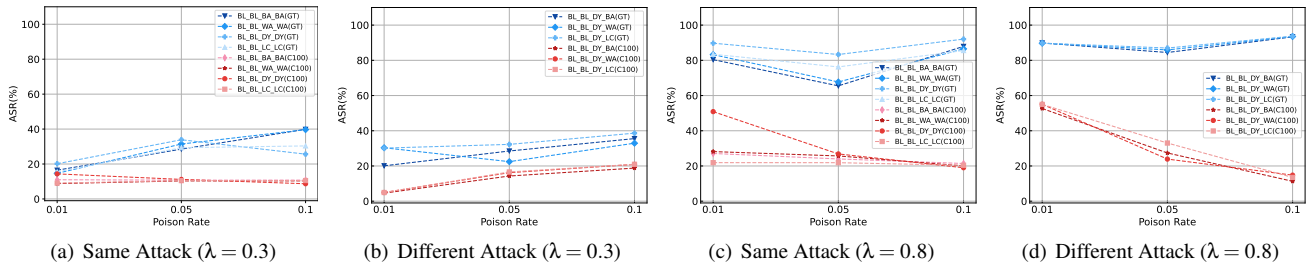


Figure 23: Comparison of results of 2 BTVs trained by backdoor attacks added by 3 clean tasks with varying poison rates. Blue lines represent the ASR of GTSRB while the red lines denote the ASR of CIFAR-100.

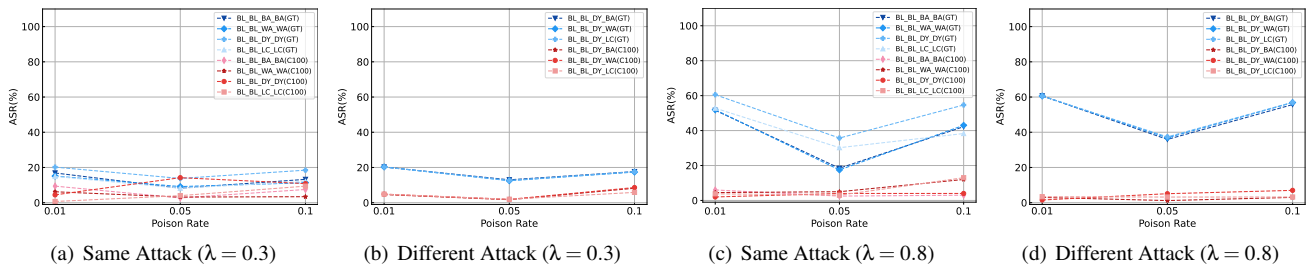


Figure 24: Comparison of results of 2 BTVs trained by backdoor attacks added by 6 clean tasks with varying poison rate rates. Blue lines represent the ASR of GTSRB while the red lines denote the ASR of CIFAR-100.

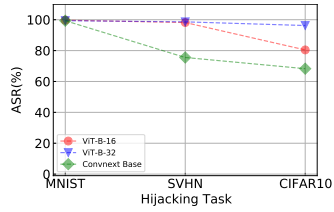


Figure 25: Comparison of model hijacking attack results with different model structures.

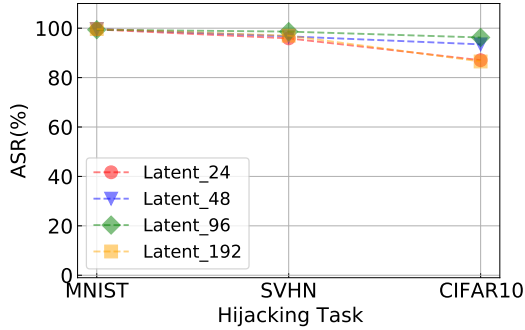


Figure 26: Comparison of model hijacking attack results with different dimensions of latent space.

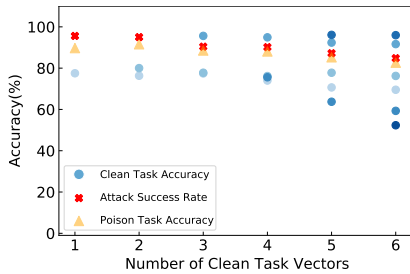


Figure 27: Comparison of ASR and Clean Accuracy (CA) across different numbers of clean task vectors, evaluating each clean task vector individually with  $\lambda = 0.3$ . The poison task vector is trained on EuroSAT by hijack attack and the hijacking task is SVHN.

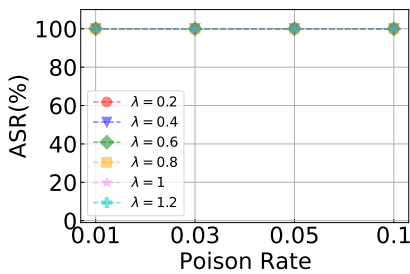


Figure 28: Comparison of the backdoor model trained on BadNets on MNIST dataset with varying the value of  $\lambda$ .

Table 5: Comparison of results for different combinations of a single BTV trained with various backdoor attacks on ViT-B-16, and a single CTV with different poison rates, across five datasets.

Model Structure	Attack Method	Poison Rate	Clean Dataset	Clean Acc	Poison Dataset	Poison Acc	ASR	cof
ViT-B-16	BadNets	0.03	SVHN	0.965542409	MNIST	0.9936	0.993	1
ViT-B-16	BadNets	0.03	CIFAR10	0.9714	MNIST	0.9941	1	1
ViT-B-16	BadNets	0.03	CIFAR100	0.8366	MNIST	0.9956	1	1
ViT-B-16	BadNets	0.03	GTSRB	0.955502771	MNIST	0.9928	1	1
ViT-B-16	BadNets	0.05	SVHN	0.961585741	MNIST	0.9932	1	1
ViT-B-16	BadNets	0.05	CIFAR10	0.9728	MNIST	0.9943	1	1
ViT-B-16	BadNets	0.05	CIFAR100	0.8225	MNIST	0.9959	1	1
ViT-B-16	BadNets	0.05	GTSRB	0.948931116	MNIST	0.9928	1	1
ViT-B-16	BadNets	0.1	SVHN	0.962891825	MNIST	0.9922	0.0032	1
ViT-B-16	BadNets	0.1	CIFAR10	0.9697	MNIST	0.994	1	1
ViT-B-16	BadNets	0.1	CIFAR100	0.8257	MNIST	0.9947	1	1
ViT-B-16	BadNets	0.1	GTSRB	0.953127474	MNIST	0.992	1	1
ViT-B-16	BadNets	0.15	SVHN	0.963160725	MNIST	0.9938	0.0023	1
ViT-B-16	BadNets	0.15	CIFAR10	0.9706	MNIST	0.9931	1	1
ViT-B-16	BadNets	0.15	CIFAR100	0.8272	MNIST	0.9955	1	1
ViT-B-16	BadNets	0.15	GTSRB	0.957007126	MNIST	0.9919	0.0066	1
ViT-B-16	BadNets	0.03	MNIST	0.9958	SVHN	0.890634604	0.998962815	1
ViT-B-16	BadNets	0.03	CIFAR10	0.9633	SVHN	0.935886601	1	1
ViT-B-16	BadNets	0.03	CIFAR100	0.8038	SVHN	0.951559619	1	1
ViT-B-16	BadNets	0.03	GTSRB	0.981155978	SVHN	0.935271973	0.999923171	1
ViT-B-16	BadNets	0.05	MNIST	0.9953	SVHN	0.904156423	0.999154886	1
ViT-B-16	BadNets	0.05	CIFAR10	0.9613	SVHN	0.943838353	1	1
ViT-B-16	BadNets	0.05	CIFAR100	0.7894	SVHN	0.956553473	1	1
ViT-B-16	BadNets	0.05	GTSRB	0.978939034	SVHN	0.93388906	0.999846343	1
ViT-B-16	BadNets	0.1	MNIST	0.9952	SVHN	0.901467425	0.9997311	1
ViT-B-16	BadNets	0.1	CIFAR10	0.9605	SVHN	0.943223725	1	1
ViT-B-16	BadNets	0.1	CIFAR100	0.7966	SVHN	0.954594345	1	1
ViT-B-16	BadNets	0.1	GTSRB	0.978780681	SVHN	0.934119545	1	1
ViT-B-16	BadNets	0.15	MNIST	0.9951	SVHN	0.899777197	0.999692686	1
ViT-B-16	BadNets	0.15	CIFAR10	0.9599	SVHN	0.946757837	1	1
ViT-B-16	BadNets	0.15	CIFAR100	0.7979	SVHN	0.956054087	1	1
ViT-B-16	BadNets	0.15	GTSRB	0.978859857	SVHN	0.935579287	1	1
ViT-B-16	BadNets	0.03	MNIST	0.9967	CIFAR10	0.9403	1	1
ViT-B-16	BadNets	0.03	SVHN	0.972956361	CIFAR10	0.9317	1	1
ViT-B-16	BadNets	0.03	CIFAR100	0.8649	CIFAR10	0.979	1	1
ViT-B-16	BadNets	0.03	GTSRB	0.984639747	CIFAR10	0.9437	1	1
ViT-B-16	BadNets	0.05	MNIST	0.9965	CIFAR10	0.937	1	1
ViT-B-16	BadNets	0.05	SVHN	0.973110018	CIFAR10	0.9343	1	1
ViT-B-16	BadNets	0.05	CIFAR100	0.8591	CIFAR10	0.9801	1	1
ViT-B-16	BadNets	0.05	GTSRB	0.980680918	CIFAR10	0.9426	1	1
ViT-B-16	BadNets	0.1	MNIST	0.9968	CIFAR10	0.9431	1	1
ViT-B-16	BadNets	0.1	SVHN	0.97357099	CIFAR10	0.929	1	1
ViT-B-16	BadNets	0.1	CIFAR100	0.8561	CIFAR10	0.9793	1	1
ViT-B-16	BadNets	0.1	GTSRB	0.983135392	CIFAR10	0.9457	1	1
ViT-B-16	BadNets	0.15	MNIST	0.9962	CIFAR10	0.9394	1	1
ViT-B-16	BadNets	0.15	SVHN	0.974800246	CIFAR10	0.9353	1	1



Model Structure	Attack Method	Poison Rate	Clean Dataset	Clean Acc	Poison Dataset	Poison Acc	ASR	cof
ViT-B-16	BadNets	0.15	CIFAR100	0.8557	CIFAR10	0.9795	1	1
ViT-B-16	BadNets	0.15	GTSRB	0.983689628	CIFAR10	0.9422	1	1
ViT-B-16	BadNets	0.03	MNIST	0.9975	CIFAR100	0.7269	0.9981	1
ViT-B-16	BadNets	0.03	SVHN	0.977297173	CIFAR100	0.6531	0.6732	1
ViT-B-16	BadNets	0.03	CIFAR10	0.9839	CIFAR100	0.8141	0.9113	1
ViT-B-16	BadNets	0.03	GTSRB	0.986935867	CIFAR100	0.657	0.9587	1
ViT-B-16	BadNets	0.05	MNIST	0.9972	CIFAR100	0.7107	0.9993	1
ViT-B-16	BadNets	0.05	SVHN	0.977105101	CIFAR100	0.6524	0.3058	1
ViT-B-16	BadNets	0.05	CIFAR10	0.9828	CIFAR100	0.8132	0.7845	1
ViT-B-16	BadNets	0.05	GTSRB	0.986302454	CIFAR100	0.6656	0.5625	1
ViT-B-16	BadNets	0.1	MNIST	0.9974	CIFAR100	0.7263	0.9989	1
ViT-B-16	BadNets	0.1	SVHN	0.977758144	CIFAR100	0.6515	0.4953	1
ViT-B-16	BadNets	0.1	CIFAR10	0.9837	CIFAR100	0.809	0.9851	1
ViT-B-16	BadNets	0.1	GTSRB	0.98685669	CIFAR100	0.6643	0.9999	1
ViT-B-16	BadNets	0.15	MNIST	0.9972	CIFAR100	0.7303	0.9992	1
ViT-B-16	BadNets	0.15	SVHN	0.977834972	CIFAR100	0.6704	0.2843	1
ViT-B-16	BadNets	0.15	CIFAR10	0.9827	CIFAR100	0.8133	0.9212	1
ViT-B-16	BadNets	0.15	GTSRB	0.986698337	CIFAR100	0.6797	0.9964	1
ViT-B-16	BadNets	0.03	MNIST	0.9962	GTSRB	0.834679335	0.80760095	1
ViT-B-16	BadNets	0.03	SVHN	0.962738168	GTSRB	0.894061758	0.311163895	1
ViT-B-16	BadNets	0.03	CIFAR10	0.9635	GTSRB	0.960174188	0.643626287	1
ViT-B-16	BadNets	0.03	CIFAR100	0.7913	GTSRB	0.968091845	0.863420428	1
ViT-B-16	BadNets	0.05	MNIST	0.9952	GTSRB	0.881947743	0.754948535	1
ViT-B-16	BadNets	0.05	SVHN	0.958397357	GTSRB	0.937133808	0.067062549	1
ViT-B-16	BadNets	0.05	CIFAR10	0.9534	GTSRB	0.960649248	0.510292953	1
ViT-B-16	BadNets	0.05	CIFAR100	0.762	GTSRB	0.969675376	0.806730008	1
ViT-B-16	BadNets	0.1	MNIST	0.9949	GTSRB	0.897307997	0.652256532	1
ViT-B-16	BadNets	0.1	SVHN	0.958935157	GTSRB	0.939350752	0.012747427	1
ViT-B-16	BadNets	0.1	CIFAR10	0.9478	GTSRB	0.965716548	0.422723674	1
ViT-B-16	BadNets	0.1	CIFAR100	0.7499	GTSRB	0.972763262	0.702058591	1
ViT-B-16	BadNets	0.15	MNIST	0.9946	GTSRB	0.919319082	0.822486144	1
ViT-B-16	BadNets	0.15	SVHN	0.952135833	GTSRB	0.963499604	0.059303246	1
ViT-B-16	BadNets	0.15	CIFAR10	0.9596	GTSRB	0.967616785	0.547585115	1
ViT-B-16	BadNets	0.15	CIFAR100	0.7697	GTSRB	0.971733967	0.814093428	1
ViT-B-16	Blend	0.03	SVHN	0.962853411	MNIST	0.993	0.2207	1
ViT-B-16	Blend	0.03	CIFAR10	0.9705	MNIST	0.993	1	1
ViT-B-16	Blend	0.03	CIFAR100	0.8307	MNIST	0.9953	1	1
ViT-B-16	Blend	0.03	GTSRB	0.952969121	MNIST	0.9906	0.4678	1
ViT-B-16	Blend	0.05	SVHN	0.959972342	MNIST	0.9934	0.2192	1
ViT-B-16	Blend	0.05	CIFAR10	0.9692	MNIST	0.9916	1	1
ViT-B-16	Blend	0.05	CIFAR100	0.8317	MNIST	0.9943	1	1
ViT-B-16	Blend	0.05	GTSRB	0.959461599	MNIST	0.9921	0.522	1
ViT-B-16	Blend	0.1	SVHN	0.959933927	MNIST	0.9936	0.1591	1
ViT-B-16	Blend	0.1	CIFAR10	0.9702	MNIST	0.9937	0.9993	1
ViT-B-16	Blend	0.1	CIFAR100	0.828	MNIST	0.996	1	1
ViT-B-16	Blend	0.1	GTSRB	0.955423595	MNIST	0.9917	0.3571	1
ViT-B-16	Blend	0.15	SVHN	0.959972342	MNIST	0.9927	0.1247	1
ViT-B-16	Blend	0.15	CIFAR10	0.9684	MNIST	0.9935	0.995	1
ViT-B-16	Blend	0.15	CIFAR100	0.8289	MNIST	0.9956	1	1
ViT-B-16	Blend	0.15	GTSRB	0.947268409	MNIST	0.9906	0.2562	1

Model Structure	Attack Method	Poison Rate	Clean Dataset	Clean Acc	Poison Dataset	Poison Acc	ASR	cof
ViT-B-16	Blend	0.03	MNIST	0.9962	SVHN	0.905616165	0.857790412	1
ViT-B-16	Blend	0.03	CIFAR10	0.9707	SVHN	0.963314382	0.999961586	1
ViT-B-16	Blend	0.03	CIFAR100	0.8209	SVHN	0.970113706	0.999961586	1
ViT-B-16	Blend	0.03	GTSRB	0.980126683	SVHN	0.948832207	0.982214198	1
ViT-B-16	Blend	0.05	MNIST	0.996	SVHN	0.904617394	0.756952981	1
ViT-B-16	Blend	0.05	CIFAR10	0.9709	SVHN	0.956361401	0.999231715	1
ViT-B-16	Blend	0.05	CIFAR100	0.8171	SVHN	0.966464352	0.999385372	1
ViT-B-16	Blend	0.05	GTSRB	0.984718923	SVHN	0.947948679	0.90872772	1
ViT-B-16	Blend	0.1	MNIST	0.9963	SVHN	0.91107099	0.711585741	1
ViT-B-16	Blend	0.1	CIFAR10	0.97	SVHN	0.960241242	0.999385372	1
ViT-B-16	Blend	0.1	CIFAR100	0.818	SVHN	0.968653964	0.999769514	1
ViT-B-16	Blend	0.1	GTSRB	0.982739509	SVHN	0.946027966	0.926820836	1
ViT-B-16	Blend	0.15	MNIST	0.9959	SVHN	0.90457898	0.715888138	1
ViT-B-16	Blend	0.15	CIFAR10	0.9678	SVHN	0.960087585	0.997426245	1
ViT-B-16	Blend	0.15	CIFAR100	0.8063	SVHN	0.968538722	0.998655501	1
ViT-B-16	Blend	0.15	GTSRB	0.979018211	SVHN	0.946681008	0.852297173	1
ViT-B-16	Blend	0.03	MNIST	0.997	CIFAR10	0.9357	0.9967	1
ViT-B-16	Blend	0.03	SVHN	0.972802704	CIFAR10	0.9271	0.9686	1
ViT-B-16	Blend	0.03	CIFAR100	0.8656	CIFAR10	0.9796	0.9638	1
ViT-B-16	Blend	0.03	GTSRB	0.98456057	CIFAR10	0.9355	0.9989	1
ViT-B-16	Blend	0.05	MNIST	0.9967	CIFAR10	0.936	0.9846	1
ViT-B-16	Blend	0.05	SVHN	0.974224032	CIFAR10	0.9286	0.9272	1
ViT-B-16	Blend	0.05	CIFAR100	0.864	CIFAR10	0.9805	0.9056	1
ViT-B-16	Blend	0.05	GTSRB	0.981472684	CIFAR10	0.9346	0.9957	1
ViT-B-16	Blend	0.1	MNIST	0.9966	CIFAR10	0.9399	0.9908	1
ViT-B-16	Blend	0.1	SVHN	0.974185618	CIFAR10	0.9232	0.9258	1
ViT-B-16	Blend	0.1	CIFAR100	0.8641	CIFAR10	0.9805	0.9111	1
ViT-B-16	Blend	0.1	GTSRB	0.983768804	CIFAR10	0.9371	0.9962	1
ViT-B-16	Blend	0.15	MNIST	0.9967	CIFAR10	0.9456	0.9989	1
ViT-B-16	Blend	0.15	SVHN	0.972572219	CIFAR10	0.9267	0.9748	1
ViT-B-16	Blend	0.15	CIFAR100	0.8618	CIFAR10	0.9813	0.9654	1
ViT-B-16	Blend	0.15	GTSRB	0.984956453	CIFAR10	0.9402	0.9995	1
ViT-B-16	Blend	0.03	MNIST	0.9972	CIFAR100	0.7057	0.9117	1
ViT-B-16	Blend	0.03	SVHN	0.977297173	CIFAR100	0.6481	0.7748	1
ViT-B-16	Blend	0.03	CIFAR10	0.984	CIFAR100	0.8205	0.6671	1
ViT-B-16	Blend	0.03	GTSRB	0.98733175	CIFAR100	0.6694	0.8682	1
ViT-B-16	Blend	0.05	MNIST	0.9976	CIFAR100	0.6951	0.8616	1
ViT-B-16	Blend	0.05	SVHN	0.977143516	CIFAR100	0.6415	0.703	1
ViT-B-16	Blend	0.05	CIFAR10	0.9825	CIFAR100	0.8237	0.5778	1
ViT-B-16	Blend	0.05	GTSRB	0.987727633	CIFAR100	0.6543	0.8302	1
ViT-B-16	Blend	0.1	MNIST	0.9973	CIFAR100	0.709	0.9216	1
ViT-B-16	Blend	0.1	SVHN	0.977988629	CIFAR100	0.663	0.7941	1
ViT-B-16	Blend	0.1	CIFAR10	0.9838	CIFAR100	0.8222	0.6728	1
ViT-B-16	Blend	0.1	GTSRB	0.985589865	CIFAR100	0.6721	0.9007	1
ViT-B-16	Blend	0.15	MNIST	0.9973	CIFAR100	0.7079	0.8873	1
ViT-B-16	Blend	0.15	SVHN	0.977220344	CIFAR100	0.6534	0.7556	1
ViT-B-16	Blend	0.15	CIFAR10	0.9832	CIFAR100	0.8257	0.6667	1
ViT-B-16	Blend	0.15	GTSRB	0.986064925	CIFAR100	0.6641	0.8914	1
ViT-B-16	Blend	0.03	MNIST	0.9959	GTSRB	0.88178939	0.805700713	1
ViT-B-16	Blend	0.03	SVHN	0.96627228	GTSRB	0.91314331	0.650435471	1

Model Structure	Attack Method	Poison Rate	Clean Dataset	Clean Acc	Poison Dataset	Poison Acc	ASR	cof
ViT-B-16	Blend	0.03	CIFAR10	0.9632	GTSRB	0.978305622	0.934758511	1
ViT-B-16	Blend	0.03	CIFAR100	0.8008	GTSRB	0.977830562	0.975692795	1
ViT-B-16	Blend	0.05	MNIST	0.9954	GTSRB	0.889786223	0.827949327	1
ViT-B-16	Blend	0.05	SVHN	0.967539951	GTSRB	0.948535234	0.662707838	1
ViT-B-16	Blend	0.05	CIFAR10	0.9652	GTSRB	0.973555028	0.940063341	1
ViT-B-16	Blend	0.05	CIFAR100	0.8023	GTSRB	0.981710214	0.980126683	1
ViT-B-16	Blend	0.1	MNIST	0.9957	GTSRB	0.885906572	0.867933492	1
ViT-B-16	Blend	0.1	SVHN	0.967002151	GTSRB	0.89976247	0.723990499	1
ViT-B-16	Blend	0.1	CIFAR10	0.9673	GTSRB	0.976801267	0.959936659	1
ViT-B-16	Blend	0.1	CIFAR100	0.7978	GTSRB	0.979018211	0.988519398	1
ViT-B-16	Blend	0.15	MNIST	0.9961	GTSRB	0.874030087	0.857719715	1
ViT-B-16	Blend	0.15	SVHN	0.970459435	GTSRB	0.93618369	0.748693587	1
ViT-B-16	Blend	0.15	CIFAR10	0.9651	GTSRB	0.97672209	0.964687253	1
ViT-B-16	Blend	0.15	CIFAR100	0.792	GTSRB	0.977909739	0.989469517	1
ViT-B-16	Wanet	0.01	SVHN	0.96239244	MNIST	0.9936	0.0937	1
ViT-B-16	Wanet	0.01	CIFAR10	0.973	MNIST	0.994	0.9687	1
ViT-B-16	Wanet	0.01	CIFAR100	0.8425	MNIST	0.9952	0.9984	1
ViT-B-16	Wanet	0.01	GTSRB	0.950277118	MNIST	0.9928	0.3199	1
ViT-B-16	Wanet	0.03	SVHN	0.963813768	MNIST	0.9931	0.0868	1
ViT-B-16	Wanet	0.03	CIFAR10	0.9737	MNIST	0.9936	0.9884	1
ViT-B-16	Wanet	0.03	CIFAR100	0.8404	MNIST	0.9952	0.9933	1
ViT-B-16	Wanet	0.03	GTSRB	0.941092637	MNIST	0.9928	0.2734	1
ViT-B-16	Wanet	0.05	SVHN	0.964697296	MNIST	0.9934	0.079	1
ViT-B-16	Wanet	0.05	CIFAR10	0.9706	MNIST	0.9934	0.8409	1
ViT-B-16	Wanet	0.05	CIFAR100	0.827	MNIST	0.9951	0.8081	1
ViT-B-16	Wanet	0.05	GTSRB	0.935154394	MNIST	0.9913	0.0818	1
ViT-B-16	Wanet	0.1	SVHN	0.964236325	MNIST	0.9921	0.0854	1
ViT-B-16	Wanet	0.1	CIFAR10	0.9714	MNIST	0.9934	0.8222	1
ViT-B-16	Wanet	0.1	CIFAR100	0.8354	MNIST	0.9945	0.8231	1
ViT-B-16	Wanet	0.1	GTSRB	0.936975455	MNIST	0.9919	0.2471	1
ViT-B-16	Wanet	0.15	SVHN	0.9590504	MNIST	0.9931	0.0878	1
ViT-B-16	Wanet	0.15	CIFAR10	0.9695	MNIST	0.994	0.5997	1
ViT-B-16	Wanet	0.15	CIFAR100	0.8258	MNIST	0.9952	0.6177	1
ViT-B-16	Wanet	0.15	GTSRB	0.925019794	MNIST	0.991	0.1544	1
ViT-B-16	Wanet	0.01	MNIST	0.9965	SVHN	0.90557775	0.400199754	1
ViT-B-16	Wanet	0.01	CIFAR10	0.9688	SVHN	0.965657652	0.925822065	1
ViT-B-16	Wanet	0.01	CIFAR100	0.8075	SVHN	0.973186847	0.960164413	1
ViT-B-16	Wanet	0.01	GTSRB	0.982106097	SVHN	0.949293178	0.818915181	1
ViT-B-16	Wanet	0.03	MNIST	0.9957	SVHN	0.892401659	0.603219115	1
ViT-B-16	Wanet	0.03	CIFAR10	0.9653	SVHN	0.936001844	0.967847265	1
ViT-B-16	Wanet	0.03	CIFAR100	0.7964	SVHN	0.952135833	0.986708666	1
ViT-B-16	Wanet	0.03	GTSRB	0.98202692	SVHN	0.927358636	0.924323909	1
ViT-B-16	Wanet	0.05	MNIST	0.995	SVHN	0.884181008	0.320682237	1
ViT-B-16	Wanet	0.05	CIFAR10	0.9624	SVHN	0.939074985	0.893592502	1
ViT-B-16	Wanet	0.05	CIFAR100	0.7965	SVHN	0.951137062	0.970881991	1
ViT-B-16	Wanet	0.05	GTSRB	0.980443389	SVHN	0.924170252	0.792755071	1
ViT-B-16	Wanet	0.1	MNIST	0.9958	SVHN	0.893592502	0.704325446	1
ViT-B-16	Wanet	0.1	CIFAR10	0.9604	SVHN	0.944222495	0.983866011	1
ViT-B-16	Wanet	0.1	CIFAR100	0.7925	SVHN	0.9582437	0.995390289	1
ViT-B-16	Wanet	0.1	GTSRB	0.980047506	SVHN	0.93362016	0.96266134	1

Model Structure	Attack Method	Poison Rate	Clean Dataset	Clean Acc	Poison Dataset	Poison Acc	ASR	cof
ViT-B-16	Wanet	0.15	MNIST	0.9953	SVHN	0.889674247	0.805162876	1
ViT-B-16	Wanet	0.15	CIFAR10	0.9585	SVHN	0.937653657	0.986900738	1
ViT-B-16	Wanet	0.15	CIFAR100	0.7817	SVHN	0.95228949	0.995428703	1
ViT-B-16	Wanet	0.15	GTSRB	0.979889153	SVHN	0.929087277	0.970382606	1
ViT-B-16	Wanet	0.01	MNIST	0.9968	CIFAR10	0.9367	0.9118	1
ViT-B-16	Wanet	0.01	SVHN	0.975222803	CIFAR10	0.9157	0.7273	1
ViT-B-16	Wanet	0.01	CIFAR100	0.8685	CIFAR10	0.9796	0.6977	1
ViT-B-16	Wanet	0.01	GTSRB	0.984639747	CIFAR10	0.9274	0.9585	1
ViT-B-16	Wanet	0.03	MNIST	0.9968	CIFAR10	0.9256	0.9264	1
ViT-B-16	Wanet	0.03	SVHN	0.974608175	CIFAR10	0.9247	0.7894	1
ViT-B-16	Wanet	0.03	CIFAR100	0.8619	CIFAR10	0.9775	0.7243	1
ViT-B-16	Wanet	0.03	GTSRB	0.98432304	CIFAR10	0.9335	0.9714	1
ViT-B-16	Wanet	0.05	MNIST	0.9966	CIFAR10	0.9192	0.9297	1
ViT-B-16	Wanet	0.05	SVHN	0.974224032	CIFAR10	0.9235	0.8112	1
ViT-B-16	Wanet	0.05	CIFAR100	0.8557	CIFAR10	0.9777	0.7575	1
ViT-B-16	Wanet	0.05	GTSRB	0.982422803	CIFAR10	0.9329	0.9687	1
ViT-B-16	Wanet	0.1	MNIST	0.9962	CIFAR10	0.9202	0.9373	1
ViT-B-16	Wanet	0.1	SVHN	0.973340504	CIFAR10	0.9164	0.844	1
ViT-B-16	Wanet	0.1	CIFAR100	0.8485	CIFAR10	0.9764	0.7025	1
ViT-B-16	Wanet	0.1	GTSRB	0.985193983	CIFAR10	0.9324	0.9823	1
ViT-B-16	Wanet	0.15	MNIST	0.9962	CIFAR10	0.9292	0.9472	1
ViT-B-16	Wanet	0.15	SVHN	0.971957591	CIFAR10	0.9325	0.8501	1
ViT-B-16	Wanet	0.15	CIFAR100	0.8544	CIFAR10	0.9768	0.7856	1
ViT-B-16	Wanet	0.15	GTSRB	0.983293745	CIFAR10	0.9379	0.9815	1
ViT-B-16	Wanet	0.01	MNIST	0.9975	CIFAR100	0.7289	0.9223	1
ViT-B-16	Wanet	0.01	SVHN	0.9784496	CIFAR100	0.6418	0.7344	1
ViT-B-16	Wanet	0.01	CIFAR10	0.9839	CIFAR100	0.8242	0.6848	1
ViT-B-16	Wanet	0.01	GTSRB	0.987806809	CIFAR100	0.6634	0.9564	1
ViT-B-16	Wanet	0.03	MNIST	0.9972	CIFAR100	0.7101	0.9383	1
ViT-B-16	Wanet	0.03	SVHN	0.977066687	CIFAR100	0.6414	0.7851	1
ViT-B-16	Wanet	0.03	CIFAR10	0.9828	CIFAR100	0.8106	0.7154	1
ViT-B-16	Wanet	0.03	GTSRB	0.986223278	CIFAR100	0.6449	0.9698	1
ViT-B-16	Wanet	0.05	MNIST	0.9972	CIFAR100	0.7101	0.9531	1
ViT-B-16	Wanet	0.05	SVHN	0.976682545	CIFAR100	0.6492	0.8098	1
ViT-B-16	Wanet	0.05	CIFAR10	0.983	CIFAR100	0.8135	0.7623	1
ViT-B-16	Wanet	0.05	GTSRB	0.986064925	CIFAR100	0.6538	0.9676	1
ViT-B-16	Wanet	0.1	MNIST	0.997	CIFAR100	0.7066	0.968	1
ViT-B-16	Wanet	0.1	SVHN	0.97691303	CIFAR100	0.6542	0.874	1
ViT-B-16	Wanet	0.1	CIFAR10	0.9833	CIFAR100	0.809	0.7796	1
ViT-B-16	Wanet	0.1	GTSRB	0.986539984	CIFAR100	0.6619	0.9819	1
ViT-B-16	Wanet	0.15	MNIST	0.9972	CIFAR100	0.7053	0.9581	1
ViT-B-16	Wanet	0.15	SVHN	0.977489244	CIFAR100	0.6468	0.8136	1
ViT-B-16	Wanet	0.15	CIFAR10	0.9832	CIFAR100	0.8098	0.726	1
ViT-B-16	Wanet	0.15	GTSRB	0.985827395	CIFAR100	0.6553	0.9788	1
ViT-B-16	Wanet	0.01	MNIST	0.9958	GTSRB	0.872525732	0.432620744	1
ViT-B-16	Wanet	0.01	SVHN	0.966733251	GTSRB	0.912430721	0.488044339	1
ViT-B-16	Wanet	0.01	CIFAR10	0.9628	GTSRB	0.973634204	0.659857482	1
ViT-B-16	Wanet	0.01	CIFAR100	0.7721	GTSRB	0.97695962	0.78939034	1
ViT-B-16	Wanet	0.03	MNIST	0.9952	GTSRB	0.862945368	0.4050673	1
ViT-B-16	Wanet	0.03	SVHN	0.961893055	GTSRB	0.900079177	0.581551861	1

Model Structure	Attack Method	Poison Rate	Clean Dataset	Clean Acc	Poison Dataset	Poison Acc	ASR	cof
ViT-B-16	Wanet	0.03	CIFAR10	0.9661	GTSRB	0.963024545	0.589786223	1
ViT-B-16	Wanet	0.03	CIFAR100	0.7775	GTSRB	0.973713381	0.750752177	1
ViT-B-16	Wanet	0.05	MNIST	0.9962	GTSRB	0.871733967	0.655265241	1
ViT-B-16	Wanet	0.05	SVHN	0.962891825	GTSRB	0.890340459	0.651860649	1
ViT-B-16	Wanet	0.05	CIFAR10	0.9677	GTSRB	0.95621536	0.714885194	1
ViT-B-16	Wanet	0.05	CIFAR100	0.7971	GTSRB	0.965479018	0.836025337	1
ViT-B-16	Wanet	0.1	MNIST	0.9944	GTSRB	0.901346002	0.722882027	1
ViT-B-16	Wanet	0.1	SVHN	0.957283344	GTSRB	0.908946952	0.722169438	1
ViT-B-16	Wanet	0.1	CIFAR10	0.9651	GTSRB	0.96128266	0.822723674	1
ViT-B-16	Wanet	0.1	CIFAR100	0.7786	GTSRB	0.973317498	0.936737926	1
ViT-B-16	Wanet	0.15	MNIST	0.9951	GTSRB	0.918923199	0.768329375	1
ViT-B-16	Wanet	0.15	SVHN	0.955247388	GTSRB	0.947901821	0.736658749	1
ViT-B-16	Wanet	0.15	CIFAR10	0.9616	GTSRB	0.963262074	0.850197941	1
ViT-B-16	Wanet	0.15	CIFAR100	0.7734	GTSRB	0.971575614	0.937767221	1
ViT-B-16	BadNets	0.01	SVHN	0.964697296	MNIST	0.9935	0.9994	1
ViT-B-16	BadNets	0.01	CIFAR10	0.9738	MNIST	0.9952	1	1
ViT-B-16	BadNets	0.01	CIFAR100	0.8404	MNIST	0.9955	1	1
ViT-B-16	BadNets	0.01	GTSRB	0.955186065	MNIST	0.9931	1	1
ViT-B-16	BadNets	0.01	MNIST	0.9962	SVHN	0.909880148	0.999308543	1
ViT-B-16	BadNets	0.01	CIFAR10	0.9701	SVHN	0.965926552	1	1
ViT-B-16	BadNets	0.01	CIFAR100	0.8171	SVHN	0.971727105	1	1
ViT-B-16	BadNets	0.01	GTSRB	0.980285036	SVHN	0.951213891	1	1
ViT-B-16	BadNets	0.01	MNIST	0.9967	CIFAR10	0.9417	1	1
ViT-B-16	BadNets	0.01	SVHN	0.975568531	CIFAR10	0.9169	1	1
ViT-B-16	BadNets	0.01	CIFAR100	0.8665	CIFAR10	0.9796	1	1
ViT-B-16	BadNets	0.01	GTSRB	0.986619161	CIFAR10	0.9362	1	1
ViT-B-16	BadNets	0.01	MNIST	0.9972	CIFAR100	0.7259	0.9887	1
ViT-B-16	BadNets	0.01	SVHN	0.97745083	CIFAR100	0.6566	0.0132	1
ViT-B-16	BadNets	0.01	CIFAR10	0.9845	CIFAR100	0.8252	0.9564	1
ViT-B-16	BadNets	0.01	GTSRB	0.989548694	CIFAR100	0.6928	0.9522	1
ViT-B-16	BadNets	0.01	MNIST	0.9965	GTSRB	0.877355503	0.645368171	1
ViT-B-16	BadNets	0.01	SVHN	0.967309465	GTSRB	0.946951702	0.459065717	1
ViT-B-16	BadNets	0.01	CIFAR10	0.9617	GTSRB	0.97212985	0.598653998	1
ViT-B-16	BadNets	0.01	CIFAR100	0.7902	GTSRB	0.975930325	0.878780681	1
ViT-B-16	Blend	0.01	SVHN	0.964121082	MNIST	0.9936	0.124	1
ViT-B-16	Blend	0.01	CIFAR10	0.973	MNIST	0.9952	1	1
ViT-B-16	Blend	0.01	CIFAR100	0.8392	MNIST	0.9957	1	1
ViT-B-16	Blend	0.01	GTSRB	0.95621536	MNIST	0.9938	0.433	1
ViT-B-16	Blend	0.01	MNIST	0.996	SVHN	0.910763675	0.819683467	1
ViT-B-16	Blend	0.01	CIFAR10	0.9719	SVHN	0.966233866	0.999615857	1
ViT-B-16	Blend	0.01	CIFAR100	0.8161	SVHN	0.972725876	0.999692686	1
ViT-B-16	Blend	0.01	GTSRB	0.98226445	SVHN	0.953595575	0.926321451	1
ViT-B-16	Blend	0.01	MNIST	0.9964	CIFAR10	0.9407	0.9838	1
ViT-B-16	Blend	0.01	SVHN	0.973955132	CIFAR10	0.9199	0.9053	1
ViT-B-16	Blend	0.01	CIFAR100	0.8668	CIFAR10	0.9795	0.8788	1
ViT-B-16	Blend	0.01	GTSRB	0.986777514	CIFAR10	0.9356	0.9872	1
ViT-B-16	Blend	0.01	MNIST	0.9972	CIFAR100	0.7223	0.8781	1
ViT-B-16	Blend	0.01	SVHN	0.978372772	CIFAR100	0.6519	0.6515	1
ViT-B-16	Blend	0.01	CIFAR10	0.984	CIFAR100	0.8261	0.5316	1
ViT-B-16	Blend	0.01	GTSRB	0.987885986	CIFAR100	0.6767	0.8159	1

Model Structure	Attack Method	Poison Rate	Clean Dataset	Clean Acc	Poison Dataset	Poison Acc	ASR	cof
ViT-B-16	Blend	0.01	MNIST	0.9961	GTSRB	0.832066508	0.840934283	1
ViT-B-16	Blend	0.01	SVHN	0.971304548	GTSRB	0.927949327	0.672446556	1
ViT-B-16	Blend	0.01	CIFAR10	0.9694	GTSRB	0.972050673	0.955819477	1
ViT-B-16	Blend	0.01	CIFAR100	0.8157	GTSRB	0.974109264	0.987806809	1
ViT-B-16	narcissus	0.01	CIFAR100	0.8181	GTSRB	0.972446556	0.870783848	1
ViT-B-16	narcissus	0.03	CIFAR100	0.812	GTSRB	0.981076801	0.882185273	1
ViT-B-16	narcissus	0.05	CIFAR100	0.8004	GTSRB	0.976880443	0.839667458	1
ViT-B-16	narcissus	0.1	CIFAR100	0.8198	GTSRB	0.974821853	0.907521774	1
ViT-B-16	dynamic_bd	0.01	CIFAR10	0.9799	CIFAR100	0.8556	0.9998	1
ViT-B-16	dynamic_bd	0.03	CIFAR10	0.9799	CIFAR100	0.845	0.9992	1
ViT-B-16	dynamic_bd	0.05	CIFAR10	0.9809	CIFAR100	0.8478	0.9997	1
ViT-B-16	dynamic_bd	0.1	CIFAR10	0.9815	CIFAR100	0.8445	0.9996	1
ViT-B-16	dynamic_bd	0.01	CIFAR10	0.9538	GTSRB	0.9802	0.998	1
ViT-B-16	dynamic_bd	0.03	CIFAR10	0.9383	GTSRB	0.9689	0.9999	1
ViT-B-16	dynamic_bd	0.05	CIFAR10	0.9403	GTSRB	0.9717	0.9998	1
ViT-B-16	dynamic_bd	0.1	CIFAR10	0.9319	GTSRB	0.9669	0.9999	1
ViT-B-16	dynamic_bd	0.01	CIFAR10	0.9425	MNIST	0.9964	0.9999	1
ViT-B-16	dynamic_bd	0.03	CIFAR10	0.9476	MNIST	0.9959	1	1
ViT-B-16	dynamic_bd	0.05	CIFAR10	0.9456	MNIST	0.9946	1	1
ViT-B-16	dynamic_bd	0.1	CIFAR10	0.945	MNIST	0.9958	1	1
ViT-B-16	dynamic_bd	0.01	CIFAR10	0.939	SVHN	0.9685	1	1
ViT-B-16	dynamic_bd	0.03	CIFAR10	0.9454	SVHN	0.9514	1	1
ViT-B-16	dynamic_bd	0.05	CIFAR10	0.9367	SVHN	0.9537	1	1
ViT-B-16	dynamic_bd	0.1	CIFAR10	0.9406	SVHN	0.9547	0.9997	1
ViT-B-16	dynamic_bd	0.01	CIFAR100	0.8331	CIFAR10	0.984	0.9999	1
ViT-B-16	dynamic_bd	0.03	CIFAR100	0.8339	CIFAR10	0.9828	0.9963	1
ViT-B-16	dynamic_bd	0.05	CIFAR100	0.8345	CIFAR10	0.9824	0.9979	1
ViT-B-16	dynamic_bd	0.1	CIFAR100	0.8304	CIFAR10	0.9799	0.9994	1
ViT-B-16	dynamic_bd	0.01	CIFAR100	0.7582	GTSRB	0.9838	0.9984	1
ViT-B-16	dynamic_bd	0.03	CIFAR100	0.7149	GTSRB	0.9743	1	1
ViT-B-16	dynamic_bd	0.05	CIFAR100	0.7121	GTSRB	0.9778	0.9998	1
ViT-B-16	dynamic_bd	0.1	CIFAR100	0.7061	GTSRB	0.9762	0.9999	1
ViT-B-16	dynamic_bd	0.01	CIFAR100	0.7455	MNIST	0.9966	1	1
ViT-B-16	dynamic_bd	0.03	CIFAR100	0.7484	MNIST	0.9969	1	1
ViT-B-16	dynamic_bd	0.05	CIFAR100	0.7565	MNIST	0.9959	1	1
ViT-B-16	dynamic_bd	0.1	CIFAR100	0.7409	MNIST	0.9961	1	1
ViT-B-16	dynamic_bd	0.01	CIFAR100	0.6957	SVHN	0.9721	1	1
ViT-B-16	dynamic_bd	0.03	CIFAR100	0.7101	SVHN	0.9582	1	1
ViT-B-16	dynamic_bd	0.05	CIFAR100	0.7034	SVHN	0.9585	1	1
ViT-B-16	dynamic_bd	0.1	CIFAR100	0.7086	SVHN	0.9576	0.9997	1
ViT-B-16	dynamic_bd	0.01	GTSRB	0.9746	CIFAR10	0.97	1	1
ViT-B-16	dynamic_bd	0.03	GTSRB	0.9687	CIFAR10	0.9675	1	1
ViT-B-16	dynamic_bd	0.05	GTSRB	0.9749	CIFAR10	0.97	0.9999	1
ViT-B-16	dynamic_bd	0.1	GTSRB	0.974	CIFAR10	0.9639	1	1
ViT-B-16	dynamic_bd	0.01	GTSRB	0.9798	CIFAR100	0.7986	0.9999	1
ViT-B-16	dynamic_bd	0.03	GTSRB	0.9795	CIFAR100	0.7754	1	1
ViT-B-16	dynamic_bd	0.05	GTSRB	0.9797	CIFAR100	0.7864	1	1
ViT-B-16	dynamic_bd	0.1	GTSRB	0.9796	CIFAR100	0.7799	1	1
ViT-B-16	dynamic_bd	0.01	GTSRB	0.9463	MNIST	0.9953	0.9992	1
ViT-B-16	dynamic_bd	0.03	GTSRB	0.9378	MNIST	0.9954	1	1

Model Structure	Attack Method	Poison Rate	Clean Dataset	Clean Acc	Poison Dataset	Poison Acc	ASR	cof
ViT-B-16	dynamic_bd	0.05	GTSRB	0.9458	MNIST	0.9947	0.9997	1
ViT-B-16	dynamic_bd	0.1	GTSRB	0.94	MNIST	0.9955	1	1
ViT-B-16	dynamic_bd	0.01	GTSRB	0.9524	SVHN	0.9632	0.9999	1
ViT-B-16	dynamic_bd	0.03	GTSRB	0.9534	SVHN	0.9518	1	1
ViT-B-16	dynamic_bd	0.05	GTSRB	0.9565	SVHN	0.9511	1	1
ViT-B-16	dynamic_bd	0.1	GTSRB	0.953	SVHN	0.9464	0.9995	1
ViT-B-16	dynamic_bd	0.01	MNIST	0.9935	CIFAR10	0.9679	1	1
ViT-B-16	dynamic_bd	0.03	MNIST	0.9949	CIFAR10	0.9633	0.9996	1
ViT-B-16	dynamic_bd	0.05	MNIST	0.9938	CIFAR10	0.9658	0.9998	1
ViT-B-16	dynamic_bd	0.1	MNIST	0.9942	CIFAR10	0.9595	1	1
ViT-B-16	dynamic_bd	0.01	MNIST	0.9958	CIFAR100	0.8184	0.9997	1
ViT-B-16	dynamic_bd	0.03	MNIST	0.9956	CIFAR100	0.8059	0.9999	1
ViT-B-16	dynamic_bd	0.05	MNIST	0.9955	CIFAR100	0.8093	0.9999	1
ViT-B-16	dynamic_bd	0.1	MNIST	0.9961	CIFAR100	0.8062	0.9999	1
ViT-B-16	dynamic_bd	0.01	MNIST	0.9951	GTSRB	0.9613	0.9972	1
ViT-B-16	dynamic_bd	0.03	MNIST	0.9908	GTSRB	0.9521	0.9997	1
ViT-B-16	dynamic_bd	0.05	MNIST	0.9913	GTSRB	0.9653	0.9995	1
ViT-B-16	dynamic_bd	0.1	MNIST	0.9935	GTSRB	0.9542	0.9997	1
ViT-B-16	dynamic_bd	0.01	MNIST	0.9934	SVHN	0.9673	0.9997	1
ViT-B-16	dynamic_bd	0.03	MNIST	0.9927	SVHN	0.9548	0.9999	1
ViT-B-16	dynamic_bd	0.05	MNIST	0.9937	SVHN	0.9578	1	1
ViT-B-16	dynamic_bd	0.1	MNIST	0.9928	SVHN	0.9536	0.9997	1
ViT-B-16	dynamic_bd	0.01	SVHN	0.9668	CIFAR10	0.9714	0.9996	1
ViT-B-16	dynamic_bd	0.03	SVHN	0.9624	CIFAR10	0.9685	0.9985	1
ViT-B-16	dynamic_bd	0.05	SVHN	0.9617	CIFAR10	0.9699	0.9988	1
ViT-B-16	dynamic_bd	0.1	SVHN	0.9626	CIFAR10	0.9656	1	1
ViT-B-16	dynamic_bd	0.01	SVHN	0.9741	CIFAR100	0.7999	0.9994	1
ViT-B-16	dynamic_bd	0.03	SVHN	0.9726	CIFAR100	0.7914	0.9995	1
ViT-B-16	dynamic_bd	0.05	SVHN	0.9726	CIFAR100	0.7941	0.9999	1
ViT-B-16	dynamic_bd	0.1	SVHN	0.9716	CIFAR100	0.796	1	1
ViT-B-16	dynamic_bd	0.01	SVHN	0.9587	GTSRB	0.9702	0.9967	1
ViT-B-16	dynamic_bd	0.03	SVHN	0.9326	GTSRB	0.9743	0.9998	1
ViT-B-16	dynamic_bd	0.05	SVHN	0.9263	GTSRB	0.9767	0.9997	1
ViT-B-16	dynamic_bd	0.1	SVHN	0.9278	GTSRB	0.9736	0.9997	1
ViT-B-16	dynamic_bd	0.01	SVHN	0.9146	MNIST	0.9958	0.9988	1
ViT-B-16	dynamic_bd	0.03	SVHN	0.9436	MNIST	0.9954	0.9999	1
ViT-B-16	dynamic_bd	0.05	SVHN	0.9455	MNIST	0.9953	0.9994	1
ViT-B-16	dynamic_bd	0.1	SVHN	0.9476	MNIST	0.9955	1	1
ViT-B-16	narcissus	0.05	CIFAR10	0.9961	GTSRB	0.889152811	0.780205859	1
ViT-B-16	narcissus	0.05	MNIST	0.967962508	GTSRB	0.936104513	0.426444972	1
ViT-B-16	narcissus	0.05	SVHN	0.9581	GTSRB	0.970783848	0.776009501	1

Table 6: Comparison of results for different combinations of a single BTV trained with various backdoor attacks on Convnext Base, and a single CTV with different poison rates, across five datasets.

Model Structure	Attack Method	Poison Rate	Clean Dataset	Clean Acc	Poison Dataset	Poison Acc	ASR	cof
convnext_base	BadNets	0.01	SVHN	0.92659035	MNIST	0.9947	1	1
convnext_base	BadNets	0.01	CIFAR10	0.9514	MNIST	0.9962	1	1
convnext_base	BadNets	0.01	CIFAR100	0.7476	MNIST	0.9963	1	1
convnext_base	BadNets	0.01	GTSRB	0.970783848	MNIST	0.9934	1	1
convnext_base	BadNets	0.03	SVHN	0.898471112	MNIST	0.993	1	1
convnext_base	BadNets	0.03	CIFAR10	0.9457	MNIST	0.9947	1	1
convnext_base	BadNets	0.03	CIFAR100	0.7426	MNIST	0.996	1	1
convnext_base	BadNets	0.03	GTSRB	0.972525732	MNIST	0.992	1	1
convnext_base	BadNets	0.05	SVHN	0.888099262	MNIST	0.9935	1	1
convnext_base	BadNets	0.05	CIFAR10	0.9566	MNIST	0.9948	1	1
convnext_base	BadNets	0.05	CIFAR100	0.7631	MNIST	0.9952	1	1
convnext_base	BadNets	0.05	GTSRB	0.972921615	MNIST	0.9914	1	1
convnext_base	BadNets	0.1	SVHN	0.899277812	MNIST	0.9932	1	1
convnext_base	BadNets	0.1	CIFAR10	0.9481	MNIST	0.9942	1	1
convnext_base	BadNets	0.1	CIFAR100	0.7535	MNIST	0.9947	1	1
convnext_base	BadNets	0.1	GTSRB	0.967695962	MNIST	0.9893	1	1
convnext_base	BadNets	0.15	SVHN	0.897625999	MNIST	0.9933	1	1
convnext_base	BadNets	0.15	CIFAR10	0.9459	MNIST	0.9947	1	1
convnext_base	BadNets	0.15	CIFAR100	0.7372	MNIST	0.9951	1	1
convnext_base	BadNets	0.15	GTSRB	0.967458432	MNIST	0.9928	1	1
convnext_base	BadNets	0.01	MNIST	0.9943	SVHN	0.919867855	1	1
convnext_base	BadNets	0.01	CIFAR10	0.9515	SVHN	0.958627843	1	1
convnext_base	BadNets	0.01	CIFAR100	0.7434	SVHN	0.963007068	1	1
convnext_base	BadNets	0.01	GTSRB	0.971338084	SVHN	0.942455439	1	1
convnext_base	BadNets	0.03	MNIST	0.9926	SVHN	0.898048556	1	1
convnext_base	BadNets	0.03	CIFAR10	0.9528	SVHN	0.930239705	1	1
convnext_base	BadNets	0.03	CIFAR100	0.7438	SVHN	0.939535956	1	1
convnext_base	BadNets	0.03	GTSRB	0.971021378	SVHN	0.927512293	1	1
convnext_base	BadNets	0.05	MNIST	0.9927	SVHN	0.886370621	1	1
convnext_base	BadNets	0.05	CIFAR10	0.9525	SVHN	0.916833128	1	1
convnext_base	BadNets	0.05	CIFAR100	0.7495	SVHN	0.92505378	1	1
convnext_base	BadNets	0.05	GTSRB	0.973159145	SVHN	0.922287953	1	1
convnext_base	BadNets	0.1	MNIST	0.9919	SVHN	0.890903503	1	1
convnext_base	BadNets	0.1	CIFAR10	0.9442	SVHN	0.910840504	1	1
convnext_base	BadNets	0.1	CIFAR100	0.7322	SVHN	0.921212354	1	1
convnext_base	BadNets	0.1	GTSRB	0.968646081	SVHN	0.917486171	1	1
convnext_base	BadNets	0.15	MNIST	0.9914	SVHN	0.888022434	1	1
convnext_base	BadNets	0.15	CIFAR10	0.9502	SVHN	0.911839275	1	1
convnext_base	BadNets	0.15	CIFAR100	0.7407	SVHN	0.920328826	1	1
convnext_base	BadNets	0.15	GTSRB	0.966429137	SVHN	0.917524585	1	1
convnext_base	BadNets	0.01	MNIST	0.9968	CIFAR10	0.9532	1	1
convnext_base	BadNets	0.01	SVHN	0.96058697	CIFAR10	0.9513	1	1
convnext_base	BadNets	0.01	CIFAR100	0.8384	CIFAR10	0.9738	1	1
convnext_base	BadNets	0.01	GTSRB	0.984956453	CIFAR10	0.8497	1	1
convnext_base	BadNets	0.03	MNIST	0.9959	CIFAR10	0.9547	1	1
convnext_base	BadNets	0.03	SVHN	0.952673632	CIFAR10	0.9561	1	1



Model Structure	Attack Method	Poison Rate	Clean Dataset	Clean Acc	Poison Dataset	Poison Acc	ASR	cof
convnext_base	BadNets	0.03	CIFAR100	0.8288	CIFAR10	0.9742	1	1
convnext_base	BadNets	0.03	GTSRB	0.984402217	CIFAR10	0.8699	1	1
convnext_base	BadNets	0.05	MNIST	0.996	CIFAR10	0.9479	1	1
convnext_base	BadNets	0.05	SVHN	0.952251076	CIFAR10	0.9531	1	1
convnext_base	BadNets	0.05	CIFAR100	0.8227	CIFAR10	0.9711	1	1
convnext_base	BadNets	0.05	GTSRB	0.985193983	CIFAR10	0.8676	1	1
convnext_base	BadNets	0.1	MNIST	0.9955	CIFAR10	0.946	1	1
convnext_base	BadNets	0.1	SVHN	0.948371235	CIFAR10	0.9548	1	1
convnext_base	BadNets	0.1	CIFAR100	0.8177	CIFAR10	0.9724	1	1
convnext_base	BadNets	0.1	GTSRB	0.984639747	CIFAR10	0.8678	1	1
convnext_base	BadNets	0.15	MNIST	0.9952	CIFAR10	0.9489	1	1
convnext_base	BadNets	0.15	SVHN	0.951329133	CIFAR10	0.9516	1	1
convnext_base	BadNets	0.15	CIFAR100	0.8228	CIFAR10	0.973	1	1
convnext_base	BadNets	0.15	GTSRB	0.984085511	CIFAR10	0.8777	1	1
convnext_base	BadNets	0.01	MNIST	0.9964	CIFAR100	0.768	1	1
convnext_base	BadNets	0.01	SVHN	0.962085126	CIFAR100	0.7479	1	1
convnext_base	BadNets	0.01	CIFAR10	0.9761	CIFAR100	0.8383	1	1
convnext_base	BadNets	0.01	GTSRB	0.987173397	CIFAR100	0.5614	1	1
convnext_base	BadNets	0.03	MNIST	0.9959	CIFAR100	0.7861	1	1
convnext_base	BadNets	0.03	SVHN	0.95382606	CIFAR100	0.7704	0.9999	1
convnext_base	BadNets	0.03	CIFAR10	0.9754	CIFAR100	0.8358	0.9999	1
convnext_base	BadNets	0.03	GTSRB	0.986144101	CIFAR100	0.5822	1	1
convnext_base	BadNets	0.05	MNIST	0.9957	CIFAR100	0.7825	1	1
convnext_base	BadNets	0.05	SVHN	0.949446835	CIFAR100	0.7644	0.9999	1
convnext_base	BadNets	0.05	CIFAR10	0.9753	CIFAR100	0.828	0.9999	1
convnext_base	BadNets	0.05	GTSRB	0.986064925	CIFAR100	0.5917	0.9997	1
convnext_base	BadNets	0.1	MNIST	0.9955	CIFAR100	0.7801	1	1
convnext_base	BadNets	0.1	SVHN	0.949177935	CIFAR100	0.76	1	1
convnext_base	BadNets	0.1	CIFAR10	0.9748	CIFAR100	0.8265	1	1
convnext_base	BadNets	0.1	GTSRB	0.987173397	CIFAR100	0.5964	1	1
convnext_base	BadNets	0.15	MNIST	0.9958	CIFAR100	0.7785	1	1
convnext_base	BadNets	0.15	SVHN	0.94840965	CIFAR100	0.7615	1	1
convnext_base	BadNets	0.15	CIFAR10	0.9741	CIFAR100	0.8253	1	1
convnext_base	BadNets	0.15	GTSRB	0.987410926	CIFAR100	0.588	1	1
convnext_base	BadNets	0.01	MNIST	0.9932	GTSRB	0.975138559	0.999841647	1
convnext_base	BadNets	0.01	SVHN	0.939228642	GTSRB	0.979572447	1	1
convnext_base	BadNets	0.01	CIFAR10	0.8334	GTSRB	0.985748219	1	1
convnext_base	BadNets	0.01	CIFAR100	0.4978	GTSRB	0.986223278	1	1
convnext_base	BadNets	0.03	MNIST	0.9873	GTSRB	0.976642914	1	1
convnext_base	BadNets	0.03	SVHN	0.880032268	GTSRB	0.977751386	1	1
convnext_base	BadNets	0.03	CIFAR10	0.8606	GTSRB	0.980126683	1	1
convnext_base	BadNets	0.03	CIFAR100	0.532	GTSRB	0.982818686	1	1
convnext_base	BadNets	0.05	MNIST	0.986	GTSRB	0.972763262	1	1
convnext_base	BadNets	0.05	SVHN	0.865780578	GTSRB	0.9746635	1	1
convnext_base	BadNets	0.05	CIFAR10	0.8482	GTSRB	0.982977039	1	1
convnext_base	BadNets	0.05	CIFAR100	0.5104	GTSRB	0.982501979	1	1
convnext_base	BadNets	0.1	MNIST	0.9816	GTSRB	0.974742676	1	1
convnext_base	BadNets	0.1	SVHN	0.850069146	GTSRB	0.976326207	1	1
convnext_base	BadNets	0.1	CIFAR10	0.8471	GTSRB	0.982343626	1	1
convnext_base	BadNets	0.1	CIFAR100	0.5255	GTSRB	0.982581156	1	1

Model Structure	Attack Method	Poison Rate	Clean Dataset	Clean Acc	Poison Dataset	Poison Acc	ASR	cof
convnext_base	BadNets	0.15	MNIST	0.9861	GTSRB	0.97189232	1	1
convnext_base	BadNets	0.15	SVHN	0.850914259	GTSRB	0.973950911	1	1
convnext_base	BadNets	0.15	CIFAR10	0.8558	GTSRB	0.978147268	1	1
convnext_base	BadNets	0.15	CIFAR100	0.5276	GTSRB	0.977117973	1	1
convnext_base	Blend	0.01	SVHN	0.928242163	MNIST	0.9952	0.3702	1
convnext_base	Blend	0.01	CIFAR10	0.9588	MNIST	0.9963	1	1
convnext_base	Blend	0.01	CIFAR100	0.7796	MNIST	0.9966	1	1
convnext_base	Blend	0.01	GTSRB	0.9797308	MNIST	0.9933	0.2074	1
convnext_base	Blend	0.03	SVHN	0.92090504	MNIST	0.994	0.5016	1
convnext_base	Blend	0.03	CIFAR10	0.9609	MNIST	0.9955	1	1
convnext_base	Blend	0.03	CIFAR100	0.7917	MNIST	0.9955	1	1
convnext_base	Blend	0.03	GTSRB	0.978068092	MNIST	0.9935	0.2527	1
convnext_base	Blend	0.05	SVHN	0.929125691	MNIST	0.9944	0.5438	1
convnext_base	Blend	0.05	CIFAR10	0.9617	MNIST	0.9951	1	1
convnext_base	Blend	0.05	CIFAR100	0.8009	MNIST	0.9956	1	1
convnext_base	Blend	0.05	GTSRB	0.979018211	MNIST	0.9934	0.2626	1
convnext_base	Blend	0.1	SVHN	0.91468193	MNIST	0.9938	0.6584	1
convnext_base	Blend	0.1	CIFAR10	0.9581	MNIST	0.9952	1	1
convnext_base	Blend	0.1	CIFAR100	0.7869	MNIST	0.9956	1	1
convnext_base	Blend	0.1	GTSRB	0.977434679	MNIST	0.9921	0.3291	1
convnext_base	Blend	0.15	SVHN	0.904386908	MNIST	0.9933	0.4239	1
convnext_base	Blend	0.15	CIFAR10	0.959	MNIST	0.9947	1	1
convnext_base	Blend	0.15	CIFAR100	0.7929	MNIST	0.9951	1	1
convnext_base	Blend	0.15	GTSRB	0.976009501	MNIST	0.992	0.2518	1
convnext_base	Blend	0.01	MNIST	0.9945	SVHN	0.922249539	0.886677935	1
convnext_base	Blend	0.01	CIFAR10	0.9559	SVHN	0.955516288	0.999769514	1
convnext_base	Blend	0.01	CIFAR100	0.765	SVHN	0.961816226	0.999346958	1
convnext_base	Blend	0.01	GTSRB	0.973713381	SVHN	0.938806085	0.742893362	1
convnext_base	Blend	0.03	MNIST	0.993	SVHN	0.915027658	0.944414567	1
convnext_base	Blend	0.03	CIFAR10	0.9582	SVHN	0.934081131	0.999923171	1
convnext_base	Blend	0.03	CIFAR100	0.7655	SVHN	0.943761524	0.999769514	1
convnext_base	Blend	0.03	GTSRB	0.972684086	SVHN	0.929509834	0.822065151	1
convnext_base	Blend	0.05	MNIST	0.9934	SVHN	0.905193608	0.960356484	1
convnext_base	Blend	0.05	CIFAR10	0.9517	SVHN	0.925706822	1	1
convnext_base	Blend	0.05	CIFAR100	0.7509	SVHN	0.938998156	0.999961586	1
convnext_base	Blend	0.05	GTSRB	0.974901029	SVHN	0.925399508	0.853564843	1
convnext_base	Blend	0.1	MNIST	0.9931	SVHN	0.909419176	0.976567302	1
convnext_base	Blend	0.1	CIFAR10	0.9547	SVHN	0.922134296	1	1
convnext_base	Blend	0.1	CIFAR100	0.7646	SVHN	0.934273202	1	1
convnext_base	Blend	0.1	GTSRB	0.973634204	SVHN	0.921596497	0.912146589	1
convnext_base	Blend	0.15	MNIST	0.9929	SVHN	0.911877689	0.97249539	1
convnext_base	Blend	0.15	CIFAR10	0.9537	SVHN	0.909457591	1	1
convnext_base	Blend	0.15	CIFAR100	0.7609	SVHN	0.923862938	1	1
convnext_base	Blend	0.15	GTSRB	0.973159145	SVHN	0.920021512	0.887561463	1
convnext_base	Blend	0.01	MNIST	0.9964	CIFAR10	0.9542	0.9878	1
convnext_base	Blend	0.01	SVHN	0.961508912	CIFAR10	0.95	0.9907	1
convnext_base	Blend	0.01	CIFAR100	0.8375	CIFAR10	0.9752	0.9513	1
convnext_base	Blend	0.01	GTSRB	0.985193983	CIFAR10	0.8628	0.9229	1
convnext_base	Blend	0.03	MNIST	0.9961	CIFAR10	0.9465	0.9837	1
convnext_base	Blend	0.03	SVHN	0.960433313	CIFAR10	0.9509	0.9899	1

Model Structure	Attack Method	Poison Rate	Clean Dataset	Clean Acc	Poison Dataset	Poison Acc	ASR	cof
convnext_base	Blend	0.03	CIFAR100	0.8335	CIFAR10	0.9751	0.9415	1
convnext_base	Blend	0.03	GTSRB	0.985035629	CIFAR10	0.8747	0.9335	1
convnext_base	Blend	0.05	MNIST	0.9956	CIFAR10	0.9434	0.9849	1
convnext_base	Blend	0.05	SVHN	0.958090043	CIFAR10	0.9472	0.99	1
convnext_base	Blend	0.05	CIFAR100	0.8306	CIFAR10	0.9747	0.9448	1
convnext_base	Blend	0.05	GTSRB	0.984956453	CIFAR10	0.8823	0.9484	1
convnext_base	Blend	0.1	MNIST	0.9958	CIFAR10	0.9389	0.9945	1
convnext_base	Blend	0.1	SVHN	0.960010756	CIFAR10	0.943	0.9946	1
convnext_base	Blend	0.1	CIFAR100	0.818	CIFAR10	0.9712	0.9778	1
convnext_base	Blend	0.1	GTSRB	0.983847981	CIFAR10	0.883	0.9726	1
convnext_base	Blend	0.15	MNIST	0.9962	CIFAR10	0.9395	0.993	1
convnext_base	Blend	0.15	SVHN	0.96058697	CIFAR10	0.9416	0.9932	1
convnext_base	Blend	0.15	CIFAR100	0.8244	CIFAR10	0.972	0.978	1
convnext_base	Blend	0.15	GTSRB	0.985193983	CIFAR10	0.8703	0.974	1
convnext_base	Blend	0.01	MNIST	0.9966	CIFAR100	0.7644	0.9926	1
convnext_base	Blend	0.01	SVHN	0.963429625	CIFAR100	0.7346	0.9874	1
convnext_base	Blend	0.01	CIFAR10	0.9769	CIFAR100	0.8405	0.9649	1
convnext_base	Blend	0.01	GTSRB	0.98709422	CIFAR100	0.5451	0.8645	1
convnext_base	Blend	0.03	MNIST	0.9962	CIFAR100	0.7687	0.9977	1
convnext_base	Blend	0.03	SVHN	0.959242471	CIFAR100	0.7401	0.9957	1
convnext_base	Blend	0.03	CIFAR10	0.9775	CIFAR100	0.8397	0.988	1
convnext_base	Blend	0.03	GTSRB	0.988123515	CIFAR100	0.5525	0.9272	1
convnext_base	Blend	0.05	MNIST	0.9967	CIFAR100	0.7581	0.9979	1
convnext_base	Blend	0.05	SVHN	0.962891825	CIFAR100	0.7236	0.995	1
convnext_base	Blend	0.05	CIFAR10	0.9781	CIFAR100	0.8366	0.9902	1
convnext_base	Blend	0.05	GTSRB	0.987173397	CIFAR100	0.5275	0.9138	1
convnext_base	Blend	0.1	MNIST	0.9961	CIFAR100	0.7554	0.9985	1
convnext_base	Blend	0.1	SVHN	0.961739398	CIFAR100	0.7209	0.9967	1
convnext_base	Blend	0.1	CIFAR10	0.977	CIFAR100	0.833	0.995	1
convnext_base	Blend	0.1	GTSRB	0.987410926	CIFAR100	0.5561	0.9544	1
convnext_base	Blend	0.15	MNIST	0.9958	CIFAR100	0.7577	0.9987	1
convnext_base	Blend	0.15	SVHN	0.961700983	CIFAR100	0.7198	0.9957	1
convnext_base	Blend	0.15	CIFAR10	0.9773	CIFAR100	0.8314	0.995	1
convnext_base	Blend	0.15	GTSRB	0.988123515	CIFAR100	0.5574	0.9577	1
convnext_base	Blend	0.01	MNIST	0.9921	GTSRB	0.973238321	0.913855899	1
convnext_base	Blend	0.01	SVHN	0.929010449	GTSRB	0.976880443	0.986460808	1
convnext_base	Blend	0.01	CIFAR10	0.8619	GTSRB	0.986935867	0.99517023	1
convnext_base	Blend	0.01	CIFAR100	0.5379	GTSRB	0.986777514	0.993982581	1
convnext_base	Blend	0.03	MNIST	0.9907	GTSRB	0.977672209	0.883372922	1
convnext_base	Blend	0.03	SVHN	0.912492317	GTSRB	0.975613618	0.973079968	1
convnext_base	Blend	0.03	CIFAR10	0.8636	GTSRB	0.987173397	0.991053048	1
convnext_base	Blend	0.03	CIFAR100	0.5535	GTSRB	0.987490103	0.991528108	1
convnext_base	Blend	0.05	MNIST	0.992	GTSRB	0.976009501	0.864766429	1
convnext_base	Blend	0.05	SVHN	0.914451444	GTSRB	0.975059382	0.968171021	1
convnext_base	Blend	0.05	CIFAR10	0.8529	GTSRB	0.986460808	0.985431512	1
convnext_base	Blend	0.05	CIFAR100	0.5283	GTSRB	0.987885986	0.984639747	1
convnext_base	Blend	0.1	MNIST	0.9908	GTSRB	0.973634204	0.866983373	1
convnext_base	Blend	0.1	SVHN	0.909611248	GTSRB	0.977276326	0.960095012	1
convnext_base	Blend	0.1	CIFAR10	0.863	GTSRB	0.985906572	0.9847981	1
convnext_base	Blend	0.1	CIFAR100	0.5382	GTSRB	0.986460808	0.983689628	1

Model Structure	Attack Method	Poison Rate	Clean Dataset	Clean Acc	Poison Dataset	Poison Acc	ASR	cof
convnext_base	Blend	0.15	MNIST	0.9891	GTSRB	0.972288203	0.808234363	1
convnext_base	Blend	0.15	SVHN	0.895974186	GTSRB	0.973238321	0.933729216	1
convnext_base	Blend	0.15	CIFAR10	0.8569	GTSRB	0.986935867	0.973713381	1
convnext_base	Blend	0.15	CIFAR100	0.5225	GTSRB	0.986777514	0.972842439	1
convnext_base	Wanet	0.01	SVHN	0.930508605	MNIST	0.9937	0.3604	1
convnext_base	Wanet	0.01	CIFAR10	0.9549	MNIST	0.9956	0.9394	1
convnext_base	Wanet	0.01	CIFAR100	0.7625	MNIST	0.996	0.9401	1
convnext_base	Wanet	0.01	GTSRB	0.977988915	MNIST	0.9924	0.1705	1
convnext_base	Wanet	0.03	SVHN	0.920482483	MNIST	0.9932	0.3782	1
convnext_base	Wanet	0.03	CIFAR10	0.9631	MNIST	0.9902	0.9842	1
convnext_base	Wanet	0.03	CIFAR100	0.7979	MNIST	0.9912	0.9792	1
convnext_base	Wanet	0.03	GTSRB	0.97672209	MNIST	0.9907	0.1973	1
convnext_base	Wanet	0.05	SVHN	0.927512293	MNIST	0.992	0.3074	1
convnext_base	Wanet	0.05	CIFAR10	0.9625	MNIST	0.9939	0.9739	1
convnext_base	Wanet	0.05	CIFAR100	0.7877	MNIST	0.9942	0.977	1
convnext_base	Wanet	0.05	GTSRB	0.977117973	MNIST	0.989	0.1838	1
convnext_base	Wanet	0.1	SVHN	0.93127689	MNIST	0.9922	0.4268	1
convnext_base	Wanet	0.1	CIFAR10	0.9609	MNIST	0.9888	0.99	1
convnext_base	Wanet	0.1	CIFAR100	0.7958	MNIST	0.9918	0.9907	1
convnext_base	Wanet	0.1	GTSRB	0.972921615	MNIST	0.9895	0.2185	1
convnext_base	Wanet	0.15	SVHN	0.927704364	MNIST	0.9922	0.6153	1
convnext_base	Wanet	0.15	CIFAR10	0.9623	MNIST	0.9896	0.9938	1
convnext_base	Wanet	0.15	CIFAR100	0.791	MNIST	0.9905	0.9936	1
convnext_base	Wanet	0.15	GTSRB	0.973317498	MNIST	0.9896	0.2429	1
convnext_base	Wanet	0.01	MNIST	0.9941	SVHN	0.913952059	0.377573755	1
convnext_base	Wanet	0.01	CIFAR10	0.9552	SVHN	0.9577059	0.906000307	1
convnext_base	Wanet	0.01	CIFAR100	0.7479	SVHN	0.961355255	0.927550707	1
convnext_base	Wanet	0.01	GTSRB	0.971100554	SVHN	0.93596343	0.111862323	1
convnext_base	Wanet	0.03	MNIST	0.9926	SVHN	0.884449908	0.4587815	1
convnext_base	Wanet	0.03	CIFAR10	0.9548	SVHN	0.912377074	0.954133374	1
convnext_base	Wanet	0.03	CIFAR100	0.7584	SVHN	0.920136755	0.96392901	1
convnext_base	Wanet	0.03	GTSRB	0.969912906	SVHN	0.912684388	0.124001229	1
convnext_base	Wanet	0.05	MNIST	0.9924	SVHN	0.868853719	0.57494622	1
convnext_base	Wanet	0.05	CIFAR10	0.9507	SVHN	0.889712661	0.961931469	1
convnext_base	Wanet	0.05	CIFAR100	0.7477	SVHN	0.903733866	0.972917947	1
convnext_base	Wanet	0.05	GTSRB	0.96935867	SVHN	0.909419176	0.157229564	1
convnext_base	Wanet	0.1	MNIST	0.9916	SVHN	0.864820221	0.542870313	1
convnext_base	Wanet	0.1	CIFAR10	0.9569	SVHN	0.872003688	0.969806392	1
convnext_base	Wanet	0.1	CIFAR100	0.7644	SVHN	0.88898279	0.97664413	1
convnext_base	Wanet	0.1	GTSRB	0.96935867	SVHN	0.907805778	0.156077136	1
convnext_base	Wanet	0.15	MNIST	0.9915	SVHN	0.866510449	0.547249539	1
convnext_base	Wanet	0.15	CIFAR10	0.9505	SVHN	0.855293485	0.974953903	1
convnext_base	Wanet	0.15	CIFAR100	0.7571	SVHN	0.873809158	0.972418562	1
convnext_base	Wanet	0.15	GTSRB	0.968566904	SVHN	0.904079594	0.138829133	1
convnext_base	Wanet	0.01	MNIST	0.9964	CIFAR10	0.9491	0.8015	1
convnext_base	Wanet	0.01	SVHN	0.961931469	CIFAR10	0.9512	0.8211	1
convnext_base	Wanet	0.01	CIFAR100	0.8407	CIFAR10	0.9748	0.7069	1
convnext_base	Wanet	0.01	GTSRB	0.986064925	CIFAR10	0.8316	0.5354	1
convnext_base	Wanet	0.03	MNIST	0.9954	CIFAR10	0.9493	0.904	1
convnext_base	Wanet	0.03	SVHN	0.951866933	CIFAR10	0.9533	0.9078	1

Model Structure	Attack Method	Poison Rate	Clean Dataset	Clean Acc	Poison Dataset	Poison Acc	ASR	cof
convnext_base	Wanet	0.03	CIFAR100	0.8297	CIFAR10	0.9758	0.796	1
convnext_base	Wanet	0.03	GTSRB	0.983847981	CIFAR10	0.85	0.6565	1
convnext_base	Wanet	0.05	MNIST	0.9956	CIFAR10	0.9461	0.9045	1
convnext_base	Wanet	0.05	SVHN	0.950291948	CIFAR10	0.9552	0.9067	1
convnext_base	Wanet	0.05	CIFAR100	0.8233	CIFAR10	0.9703	0.8019	1
convnext_base	Wanet	0.05	GTSRB	0.983768804	CIFAR10	0.8669	0.7033	1
convnext_base	Wanet	0.1	MNIST	0.9956	CIFAR10	0.9296	0.9274	1
convnext_base	Wanet	0.1	SVHN	0.944683467	CIFAR10	0.9448	0.927	1
convnext_base	Wanet	0.1	CIFAR100	0.8215	CIFAR10	0.9688	0.8515	1
convnext_base	Wanet	0.1	GTSRB	0.983689628	CIFAR10	0.8418	0.775	1
convnext_base	Wanet	0.15	MNIST	0.9957	CIFAR10	0.9341	0.9178	1
convnext_base	Wanet	0.15	SVHN	0.947487707	CIFAR10	0.9502	0.9068	1
convnext_base	Wanet	0.15	CIFAR100	0.8239	CIFAR10	0.9691	0.8142	1
convnext_base	Wanet	0.15	GTSRB	0.984877276	CIFAR10	0.8526	0.7274	1
convnext_base	Wanet	0.01	MNIST	0.9967	CIFAR100	0.7628	0.6777	1
convnext_base	Wanet	0.01	SVHN	0.962200369	CIFAR100	0.7407	0.8159	1
convnext_base	Wanet	0.01	CIFAR10	0.9761	CIFAR100	0.8368	0.5159	1
convnext_base	Wanet	0.01	GTSRB	0.987490103	CIFAR100	0.5285	0.4494	1
convnext_base	Wanet	0.03	MNIST	0.9958	CIFAR100	0.783	0.8752	1
convnext_base	Wanet	0.03	SVHN	0.954171789	CIFAR100	0.7675	0.8751	1
convnext_base	Wanet	0.03	CIFAR10	0.9751	CIFAR100	0.8331	0.8241	1
convnext_base	Wanet	0.03	GTSRB	0.987015044	CIFAR100	0.5882	0.5684	1
convnext_base	Wanet	0.05	MNIST	0.9958	CIFAR100	0.7693	0.8897	1
convnext_base	Wanet	0.05	SVHN	0.952673632	CIFAR100	0.7534	0.893	1
convnext_base	Wanet	0.05	CIFAR10	0.975	CIFAR100	0.8261	0.8204	1
convnext_base	Wanet	0.05	GTSRB	0.98709422	CIFAR100	0.5626	0.6628	1
convnext_base	Wanet	0.1	MNIST	0.9952	CIFAR100	0.7722	0.908	1
convnext_base	Wanet	0.1	SVHN	0.951713276	CIFAR100	0.7533	0.892	1
convnext_base	Wanet	0.1	CIFAR10	0.9753	CIFAR100	0.824	0.8267	1
convnext_base	Wanet	0.1	GTSRB	0.98685669	CIFAR100	0.5814	0.7044	1
convnext_base	Wanet	0.15	MNIST	0.9952	CIFAR100	0.775	0.9162	1
convnext_base	Wanet	0.15	SVHN	0.946565765	CIFAR100	0.7518	0.9017	1
convnext_base	Wanet	0.15	CIFAR10	0.9757	CIFAR100	0.8201	0.8469	1
convnext_base	Wanet	0.15	GTSRB	0.986223278	CIFAR100	0.5833	0.7049	1
convnext_base	Wanet	0.01	MNIST	0.9928	GTSRB	0.974980206	0.694536817	1
convnext_base	Wanet	0.01	SVHN	0.928050092	GTSRB	0.975613618	0.752652415	1
convnext_base	Wanet	0.01	CIFAR10	0.8614	GTSRB	0.985669042	0.892715756	1
convnext_base	Wanet	0.01	CIFAR100	0.5473	GTSRB	0.986619161	0.87695962	1
convnext_base	Wanet	0.03	MNIST	0.9837	GTSRB	0.975771971	0.701662708	1
convnext_base	Wanet	0.03	SVHN	0.849915489	GTSRB	0.977276326	0.716627078	1
convnext_base	Wanet	0.03	CIFAR10	0.8688	GTSRB	0.979176564	0.856057007	1
convnext_base	Wanet	0.03	CIFAR100	0.5701	GTSRB	0.980205859	0.847901821	1
convnext_base	Wanet	0.05	MNIST	0.9854	GTSRB	0.97442597	0.703642122	1
convnext_base	Wanet	0.05	SVHN	0.847917947	GTSRB	0.97672209	0.707046714	1
convnext_base	Wanet	0.05	CIFAR10	0.8675	GTSRB	0.980285036	0.875534442	1
convnext_base	Wanet	0.05	CIFAR100	0.5575	GTSRB	0.97949327	0.855423595	1
convnext_base	Wanet	0.1	MNIST	0.9821	GTSRB	0.975534442	0.707680127	1
convnext_base	Wanet	0.1	SVHN	0.825522434	GTSRB	0.976880443	0.712747427	1
convnext_base	Wanet	0.1	CIFAR10	0.8707	GTSRB	0.976801267	0.824386382	1
convnext_base	Wanet	0.1	CIFAR100	0.5758	GTSRB	0.978384798	0.799920823	1

Model Structure	Attack Method	Poison Rate	Clean Dataset	Clean Acc	Poison Dataset	Poison Acc	ASR	cof
convnext_base	Wanet	0.15	MNIST	0.979	GTSRB	0.976167854	0.771496437	1
convnext_base	Wanet	0.15	SVHN	0.802320221	GTSRB	0.975296912	0.766033254	1
convnext_base	Wanet	0.15	CIFAR10	0.8849	GTSRB	0.975930325	0.88685669	1
convnext_base	Wanet	0.15	CIFAR100	0.5886	GTSRB	0.977513856	0.855027712	1
convnext_base	narcissus	0.01	CIFAR100	0.5411	GTSRB	0.98456057	0.628186857	1
convnext_base	narcissus	0.03	CIFAR100	0.5511	GTSRB	0.984877276	0.482422803	1
convnext_base	narcissus	0.05	CIFAR100	0.5743	GTSRB	0.981631037	0.809659541	1
convnext_base	narcissus	0.1	CIFAR100	0.5614	GTSRB	0.98432304	0.778939034	1
convnext_base	dynamic_bd	0.01	CIFAR100	0.5622	GTSRB	0.987569279	0.9949327	1
convnext_base	dynamic_bd	0.03	CIFAR100	0.5564	GTSRB	0.982581156	0.999841647	1
convnext_base	dynamic_bd	0.05	CIFAR100	0.548	GTSRB	0.982818686	0.99976247	1
convnext_base	dynamic_bd	0.1	CIFAR100	0.523	GTSRB	0.9797308	0.999920823	1

Table 7: Comparison of results for different combinations of a single BTW trained with various backdoor attacks on ViT-B-32, and a single CTV with different poison rates, across five datasets.

Model Structure	Attack Method	Poison Rate	Clean Dataset	Clean Acc	Poison Dataset	Poison Acc	ASR	cof
ViT-B-32	BadNets	0.01	SVHN	0.955477873	MNIST	0.9881	0	1
ViT-B-32	BadNets	0.01	CIFAR10	0.9511	MNIST	0.9929	1	1
ViT-B-32	BadNets	0.01	CIFAR100	0.7709	MNIST	0.9949	1	1
ViT-B-32	BadNets	0.01	GTSRB	0.959857482	MNIST	0.9847	1	1
ViT-B-32	BadNets	0.03	SVHN	0.941533497	MNIST	0.9881	0	1
ViT-B-32	BadNets	0.03	CIFAR10	0.9547	MNIST	0.9894	1	1
ViT-B-32	BadNets	0.03	CIFAR100	0.7851	MNIST	0.992	1	1
ViT-B-32	BadNets	0.03	GTSRB	0.954869359	MNIST	0.9841	1	1
ViT-B-32	BadNets	0.05	SVHN	0.942263368	MNIST	0.9853	0	1
ViT-B-32	BadNets	0.05	CIFAR10	0.9526	MNIST	0.9908	1	1
ViT-B-32	BadNets	0.05	CIFAR100	0.7701	MNIST	0.9931	1	1
ViT-B-32	BadNets	0.05	GTSRB	0.943072051	MNIST	0.9838	1	1
ViT-B-32	BadNets	0.1	SVHN	0.942570682	MNIST	0.9895	0	1
ViT-B-32	BadNets	0.1	CIFAR10	0.9476	MNIST	0.9897	1	1
ViT-B-32	BadNets	0.1	CIFAR100	0.775	MNIST	0.9927	1	1
ViT-B-32	BadNets	0.1	GTSRB	0.950593824	MNIST	0.985	1	1
ViT-B-32	BadNets	0.15	SVHN	0.934734173	MNIST	0.9874	0	1
ViT-B-32	BadNets	0.15	CIFAR10	0.9473	MNIST	0.9897	1	1
ViT-B-32	BadNets	0.15	CIFAR100	0.774	MNIST	0.9918	1	1
ViT-B-32	BadNets	0.15	GTSRB	0.933570863	MNIST	0.9828	1	1
ViT-B-32	BadNets	0.01	MNIST	0.9954	SVHN	0.880416411	0.999539029	1
ViT-B-32	BadNets	0.01	CIFAR10	0.9488	SVHN	0.942032883	1	1
ViT-B-32	BadNets	0.01	CIFAR100	0.7883	SVHN	0.952635218	1	1
ViT-B-32	BadNets	0.01	GTSRB	0.973079968	SVHN	0.912838045	0.999308543	1
ViT-B-32	BadNets	0.03	MNIST	0.9949	SVHN	0.836969883	1	1
ViT-B-32	BadNets	0.03	CIFAR10	0.9442	SVHN	0.873732329	1	1
ViT-B-32	BadNets	0.03	CIFAR100	0.7717	SVHN	0.900314997	1	1
ViT-B-32	BadNets	0.03	GTSRB	0.971733967	SVHN	0.873617087	0.035456361	1
ViT-B-32	BadNets	0.05	MNIST	0.9947	SVHN	0.85010756	1	1
ViT-B-32	BadNets	0.05	CIFAR10	0.9411	SVHN	0.865895821	1	1

Model Structure	Attack Method	Poison Rate	Clean Dataset	Clean Acc	Poison Dataset	Poison Acc	ASR	cof
ViT-B-32	BadNets	0.05	CIFAR100	0.7672	SVHN	0.89962354	1	1
ViT-B-32	BadNets	0.05	GTSRB	0.970387965	SVHN	0.87138906	0.031807007	1
ViT-B-32	BadNets	0.1	MNIST	0.9946	SVHN	0.846074063	1	1
ViT-B-32	BadNets	0.1	CIFAR10	0.9386	SVHN	0.875768285	1	1
ViT-B-32	BadNets	0.1	CIFAR100	0.7609	SVHN	0.897856484	1	1
ViT-B-32	BadNets	0.1	GTSRB	0.968804434	SVHN	0.881376767	0.991472034	1
ViT-B-32	BadNets	0.15	MNIST	0.9947	SVHN	0.849147203	1	1
ViT-B-32	BadNets	0.15	CIFAR10	0.9359	SVHN	0.872771973	1	1
ViT-B-32	BadNets	0.15	CIFAR100	0.7498	SVHN	0.893208359	1	1
ViT-B-32	BadNets	0.15	GTSRB	0.968171021	SVHN	0.872541487	0.745467117	1
ViT-B-32	BadNets	0.01	MNIST	0.9959	CIFAR10	0.9092	1	1
ViT-B-32	BadNets	0.01	SVHN	0.971381377	CIFAR10	0.9276	1	1
ViT-B-32	BadNets	0.01	CIFAR100	0.8406	CIFAR10	0.9708	1	1
ViT-B-32	BadNets	0.01	GTSRB	0.983214568	CIFAR10	0.9071	1	1
ViT-B-32	BadNets	0.03	MNIST	0.9953	CIFAR10	0.8834	1	1
ViT-B-32	BadNets	0.03	SVHN	0.96681008	CIFAR10	0.9117	0.9994	1
ViT-B-32	BadNets	0.03	CIFAR100	0.8109	CIFAR10	0.9643	1	1
ViT-B-32	BadNets	0.03	GTSRB	0.979018211	CIFAR10	0.878	1	1
ViT-B-32	BadNets	0.05	MNIST	0.9957	CIFAR10	0.865	1	1
ViT-B-32	BadNets	0.05	SVHN	0.967309465	CIFAR10	0.8934	1	1
ViT-B-32	BadNets	0.05	CIFAR100	0.7928	CIFAR10	0.9521	1	1
ViT-B-32	BadNets	0.05	GTSRB	0.962074426	CIFAR10	0.8493	1	1
ViT-B-32	BadNets	0.1	MNIST	0.9951	CIFAR10	0.8822	1	1
ViT-B-32	BadNets	0.1	SVHN	0.965081438	CIFAR10	0.9141	0.9994	1
ViT-B-32	BadNets	0.1	CIFAR100	0.7939	CIFAR10	0.9573	1	1
ViT-B-32	BadNets	0.1	GTSRB	0.977434679	CIFAR10	0.8813	1	1
ViT-B-32	BadNets	0.15	MNIST	0.9942	CIFAR10	0.8828	1	1
ViT-B-32	BadNets	0.15	SVHN	0.964850953	CIFAR10	0.9019	0.9998	1
ViT-B-32	BadNets	0.15	CIFAR100	0.791	CIFAR10	0.9485	1	1
ViT-B-32	BadNets	0.15	GTSRB	0.965716548	CIFAR10	0.8718	1	1
ViT-B-32	BadNets	0.01	MNIST	0.996	CIFAR100	0.6254	0	1
ViT-B-32	BadNets	0.01	SVHN	0.97357099	CIFAR100	0.6383	0.0006	1
ViT-B-32	BadNets	0.01	CIFAR10	0.9744	CIFAR100	0.8023	0.0151	1
ViT-B-32	BadNets	0.01	GTSRB	0.987015044	CIFAR100	0.6328	0.0117	1
ViT-B-32	BadNets	0.03	MNIST	0.9961	CIFAR100	0.5965	0	1
ViT-B-32	BadNets	0.03	SVHN	0.969844806	CIFAR100	0.6213	0	1
ViT-B-32	BadNets	0.03	CIFAR10	0.9722	CIFAR100	0.7746	0	1
ViT-B-32	BadNets	0.03	GTSRB	0.981710214	CIFAR100	0.5836	0	1
ViT-B-32	BadNets	0.05	MNIST	0.9963	CIFAR100	0.6023	0	1
ViT-B-32	BadNets	0.05	SVHN	0.967501537	CIFAR100	0.6238	0	1
ViT-B-32	BadNets	0.05	CIFAR10	0.9713	CIFAR100	0.7686	0	1
ViT-B-32	BadNets	0.05	GTSRB	0.973555028	CIFAR100	0.5969	0	1
ViT-B-32	BadNets	0.1	MNIST	0.9955	CIFAR100	0.5822	0	1
ViT-B-32	BadNets	0.1	SVHN	0.966771666	CIFAR100	0.6134	0	1
ViT-B-32	BadNets	0.1	CIFAR10	0.9701	CIFAR100	0.7632	0	1
ViT-B-32	BadNets	0.1	GTSRB	0.967933492	CIFAR100	0.5738	0	1
ViT-B-32	BadNets	0.15	MNIST	0.9962	CIFAR100	0.6037	0	1
ViT-B-32	BadNets	0.15	SVHN	0.966502766	CIFAR100	0.6175	0	1
ViT-B-32	BadNets	0.15	CIFAR10	0.9699	CIFAR100	0.772	0	1
ViT-B-32	BadNets	0.15	GTSRB	0.978384798	CIFAR100	0.5927	0	1

Model Structure	Attack Method	Poison Rate	Clean Dataset	Clean Acc	Poison Dataset	Poison Acc	ASR	cof
ViT-B-32	BadNets	0.01	MNIST	0.9938	GTSRB	0.822248614	0.885273159	1
ViT-B-32	BadNets	0.01	SVHN	0.957475415	GTSRB	0.911559778	0.925890736	1
ViT-B-32	BadNets	0.01	CIFAR10	0.9417	GTSRB	0.949010293	0.952414885	1
ViT-B-32	BadNets	0.01	CIFAR100	0.7432	GTSRB	0.961995249	0.965874901	1
ViT-B-32	BadNets	0.03	MNIST	0.9793	GTSRB	0.716389549	0.737688044	1
ViT-B-32	BadNets	0.03	SVHN	0.93488783	GTSRB	0.82280285	0.775296912	1
ViT-B-32	BadNets	0.03	CIFAR10	0.9156	GTSRB	0.839113222	0.865241489	1
ViT-B-32	BadNets	0.03	CIFAR100	0.6886	GTSRB	0.865637371	0.86658749	1
ViT-B-32	BadNets	0.05	MNIST	0.9843	GTSRB	0.703008709	0.818923199	1
ViT-B-32	BadNets	0.05	SVHN	0.940842041	GTSRB	0.858194774	0.883689628	1
ViT-B-32	BadNets	0.05	CIFAR10	0.9317	GTSRB	0.850752177	0.926128266	1
ViT-B-32	BadNets	0.05	CIFAR100	0.7096	GTSRB	0.883610451	0.935787807	1
ViT-B-32	BadNets	0.1	MNIST	0.968	GTSRB	0.671258907	0.856927949	1
ViT-B-32	BadNets	0.1	SVHN	0.937845728	GTSRB	0.86152019	0.901266825	1
ViT-B-32	BadNets	0.1	CIFAR10	0.9217	GTSRB	0.801821061	0.927553444	1
ViT-B-32	BadNets	0.1	CIFAR100	0.6969	GTSRB	0.838796516	0.936737926	1
ViT-B-32	BadNets	0.15	MNIST	0.9583	GTSRB	0.677672209	0.872288203	1
ViT-B-32	BadNets	0.15	SVHN	0.932736632	GTSRB	0.826840855	0.911243072	1
ViT-B-32	BadNets	0.15	CIFAR10	0.9137	GTSRB	0.794457641	0.92858274	1
ViT-B-32	BadNets	0.15	CIFAR100	0.6801	GTSRB	0.831987332	0.934600158	1
ViT-B-32	Blend	0.01	SVHN	0.953096189	MNIST	0.9883	0.0999	1
ViT-B-32	Blend	0.01	CIFAR10	0.9547	MNIST	0.9929	0.9133	1
ViT-B-32	Blend	0.01	CIFAR100	0.795	MNIST	0.9953	0.9975	1
ViT-B-32	Blend	0.01	GTSRB	0.960095012	MNIST	0.9857	0.1588	1
ViT-B-32	Blend	0.03	SVHN	0.94372311	MNIST	0.9897	0.1027	1
ViT-B-32	Blend	0.03	CIFAR10	0.9515	MNIST	0.9902	0.8419	1
ViT-B-32	Blend	0.03	CIFAR100	0.7897	MNIST	0.9925	0.9968	1
ViT-B-32	Blend	0.03	GTSRB	0.945764054	MNIST	0.9769	0.2762	1
ViT-B-32	Blend	0.05	SVHN	0.942993239	MNIST	0.9873	0.1134	1
ViT-B-32	Blend	0.05	CIFAR10	0.9511	MNIST	0.9868	0.7456	1
ViT-B-32	Blend	0.05	CIFAR100	0.7795	MNIST	0.9902	0.9772	1
ViT-B-32	Blend	0.05	GTSRB	0.958828187	MNIST	0.9816	0.2088	1
ViT-B-32	Blend	0.1	SVHN	0.941456669	MNIST	0.9887	0.1056	1
ViT-B-32	Blend	0.1	CIFAR10	0.9504	MNIST	0.9903	0.6953	1
ViT-B-32	Blend	0.1	CIFAR100	0.7759	MNIST	0.9923	0.9431	1
ViT-B-32	Blend	0.1	GTSRB	0.950277118	MNIST	0.9842	0.2196	1
ViT-B-32	Blend	0.15	SVHN	0.938959742	MNIST	0.9897	0.1045	1
ViT-B-32	Blend	0.15	CIFAR10	0.949	MNIST	0.9899	0.6759	1
ViT-B-32	Blend	0.15	CIFAR100	0.7715	MNIST	0.9919	0.9475	1
ViT-B-32	Blend	0.15	GTSRB	0.946239113	MNIST	0.9864	0.222	1
ViT-B-32	Blend	0.01	MNIST	0.9956	SVHN	0.890941918	0.56403657	1
ViT-B-32	Blend	0.01	CIFAR10	0.9524	SVHN	0.947295636	0.994391518	1
ViT-B-32	Blend	0.01	CIFAR100	0.7885	SVHN	0.958435771	0.998079287	1
ViT-B-32	Blend	0.01	GTSRB	0.971179731	SVHN	0.913798402	0.870736017	1
ViT-B-32	Blend	0.03	MNIST	0.9953	SVHN	0.866894591	0.759987707	1
ViT-B-32	Blend	0.03	CIFAR10	0.9493	SVHN	0.902158881	0.998079287	1
ViT-B-32	Blend	0.03	CIFAR100	0.7887	SVHN	0.919291641	0.999654272	1
ViT-B-32	Blend	0.03	GTSRB	0.966112431	SVHN	0.903272895	0.929125691	1
ViT-B-32	Blend	0.05	MNIST	0.9947	SVHN	0.868315919	0.676628765	1
ViT-B-32	Blend	0.05	CIFAR10	0.9522	SVHN	0.894437615	0.997003688	1



Model Structure	Attack Method	Poison Rate	Clean Dataset	Clean Acc	Poison Dataset	Poison Acc	ASR	cof
ViT-B-32	Blend	0.05	CIFAR100	0.7821	SVHN	0.919714198	0.999308543	1
ViT-B-32	Blend	0.05	GTSRB	0.965241489	SVHN	0.901121696	0.914182545	1
ViT-B-32	Blend	0.1	MNIST	0.9946	SVHN	0.864320836	0.78057775	1
ViT-B-32	Blend	0.1	CIFAR10	0.9493	SVHN	0.88798402	0.99765673	1
ViT-B-32	Blend	0.1	CIFAR100	0.786	SVHN	0.912453903	0.999423786	1
ViT-B-32	Blend	0.1	GTSRB	0.967933492	SVHN	0.897049785	0.929778734	1
ViT-B-32	Blend	0.15	MNIST	0.9949	SVHN	0.874539029	0.711009527	1
ViT-B-32	Blend	0.15	CIFAR10	0.9481	SVHN	0.910456361	0.997118931	1
ViT-B-32	Blend	0.15	CIFAR100	0.7771	SVHN	0.926936079	0.9994622	1
ViT-B-32	Blend	0.15	GTSRB	0.964766429	SVHN	0.906230793	0.919637369	1
ViT-B-33	dynamic_bd	0.01	CIFAR100	0.7075	GTSRB	0.9773	0.9679	1
ViT-B-34	dynamic_bd	0.03	CIFAR100	0.6996	GTSRB	0.9644	0.9949	1
ViT-B-35	dynamic_bd	0.05	CIFAR100	0.6965	GTSRB	0.9625	0.9947	1
ViT-B-36	dynamic_bd	0.1	CIFAR100	0.7137	GTSRB	0.9493	0.996	1
ViT-B-32	Wanet	0.01	SVHN	0.95643823	MNIST	0.9878	0.1152	1
ViT-B-32	Wanet	0.01	CIFAR10	0.9522	MNIST	0.9928	0.9877	1
ViT-B-32	Wanet	0.01	CIFAR100	0.7803	MNIST	0.9944	0.9981	1
ViT-B-32	Wanet	0.01	GTSRB	0.960174188	MNIST	0.9869	0.8978	1
ViT-B-32	Wanet	0.03	SVHN	0.944606638	MNIST	0.9876	0.113	1
ViT-B-32	Wanet	0.03	CIFAR10	0.9481	MNIST	0.9908	0.9973	1
ViT-B-32	Wanet	0.03	CIFAR100	0.7759	MNIST	0.9917	0.9997	1
ViT-B-32	Wanet	0.03	GTSRB	0.93594616	MNIST	0.9844	0.9538	1
ViT-B-32	Wanet	0.05	SVHN	0.943607867	MNIST	0.9857	0.0971	1
ViT-B-32	Wanet	0.05	CIFAR10	0.953	MNIST	0.9904	0.9849	1
ViT-B-32	Wanet	0.05	CIFAR100	0.7803	MNIST	0.9924	0.9992	1
ViT-B-32	Wanet	0.05	GTSRB	0.933570863	MNIST	0.9862	0.9534	1
ViT-B-32	Wanet	0.1	SVHN	0.940419484	MNIST	0.9842	0.1469	1
ViT-B-32	Wanet	0.1	CIFAR10	0.9452	MNIST	0.9843	0.9996	1
ViT-B-32	Wanet	0.1	CIFAR100	0.7757	MNIST	0.9892	1	1
ViT-B-32	Wanet	0.1	GTSRB	0.924623911	MNIST	0.9789	0.9865	1
ViT-B-32	Wanet	0.15	SVHN	0.935809773	MNIST	0.9858	0.1608	1
ViT-B-32	Wanet	0.15	CIFAR10	0.944	MNIST	0.9902	0.9975	1
ViT-B-32	Wanet	0.15	CIFAR100	0.7716	MNIST	0.9929	1	1
ViT-B-32	Wanet	0.15	GTSRB	0.90530483	MNIST	0.9861	0.9545	1
ViT-B-32	Wanet	0.01	MNIST	0.9957	SVHN	0.880762139	0.134603565	1
ViT-B-32	Wanet	0.01	CIFAR10	0.951	SVHN	0.934657345	0.827673632	1
ViT-B-32	Wanet	0.01	CIFAR100	0.7875	SVHN	0.948371235	0.933236017	1
ViT-B-32	Wanet	0.01	GTSRB	0.975613618	SVHN	0.906038722	0.636524278	1
ViT-B-32	Wanet	0.03	MNIST	0.9943	SVHN	0.841925323	0.168677013	1
ViT-B-32	Wanet	0.03	CIFAR10	0.9484	SVHN	0.867278734	0.885064536	1
ViT-B-32	Wanet	0.03	CIFAR100	0.782	SVHN	0.891133989	0.972533805	1
ViT-B-32	Wanet	0.03	GTSRB	0.969437846	SVHN	0.864704978	0.730447142	1
ViT-B-32	Wanet	0.05	MNIST	0.9948	SVHN	0.854640443	0.145666872	1
ViT-B-32	Wanet	0.05	CIFAR10	0.9425	SVHN	0.861401352	0.869468347	1
ViT-B-32	Wanet	0.05	CIFAR100	0.774	SVHN	0.886447449	0.968999693	1
ViT-B-32	Wanet	0.05	GTSRB	0.973396675	SVHN	0.857982483	0.670866626	1
ViT-B-32	Wanet	0.1	MNIST	0.9946	SVHN	0.837738168	0.147741242	1
ViT-B-32	Wanet	0.1	CIFAR10	0.9479	SVHN	0.863706208	0.844537492	1
ViT-B-32	Wanet	0.1	CIFAR100	0.7782	SVHN	0.891902274	0.957206515	1
ViT-B-32	Wanet	0.1	GTSRB	0.970308789	SVHN	0.866279963	0.673670867	1

Model Structure	Attack Method	Poison Rate	Clean Dataset	Clean Acc	Poison Dataset	Poison Acc	ASR	cof
ViT-B-32	Wanet	0.15	MNIST	0.9942	SVHN	0.833704671	0.13302858	1
ViT-B-32	Wanet	0.15	CIFAR10	0.945	SVHN	0.870390289	0.834895513	1
ViT-B-32	Wanet	0.15	CIFAR100	0.7704	SVHN	0.896319914	0.962161955	1
ViT-B-32	Wanet	0.15	GTSRB	0.96912114	SVHN	0.877650584	0.712507683	1
ViT-B-32	Wanet	0.01	MNIST	0.9962	CIFAR10	0.9021	0.254	1
ViT-B-32	Wanet	0.01	SVHN	0.970228949	CIFAR10	0.915	0.2127	1
ViT-B-32	Wanet	0.01	CIFAR100	0.8419	CIFAR10	0.9701	0.3462	1
ViT-B-32	Wanet	0.01	GTSRB	0.9847981	CIFAR10	0.8914	0.6602	1
ViT-B-32	Wanet	0.03	MNIST	0.9948	CIFAR10	0.8002	0.3191	1
ViT-B-32	Wanet	0.03	SVHN	0.966310695	CIFAR10	0.8533	0.2547	1
ViT-B-32	Wanet	0.03	CIFAR100	0.7919	CIFAR10	0.9436	0.4117	1
ViT-B-32	Wanet	0.03	GTSRB	0.97442597	CIFAR10	0.8008	0.7188	1
ViT-B-32	Wanet	0.05	MNIST	0.9907	CIFAR10	0.7847	0.3451	1
ViT-B-32	Wanet	0.05	SVHN	0.964850953	CIFAR10	0.8416	0.2957	1
ViT-B-32	Wanet	0.05	CIFAR100	0.7696	CIFAR10	0.9254	0.3666	1
ViT-B-32	Wanet	0.05	GTSRB	0.958511481	CIFAR10	0.7774	0.6882	1
ViT-B-32	Wanet	0.1	MNIST	0.9946	CIFAR10	0.7982	0.4402	1
ViT-B-32	Wanet	0.1	SVHN	0.968999693	CIFAR10	0.8497	0.3504	1
ViT-B-32	Wanet	0.1	CIFAR100	0.7798	CIFAR10	0.9396	0.4069	1
ViT-B-32	Wanet	0.1	GTSRB	0.976326207	CIFAR10	0.8002	0.8162	1
ViT-B-32	Wanet	0.15	MNIST	0.9954	CIFAR10	0.7956	0.4724	1
ViT-B-32	Wanet	0.15	SVHN	0.966925323	CIFAR10	0.8437	0.4182	1
ViT-B-32	Wanet	0.15	CIFAR100	0.7887	CIFAR10	0.9342	0.5061	1
ViT-B-32	Wanet	0.15	GTSRB	0.976247031	CIFAR10	0.7891	0.8587	1
ViT-B-32	Wanet	0.01	MNIST	0.9963	CIFAR100	0.6124	0.0695	1
ViT-B-32	Wanet	0.01	SVHN	0.97303319	CIFAR100	0.618	0.1365	1
ViT-B-32	Wanet	0.01	CIFAR10	0.9741	CIFAR100	0.8008	0.166	1
ViT-B-32	Wanet	0.01	GTSRB	0.985431512	CIFAR100	0.6098	0.5011	1
ViT-B-32	Wanet	0.03	MNIST	0.9959	CIFAR100	0.5793	0.0805	1
ViT-B-32	Wanet	0.03	SVHN	0.968423479	CIFAR100	0.5819	0.1453	1
ViT-B-32	Wanet	0.03	CIFAR10	0.9692	CIFAR100	0.7646	0.156	1
ViT-B-32	Wanet	0.03	GTSRB	0.977751386	CIFAR100	0.554	0.5039	1
ViT-B-32	Wanet	0.05	MNIST	0.9955	CIFAR100	0.5628	0.0639	1
ViT-B-32	Wanet	0.05	SVHN	0.965888138	CIFAR100	0.569	0.13	1
ViT-B-32	Wanet	0.05	CIFAR10	0.965	CIFAR100	0.7477	0.1317	1
ViT-B-32	Wanet	0.05	GTSRB	0.966983373	CIFAR100	0.5383	0.4715	1
ViT-B-32	Wanet	0.1	MNIST	0.9955	CIFAR100	0.5794	0.0777	1
ViT-B-32	Wanet	0.1	SVHN	0.967155808	CIFAR100	0.5825	0.1366	1
ViT-B-32	Wanet	0.1	CIFAR10	0.9671	CIFAR100	0.7517	0.1206	1
ViT-B-32	Wanet	0.1	GTSRB	0.973634204	CIFAR100	0.5588	0.4518	1
ViT-B-32	Wanet	0.15	MNIST	0.9962	CIFAR100	0.5632	0.0499	1
ViT-B-32	Wanet	0.15	SVHN	0.967847265	CIFAR100	0.58	0.1562	1
ViT-B-32	Wanet	0.15	CIFAR10	0.9664	CIFAR100	0.7512	0.1426	1
ViT-B-32	Wanet	0.15	GTSRB	0.954315123	CIFAR100	0.5501	0.442	1
ViT-B-32	Wanet	0.01	MNIST	0.9946	GTSRB	0.818527316	0.151939826	1
ViT-B-32	Wanet	0.01	SVHN	0.960394899	GTSRB	0.913935075	0.222644497	1
ViT-B-32	Wanet	0.01	CIFAR10	0.939	GTSRB	0.94330958	0.568646081	1
ViT-B-32	Wanet	0.01	CIFAR100	0.739	GTSRB	0.961361837	0.652969121	1
ViT-B-32	Wanet	0.03	MNIST	0.9839	GTSRB	0.704117181	0.270229612	1
ViT-B-32	Wanet	0.03	SVHN	0.944299324	GTSRB	0.860332542	0.314964371	1

Model Structure	Attack Method	Poison Rate	Clean Dataset	Clean Acc	Poison Dataset	Poison Acc	ASR	cof
ViT-B-32	Wanet	0.03	CIFAR10	0.9326	GTSRB	0.845922407	0.648456057	1
ViT-B-32	Wanet	0.03	CIFAR100	0.7126	GTSRB	0.872367379	0.758194774	1
ViT-B-32	Wanet	0.05	MNIST	0.9755	GTSRB	0.681947743	0.370942201	1
ViT-B-32	Wanet	0.05	SVHN	0.939267056	GTSRB	0.849564529	0.400791766	1
ViT-B-32	Wanet	0.05	CIFAR10	0.928	GTSRB	0.815281077	0.679889153	1
ViT-B-32	Wanet	0.05	CIFAR100	0.6993	GTSRB	0.854711006	0.807125891	1
ViT-B-32	Wanet	0.1	MNIST	0.967	GTSRB	0.726920032	0.431195566	1
ViT-B-32	Wanet	0.1	SVHN	0.945759066	GTSRB	0.865320665	0.404671417	1
ViT-B-32	Wanet	0.1	CIFAR10	0.9241	GTSRB	0.846239113	0.753840063	1
ViT-B-32	Wanet	0.1	CIFAR100	0.6921	GTSRB	0.880443389	0.842042755	1
ViT-B-32	Wanet	0.15	MNIST	0.9734	GTSRB	0.71821061	0.390023753	1
ViT-B-32	Wanet	0.15	SVHN	0.939958513	GTSRB	0.86429137	0.435629454	1
ViT-B-32	Wanet	0.15	CIFAR10	0.904	GTSRB	0.836025337	0.755819477	1
ViT-B-32	Wanet	0.15	CIFAR100	0.6738	GTSRB	0.868725257	0.860649248	1
ViT-B-32	Blend	0.01	CIFAR100	0.7543	GTSRB	0.976247031	0.872921615	1
ViT-B-32	Blend	0.03	CIFAR100	0.7224	GTSRB	0.954711006	0.656532067	1
ViT-B-32	Blend	0.05	CIFAR100	0.7008	GTSRB	0.920902613	0.770150435	1
ViT-B-32	Blend	0.1	CIFAR100	0.7239	GTSRB	0.946634996	0.850514648	1
ViT-B-32	Blend	0.15	CIFAR100	0.6929	GTSRB	0.913460016	0.786619161	1
ViT-B-32	narcissus	0.01	CIFAR100	0.7472	GTSRB	0.97189232	0.667300079	1
ViT-B-32	narcissus	0.03	CIFAR100	0.7535	GTSRB	0.973159145	0.673238321	1
ViT-B-32	narcissus	0.05	CIFAR100	0.7467	GTSRB	0.968250198	0.84101346	1
ViT-B-32	narcissus	0.1	CIFAR100	0.7486	GTSRB	0.966745843	0.599208234	1